ISTANBUL TECHNICAL UNIVERSITY ★ GRADUATE SCHOOL OF SCIENCE ENGINEERING AND TECHNOLOGY

ASSESSMENT OF SEISMIC PERFORMANCE OF RC MEMBERS AFTER FIRE EXPOSURE THROUGH LARGE-SCALE TESTING

Ph.D. THESIS

Ugur DEMIR

Department of Civil Engineering

Structural Engineering Programme

SEPTEMBER 2020

ISTANBUL TECHNICAL UNIVERSITY ★ GRADUATE SCHOOL OF SCIENCE ENGINEERING AND TECHNOLOGY

ASSESSMENT OF SEISMIC PERFORMANCE OF RC MEMBERS AFTER FIRE EXPOSURE THROUGH LARGE-SCALE TESTING

Ph.D. THESIS

Ugur DEMIR
(501122022)

Department of Civil Engineering

Structural Engineering Programme

Thesis Advisor: Prof. Dr. Alper ILKI
Thesis Co-Advisor: Prof. Dr. Mark F. GREEN

SEPTEMBER 2020

İSTANBUL TEKNİK ÜNİVERSİTESİ ★ FEN BİLİMLERİ ENSTİTÜSÜ

BETONARME YAPI ELEMANLARININ YANGIN SONRASI DEPREM PERFORMANSLARININ GENİŞ ÖLÇEKLİ DENEYLERLE BELİRLENMESİ

DOKTORA TEZİ

Uğur DEMİR
(501122022)

İnşaat Mühendisliği Anabilim Dalı

Yapı Mühendisliği Programı

Tez Danışmanı: Prof. Dr. Alper İLKİ
Eş Danışman: Prof. Dr. Mark F. GREEN

EYLÜL 2020

Ugur DEMIR, a Ph.D. student of ITU Graduate School of Science Engineering and Technology student ID 501122022, successfully defended the thesis entitled "ASSESSMENT OF SEISMIC PERFORMANCE OF RC MEMBERS AFTER FIRE EXPOSURE THROUGH LARGE-SCALE TESTING", which he prepared after fulfilling the requirements specified in the associated legislations, before the jury whose signatures are below.

Thesis Advisor :	**Prof. Dr. Alper ILKI** Istanbul Technical University	.....
Co-advisor :	**Prof.Dr. Mark F. GREEN** Queen's University	.....
Jury Members :	**Prof. Dr. Rustem GUL** Igdır University	.....
	Prof. Dr. Kutlu DARILMAZ Istanbul Technical University	.....
	Asst. Prof. Dr. Mecit CELIK Istanbul Technical University	.....
	Prof. Dr. Kutay ORAKCAL Bogazici University	.....
	Prof. Dr. Tulay AKSU OZKUL Istanbul Technical University	.....

Date of Submission : 1 June 2020
Date of Defense : 17 September 2020

To my spouse and sons Aren and Uras,

FOREWORD

The effects of fire induced damage on seismic performance of reinforced concrete members are not well understood up to now. This thesis investigates the post-fire seismic behavior of reinforced concrete columns in a comprehensive manner in order to fulfill this gap.

Many people have assisted me during the course of this research and I would like to extend my thanks to several in particular. My thesis supervisor at Istanbul Technical University Prof.Dr. Alper Ilki and co-supervisor at Queen's University Prof.Dr. Mark F. Green have been of tremendous help continually throughout the study. I appreciate the contributions of steering committee members of the thesis Prof.Dr. Rustem Gul, Prof.Dr. Kutlu Darilmaz and Asst.Prof.Dr. Mecit Celik. I also very much appreciate the invaluable support and eternal patience of Dr. Caglar Goksu. Others who have provided me with a great deal of help and support include Mr. Ergun Binbir and Mr. Goktug Unal for which I am grateful. This study could not have been conducted without the support and encouragement of my spouse for which I am extremely grateful.

Funding for this study was provided jointly by Research Council of Turkey (TUBITAK-216M535), ITU scientific research project department (BAP-39548), Yapi Merkezi Construction Co., Allianz Insurance Co., Ytong-Turk and Fibrobeton Co. and I would like to thank them for this opportunity.

September 2020

Ugur DEMIR
(M.Sc.)

TABLE OF CONTENTS

Page

SYMBOLS

A_o	: Area of lateral reinforcement
A_{cc}	: Area of core section
A_g	: Gross-sectional area
A_s	: Area of longitudinal steel
c	: Specific heat
d_c	: Concrete core dimension to center line of the perimeter hoop
Δ	: Lateral displacement
Δ_p	: Lateral plastic displacement
Δ_{res}	: Residual lateral plastic displacement
Δ_u	: Lateral ultimate displacement
Δ_{un}	: Specified peak displacement for each drift ratio
Δ_y	: Lateral yield displacement
EDC	: Cumulative energy dissipation
ε	: Emissivity of the solid
ε_c	: Compressive strain of unconfined concrete
ε_{cc}	: Compressive strain of confined concrete
ε_s	: Tensile strain of longitudinal steel
ε_o	: Peak compressive strain of concrete at ambient temperature
ε_{oT}	: Residual peak compressive strain of concrete after fire exposure
f'_c	: Compressive strength of concrete at ambient temperature
f'_{cT}	: Residual compressive strength of concrete after fire exposure
h	: Coefficient of convection
h_c	: Convective heat flux between gas and solid
h_r	: Radiative heat flux emitted by a solid
k	: Thermal conductivity
K	: Secant stiffness
l	: Shear span
l_p	: Plastic hinge length
M	: Moment
μ_Δ	: Ductility factor
n	: Axial load ratio
N	: Applied axial load
N_0	: Axial load capacity
P	: Lateral load
ϕ	: Curvature
ϕ_y	: Yield curvature
Q	: Constant for internal generation of heat
r	: Residual displacement ratio
ρ	: Specific mass
ρ_{cc}	: Ratio of longitudinal steel
ρ_s	: Ratio of lateral reinforcement
s	: Spacing of the lateral reinforcement

σ	: Stefan -Boltzman constant
t	: Time
T	: Temperature
T_g	: Temperature of the gas
T_s	: Temperature at the surface of the solid
Θ_p	: Plastic rotation

LIST OF TABLES

Page

LIST OF FIGURES

Page

ASSESSMENT OF SEISMIC PERFORMANCE OF RC MEMBERS AFTER FIRE EXPOSURE THROUGH LARGE-SCALE TESTING

SUMMARY

Quantifying the seismic resistance of reinforced concrete (RC) buildings after fire is currently difficult because of the lack of information regarding their strength and ductility under earthquake loads. This thesis presents the results of an experimental study, which was carried out to investigate the post-fire seismic behavior of reinforced concrete columns. The thesis is mainly comprised of three papers accepted by high quality journals.

In the first chapter, the factors affecting the post-fire seismic behavior of RC columns are analyzed with a particular focus on the behavior of concrete and steel under elevated temperatures and after cooling.

In the second chapter, post-fire seismic behavior of cast-in-situ RC columns are investigated. Five cast-in-place RC columns were tested to failure under constant axial load and reversed cyclic lateral displacements after being exposed to ISO-834 standard fire for 30, 60 or 90 minutes. All of the columns are full-scale and designed to behave in flexure-controlled manner complying with major design codes (e.g. ACI 318-14). Other than the effects of fire exposure durations, the effects of thickness of concrete cover (25 and 40 mm) on structural performance was also investigated for the short fire exposure duration (30 minutes). The responses of the columns are analyzed in terms of lateral load-displacement relationships, ductility, stiffness, energy dissipation capacities and residual displacements. The test results indicated that fire exposure reduced the lateral load capacity of the columns whereas the deformability capabilities were found to be satisfactory in terms of structural response. It was also seen that the thickness of the concrete cover has only a slight influence on the post-fire seismic behavior of the columns which is attributed to the fact that lower concrete cover thickness results in higher effective depth which in turn leads to higher bending moment capacity and thereby higher lateral load capacity. Furthermore, a theoretical study was conducted to predict the load-displacement response of the fire exposed columns. The comparison of the experimentally and theoretically obtained load-displacement relationships indicated that the principals of structural mechanics usually applied to conventional columns are also valid for the columns exposed to fire in case the proposed algorithm is followed.

In the third chapter, a similar approach as stated for the cast-in-situ columns is followed for precast RC columns as well. The precast columns had the same cross-section and reinforcement configuration and had been exposed to the same fire scenarios with the cast-in-situ columns. These columns were inserted into a socket foundation and had a lower axial load ratio (i.e. 10%) in order to represent the condition in common industrial buildings. The findings indicated that the repair mortar

between the columns and foundation behaved in a satisfactory manner and therefore, similar post-fire seismic behavior was observed for cast-in-situ and precast columns.

In the fourth chapter of the thesis, an experimental study is presented to examine the impact of time after fire on (i) post-fire behavior of small-scale specimens (cubes and cylinders), (ii) seismic behavior of full-scale reinforced concrete columns. The post-fire seismic response of the columns are analyzed 30, 60 and 360 days after fire exposure. Impact of time after fire exposure on residual lateral load capacity and ductility of the columns was found to be limited while the column subjected to seismic test 30 days after fire exposure, exhibited less stiff behavior with respect to the columns tested later. Furthermore, an analytical study is conducted for the prediction of seismic behavior of reinforced concrete columns after fire exposure considering the variations in residual properties of concrete by time, and the proposed model is found to be in good agreement with the test results.

BETONARME YAPI ELEMANLARININ YANGIN SONRASI DEPREM PERFORMANSLARININ GENİŞ ÖLÇEKLİ DENEYLERLE BELİRLENMESİ

ÖZET

Betonarme yapılar şiddetli yangınlara maruz kalmaya duyarlıdır. Bu tür yapılarda, aktif ve pasif yangından koruma yöntemleri; depremler, tsunamiler, kundaklama ve terörist saldırılar nedeniyle veya çoğunlukla kaza ile oluşan yangınlarda uygulanamayabilir veya işe yaramayabilir. Bu durumda yapıya hasar verebilecek şiddette yangınlar meydana gelebilir. İstanbul Büyükşehir Belediyesi İtfaiye Daire Başkanlığı tarafından yayımlanan rapora göre, 2014-2018 yılları arasında İstanbul'da yılda ortalama 15.000 yapısal meydana gelmiştir. Uluslararası Yangın ve Kurtarma Birliği'nin raporuna göre 1993-2014 yılları arasında oluşan yangınların yaklaşık %40'ı yapılardan kaynaklanmıştır ve bu yangınlar nedeniyle hayatını kaybeden insan sayısı bir milyonu aşmıştır. Bu durum yangın sonrası betonarme yapıların davranışlarının belirlenmesine yönelik çalışmaların gerekliliğini göstermektedir. Betonarme yapılarda, yangın nedeniyle betonun ve donatıların mekanik özelliklerinde bir miktar azalma görülebilir. Bu azalma genellikle yangın sırasında ulaşılan en yüksek sıcaklığa, kullanılan beton ve donatının özelliklerine ve betonarme yapı elemanlarının üzerinde bulunan yük durumuna bağlıdır. Ülkemiz ve dünyada mevcut yangın yönetmeliklerinin hemen hepsinde, betonarme yapı elemanları için gerekli paspayı kalınlıkları önerilmekte ve bu paspayını sağlayan elemanlardan teşkil edilmiş betonarme yapıların, servis yükleri altında yangın sonrası can güvenliğini sağlayacağı öngörülmektedir.

Bunun yanında ülkemiz ve dünyanın önemli miktarda nüfusuna ev sahipliği yapan birçok ülke (Ör. Çin, Hindistan, Pakistan, Amerika Birleşik Devletleri, Japonya, İtalya v.b.) deprem fay hatları üzerinde yer almaktadır. Deprem riski altındaki bu ülkelerde, yangın geçiren betonarme yapılarda meydana gelmesi olası depremler dikkate alınarak tasarım ve yangın sonrası performans değerlendirmesi yapılmalıdır. Bu durum, betonarme yapıların yangın sonrası deprem performansının belirlenmesine yönelik araştırmaları gerektirmektedir. Betonarme kolonlar çerçeve tipi yapılarda ana taşıyıcı elemanlar olduğundan, bu tez kapsamında betonarme kolonların yangın sonrası deprem performansı incelenmiştir. Yangına maruz kalmış kolonların olası depremler sonrası performansının değerlendirilmesine yönelik yeterli miktarda araştırma literatürde bulunmamaktadır. Şimdiye dek bu konuda yapılan deneysel çalışmalar, mevcut yapılarda uygulama açısından belirli yetersizlikleri bulunan (Ör. kesme kritik) ve görece küçük ölçekli betonarme kolonlara yöneliktir. Bu çalışmaların büyük çoğunluğu, yangın sonrası betonarme kolonların onarım ve güçlendirilmesine yönelik gerçekleştirilmiştir.

Tüm bu bilgiler ışığında tez kapsamında; önemli deprem ve yangın yönetmeliklerine uygun olarak tasarlanmış, eğilme-kritik, tam ölçekli betonarme kolonların yangın sonrası deprem performansının belirlenmesine yönelik bir deneysel çalışma literatürde

ilk kez gerçekleştirilmiştir. Tez, İTÜ Fen Bilimleri Enstitüsü tarafından yayımlanan "*Doktora Tezlerinin Bilimsel Yayınlardan Hazırlanmasına İlişkin Yönerge*" kapsamında dört adet makalenin birleştirilmesinden oluşmaktadır. Bunlardan tezin iki, üç ve dördüncü bölümünü oluşturanlar, Scopus tarafından Q1 olarak taranan dergilerde yayımlanmak üzere kabul edilmiştir.

Tezin ilk bölümünde, betonarme yapılarda yangın sonrası deprem performansını etkileyen faktörler tartışılmıştır. Geniş kapsamlı literatür taraması sonucu, beton ve donatıda yüksek sıcaklık nedeniyle oluşan değişiklikler, soğuduktan sonraki durumu da dikkate alacak şekilde ortaya konmuştur.

Tezin ikinci bölümünde, az ve orta katlı betonarme yapılardaki genel durumu temsil etmek üzere, yerinde döküm yöntemiyle inşa edilmiş betonarme kolonların yangın sonrası deprem performansı, analitik ve deneysel yöntemlerle incelenmiştir. İlgili kolonlarda deprem yönetmeliklerinde verilen minimum koşullar dikkate alınarak yapılan tasarımda, beton paspayı tüm yangın yönetmeliklerine uygun şekilde 40 mm olarak seçilmiş, deprem yönetmeliklerinin izin verdiği fakat yangın yönetmeliklerine uymayan, mevcut yapılarda sıkça karşılaşılan durumu temsil etmek üzere, numunelerin bir tanesinde paspayı 25 mm olarak uygulanmıştır. Betonarme kolonlar, üretildikten sonra nihai dayanımlarına ulaşana kadar yaklaşık 14 ay bekletildikten sonra yangın testleri gerçekleştirilmiştir. Yangın testleri, ISO-834 yangın yönetmeliği tarafından önerilen standart yangın eğrisi, 30, 60 ve 90 dakika izlenerek gerçekleştirilmiş, kolon numuneler yangına maruz bırakıldıktan 60 gün sonra deprem testlerine maruz bırakılmıştır. Altmış günlük süre, yangından sonra performans tayini için gerekli incelemeler ve analizler için geçen yaklaşık süreyi temsil etmektedir. Deprem testleri sabit düşey yüklerle kombine edilmiş yatay tersinir tekrarlı yükler altında gerçekleştirilmiştir. Kolonlardaki düşey yükler, az ve orta yükseklikteki betonarme yapıları temsil etmek üzere, eksenel yük kapasitesinin yaklaşık %20'si mertebesinde uygulanmıştır. Deprem testleri sonucunda, betonarme kolonlara ait çevrimsel yatay yük-yatay yerdeğiştirme ilişkileri, süneklik faktörleri, rijitlikler, enerji yutma kapasiteleri ve nihai kalıcı yerdeğiştirmeler elde edilmiştir. Deney sonuçları, kolonlarda standart yangınlar sonrasında yatay yük taşıma kapasitelerinde %20'ye varan kayıplar oluştuğunu göstermiştir. Betonun elastisite modülünde yangın hasarına bağlı olarak oluşan önemli azalmalar, betonarme kolonlarda akmaya karşı gelen ötelemelerde artışa neden olurken, nihai ötelemelerde kaydadeğer herhangi bir değişikliğe yol açmamıştır. Bu nedenle, 30 ve 60 dakikalık yangınlara maruz kalmış kolonlarda kolon sünekliklerinde önemli bir değişiklik görülmezken, akma yerdeğiştirmesinde görece daha yüksek miktarda artış meydana gelen, 90 dakika yangına maruz kalmış kolonda süneklik %20 mertebelerinde azalmıştır. Test edilen tüm kolonlarda süneklik faktörü 3.5'in üzerinde olduğundan, incelenen şiddette yangın hasarının incelenen koşullar altında betonarme kolonların sünekliği üzerinde önemli bir etkisi olmadığı değerlendirilebilir. Beton elastisite modülünde yangın hasarı nedeniyle meydana gelen azalma, kolon rijitliklerinde azalmaya neden olmuştur. Bu azalma yangın süresi ile orantılıdır. Enerji yutma kapasitelerinde yangın hasarına bağlı olarak, yangın süresine orantılı şekilde azalmalar gözlemlenmiştir. Kalıcı yerdeğiştirmelerde pik yük değerine kadar önemli bir değişiklik gözlenmezken, bu noktadan sonra yangın süresi ile orantılı azalmalar gözlenmiştir. Beton paspayının azalması bir taraftan donatıdaki sıcaklıkların artmasına neden olmakla birlikte, diğer taraftan kesit faydalı yüksekliğini ve dolayısıyla moment kapasitesini arttırdığından, incelenen koşullar altında yangın sonrası deprem performansını önemli ölçüde etkilememiştir. İncelenen koşullar altında donatının yangın sonrası mekanik

özelliklerinde herhangi bir değişiklik gözlenmemiş olduğu ve donatı nihai mekanik özelliklerinde bir azalma olması durumunda paspayı azalmasının aynı sonucu doğurmayacağı akılda tutulmalıdır. Deneysel çalışma neticesinde elde edilen veriler kullanılarak, betonarme kolonlarda yatay yük-yatay yerdeğiştirme ilişkisi nümerik olarak modellenmiştir. Modelleme sırasında sonlu elemanlar yöntemi kullanılarak kolon kesitlerindeki sıcaklık dağılımları belirlenmiş, bu değerlere karşı gelen dayanım kayıpları literatürde yer alan dayanım azalması ilişkileri kullanılarak elde edilmiş ve geleneksel yapı mekaniği ilkeleri uyarınca davranış modellenmiştir. Geliştirilen nümerik algoritmanın deney sonuçlarını tahmin etme konusunda başarılı olduğu görülmüştür.

Tezin üçüncü bölümünde, sanayi yapılarında sıklıkla uygulandığı bilinen öndökümlü betonarme kolonları temsil etmek üzere tam ölçekli, soket temelli kolonlar imal edilmiştir. Kolonların tasarımı deprem ve yangın yönetmeliklerine uygundur. Bu kolonlara da yerinde dökümlü betonarme kolonlarla kıyas yapılabilmesi için aynı yangın senaryoları uygulanmıştır. Yangına maruz bırakıldıktan sonra kolonların deprem perfromansları incelenmiştir. Bu kolonlarda, soket temel ile kolonlar arasına pratikte uygulanan tamir harcının yangın sonrası yeterli performansı gösterdiği görülmüştür. Yangın sonrası öndökümlü kolonların, yerinde döküm kolonlara yakın davranış sergilediği gözlenmiştir. Öndökümlü kolonların yangın sonrası deprem sonrası davranışı ikinci bölümde belirtilen şekilde nümerik olarak modellenmiştir. Geliştirilen nümerik algoritmanın deney sonuçlarını tahmin etme konusunda başarılı olduğu görülmüştür.

Tezin dördüncü bölümünde yangın sonrası geçen sürenin deprem performansına etkisi incelenmiştir. Yukarıda belirtildiği gibi, yapılan literatür taraması sonucu yangın sonrası beton mekanik özelliklerinin zamanla değiştiği bilinmektedir. Tez kapsamında küçük ölçekli silindir ve küp numunelerden elde edilen sonuçlar da bu durumu desteklemektedir. Fakat literatürde mevcut sınırlı sayıdaki çalışmalar, farklı koşullar altında gerçekleştirilmiş ve farklı sonuçlar rapor etmiştir. Genel olarak, maruz kalınan en yüksek sıcaklıktan bağımsız olarak, yangından 60 gün sonraki beton basınç dayanımı, yangından 30 gün sonrasına kıyaslandığında bazı çalışmalara göre değişmez iken bazı çalışmalara göre % 15 daha artmaktadır. Literatürde rapor edilen bu çelişkili durumu netleştirmek ve yangın sonrası geçen sürenin deprem performansına etkisini incelemek üzere, yangından 60 gün sonra test edilmek üzere yukarıda bahsedilen kolonlarla aynı özelliklere sahip iki kolon daha üretilmiş, 90 dakikalık standart yangına maruz bırakılmış ve yangından 30 ve 360 gün sonra aynı deprem yüklerine maruz bırakılmıştır. Deneyler sonucunda, yangından 30 ve 60 gün sonra test edilen kolonların yatay yük-yatay yerdeğiştirme ilişkilerinde ve sünekliklerinde önemli miktarda farklılıklar görülmezken, yangından 60 gün sonra test edilen kolondaki rijitliğin, 30 gün sonra test edilene kıyasla daha yüksek olduğu gözlenmiştir. Yukarıda bahsedilen nümerik çalışma tezin bu bölümü için de yangın sonrası davranışın modellenmesine yönelik olarak tekrarlanmıştır. Yapılan hesaplarda, yangından 60 gün sonra test edilen kolonun beton basınç dayanımı, 30 gün sonra test edilen kolonunkine kıyasla %15 fazla alındığında nümerik ve deneysel sonuçların birbirine yaklaştığı görülmüştür.

Tez kapsamında gerçekleştirilen deneysel ve nümerik çalışmanın, konunun önemi ve insanların can güvenliği perspektifinden bakıldığında, kaydadeğer bir katkı sunduğu değerlendirilmelidir. Bu çalışma, ayrıca beraberinde incelenmesi gereken yeni sorunların varlığını ortaya koymaktadır. Bu nedenle, daha sonra yapılması gerekli çalışmalara ön ayak olacağı düşünülmektedir.

1. INTRODUCTION

In majority of the fires originated from reinforced concrete (RC) structures, structural damage is observed due to the deterioration of the materials, such as concrete and steel reinforcement. Furthermore, probable future earthquakes may cause unanticipated strength and stiffness degradation to this kind of fire-damaged structures which is critical in terms of lateral dynamic instability in earthquake prone areas. This instability is manifested in RC structures as side-sway collapse caused by loss of lateral-force-resisting capacity or remarkable increases in peak displacement demands. In other respects, RC columns form the main load bearing component of a RC structure and therefore, provision of appropriate fire safety measures is one of the major safety requirements in design. Protecting columns from losing the load-carrying capacity is the most crucial part in the ductility design of RC frame structures to withstand seismic actions, which complies with the principles and requirements for the safety and serviceability of structures.

In the scope of the thesis, first, impact of high temperatures on mechanical properties of concrete and reinforcement is investigated in this chapter considering the influence of post-fire cooling phase. Then, post-fire seismic behavior of cast-in-situ and precast columns is analyzed through large-scale testing and numerical modelling. The impact of time after fire also affects the post-fire seismic behavior, and this impact is also discussed within the thesis. It should be noted that this chapter is based on a perivously published research of the author and the thesis advisor (Ilki and Demir, 2019), while the following three chapters are comprised of three journal papers i.e. Demir et al., 2020a; Demir et al., 2020b and Demir et al., 2020c. These papers are constructed in the scope of the presented thesis and accepted for publishing in ASCE Journal of Structural Engineering, PCI Journal and Structures Journal. At the last chapter of the thesis, findings are presented and needs for further studies are addressed.

This chapter is to a large extent from: Ilki, A. and Demir, U. (2019). Factors affecting seismic behavior of reinforced concrete structures after fire exposure. NED University Journal of Research, 1, 31-41.

1.1 Literature Review

Post-fire behavior of structural components should be investigated carefully to make a realistic determination of residual seismic performance of structures after a fire. Within the scope of this chapter, the factors affecting the mechanical behavior of the structural members under elevated temperatures and after cooling phase are discussed. Proper evaluation of seismic vulnerability of RC structures after a fire is a challenging and key issue for earthquake prone countries. The post-fire seismic performance assessment is generally based on the damage of concrete cover and material deterioration over the RC members. Most of the issues related to concrete cover and material deteriorations are codified and a comparison between the recommendations of some of the major codes (Turkish fire regulation, 2007; ACI 216; CEN, 2004; Concrete Society, 2008) is investigated in this chapter. In the light of existing knowledge in literature, when subjected to fire, some of physical and chemical changes which occur in concrete and reinforcing steel are reversible upon cooling, while others are irreversible and may significantly weaken the RC structure after a fire (Harada et al., 1972; Schneider and Nagele, 1990; Papayianni and Valiasis, 1991; Khoury, 2000; Felicetti and Meda, 2005; Hertz, 2005; Fletcher et al., 2007; Concrete Society, 2008; fib, 2008). The changes in mechanical properties of concrete and steel reinforcement, under elevated temperatures and after cooling are discussed below as well as the effect of fire on bond behavior.

1.2 Effect of Concrete Cover

In RC structural members, current design criteria have been typically expressed only in terms of required concrete cover thickness for the considered design fire (Table 1.1). For example, Turkish fire regulation (2007) (hereafter TFR) demands minimum clear concrete cover of 35, 25 and 20 mm for columns, beams and slabs, respectively, for 120 minutes of standard fire resistance. According to ACI 216 (1997), minimum concrete cover, regardless of any other parameters, shall not be less than 25.4 mm (1 in.) times the number of hours of required fire resistance, or 50.8 mm (2 in.), whichever is less for columns. For 120 minutes of fire resistance, minimum concrete cover for beams is given depending on width and restrain conditions (i.e. 19.05 mm for 300 mm wide restrained beams). Minimum concrete cover for slabs is given depending on aggregate type and restrain conditions (i.e. 19.05 mm for siliceous aggregate made

restrained slabs). EN-1992-1-2 (CEN, 2004)) (Eurocode-2, hereafter EC-2) defines axis distance (concrete cover) and minimum dimensions of RC members for required fire resistance (i.e. for 120 minutes of fire resistance of columns and for mechanical reinforcement ratio (w) of 0.5 and axial load level (n) of 0.5, minimum dimension of the cross-section is 450 mm and minimum axis distance is 50 mm. Axis distance is defined depending on the width for beams. For example, for 120 minutes of fire resistance, axis distance shall be at least 35 mm in case the width of the continuous beam is 300 mm. Minimum concrete cover for slabs is given considering the thickness and type of the slabs (one-way or two-way slabs). For 120 minutes of fire resistance, minimum slab thickness shall be 120 mm and for a two-way slab minimum axis distance shall be 20 mm. It should be noted that for all codes investigated here, concrete cover is measured from concrete surface to surface of longitudinal reinforcement. As seen in Table 1.1, although given values are similar for slabs, EC-2 gives the most conservative values for other types of structural members. For columns, ACI 216.1-97 and EC-2 give similar values whilst TFR demands relatively thinner concrete cover. It is worth to note that columns are generally major lateral load carrying members in frame buildings under lateral loading. Therefore, when the post-fire seismic behavior of RC buildings is considered, TFR cover requirement seems to be less conservative in comparison with ACI 216.1-97 and EC-2.

Table 1.1 : Minimum concrete cover for 2 hours of fire resistance.

	Minimum concrete cover (mm)		
	ACI 216.1	EC-2	TFR
Slab	19.05 (a)	20	20
Beam	19.05 (b)	35 (c)	25
Column	50.8	50 (d)	35

(a) for unrestrained slabs, cover shall be larger than 25.4 mm
(b) for unrestrained beams with smaller width than 127 mm, cover shall be larger than 31.75 mm
(c) for beams with a width of 500 mm, cover shall be larger than 30 mm
(d) given for columns with minimum dimension of 500 mm, w and n are 0.5

1.3 Behavior under Elevated Temperatures

Deterioration in mechanical properties of RC members under elevated temperatures has been one of the major concerns for structural engineers since the fire resistance of the members should be considered in design. As concrete is a less combustible and a good insulating material possessing a low thermal diffusivity when compared to steel, RC structures are known as less sensitive to heat exposure with respect to steel

structures. However, there are two problems of concrete in fire mainly i) deterioration in mechanical properties as temperature rises, and ii) explosive spalling, which results in loss of material, reduction in section size and exposure of the reinforcing steel to excessive temperatures (Khoury, 2000). Under elevated temperatures, concrete mechanical properties such as compressive and flexural strengths, modulus of elasticity and volume stability are significantly affected (Arioz, 2007; Netinger et.al., 2011). If the temperature exceeds 100 °C, water in concrete evaporates causing a pressure within the concrete and thus stimulating spalling. Chemically bound water is initiate to be released from hydrated calcium silicate above 150 °C and reaches to a peak at 270 °C. After 300 °C, micro cracks occur. At about 400 °C, the calcium hydroxide in the cement begins to dehydrate, generating more water vapor. This dehydration of the cement brings a significant reduction in the physical strength of the material crystals of calcium hydroxide which decompose with the highest intensity at about 535 °C. Finally, at 800 °C, concrete can be crumbled to gravel where above 1150 °C it melts and the cement paste turns into glass phase (Khoury, 2000). The critical temperatures for significant strength reduction depend strongly on aggregate type. Quartz-based aggregates increase in volume at about 575 °C, whilst limestone aggregates will begin to decompose at about 800 °C. This volume increase reduces the compressive strength of the material for approximate values of at 650 °C for sand light-weight concrete, 660 °C for carbonate, and 430 °C for siliceous (Hertz, 2005). Similar results were also reported in the study of Rangan and Warner (2006). According to this study, concrete resistance to heat is governed by the type of aggregate used: while siliceous aggregates decompose at temperature slightly above 500 ˚C, those of carbonic composition decompose at considerably higher temperatures. As a function of the degree of heat exposure and based on the physical and chemical changes summarized above, a strength reduction is expected in concrete of RC members. ACI 216.1-97 and EC-2 give values for the change in the characteristic compressive strength of concrete, to be used with the simplified cross-section calculation methods (Figure 1.1). As seen in this figure, both codes give compressive strength as percentage of initial strength and report that when compared to calcareous, siliceous concrete is more sensitive to heat exposure. EC-2 curves recommend no compressive strength loss up to 100 °C and the compressive strength loss at 700 °C is about 70% for siliceous concrete and 60% for calcareous, respectively. On the other hand, ACI curves demonstrate that there is no loss in compressive strength until approximately 400°C

and 600 °C, respectively, both for siliceous and calcareous concrete. The trend for reduction in strength given by the codes is similar for siliceous concrete. However, for calcareous concrete at about 700 °C, EC-2 gives a reduction of 60% of undamaged case while ACI 216.1-97 recommends only 10%. This remarkable difference can be based on the fact that behavior under elevated temperatures is related to the mix proportion, aggregate and cement type, loading and restrain conditions etc. On the other hand, as shown in Figure 1.2, no changes in yield strength of steel reinforcement is expected under temperatures up to 400 °C according to EC-2 while the yield strength is reduced to about 20% of the initial value (80% loss in yield strength) at a temperature of 700 °C. ACI 216.1-97 recommends similar trend in yield strength reduction. However, ACI 216.1-97 reports a strength increase of about 10% at a temperature of 200 °C and decrease of 10% at temperature of 400 °C unlike given in EC-2.

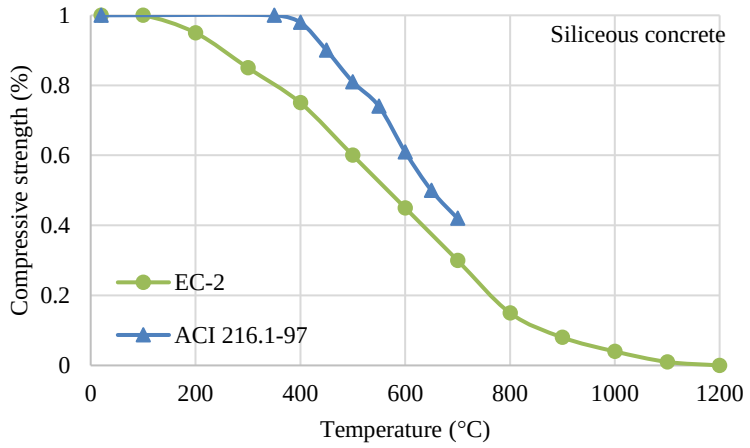

a)

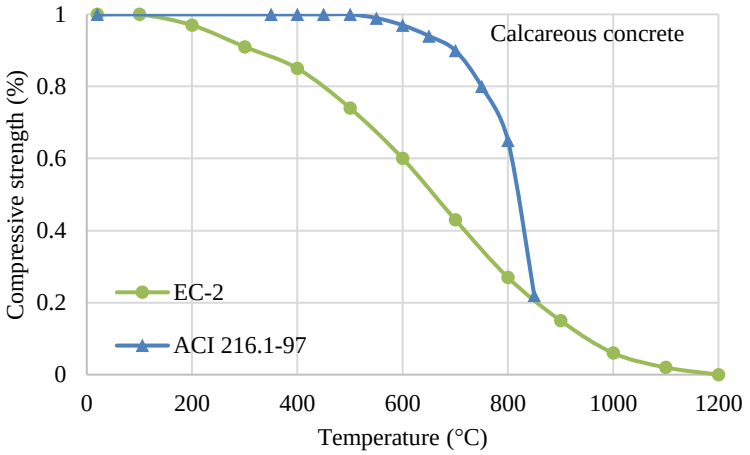

b)

Figure 1.1 : Compressive strength of concrete made of a) siliceous aggregate and b) calcareous concrete at high temperatures.

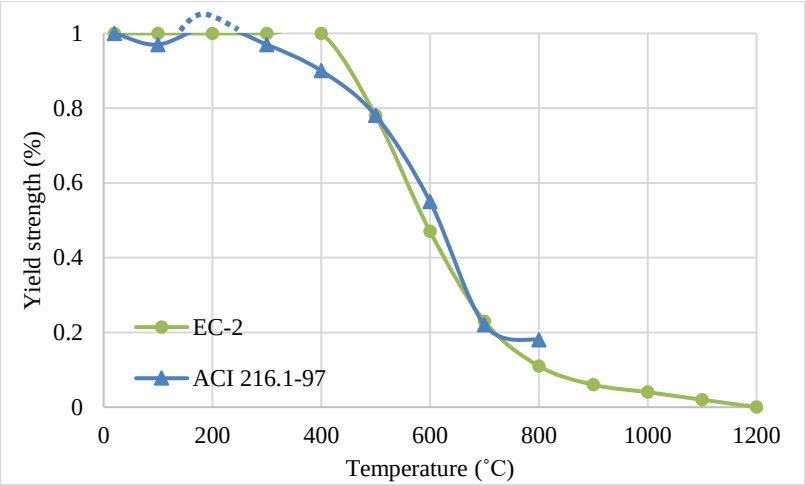

Figure 1.2 : Yield strength of reinforcement steel at high temperatures.

It should be noted that the post-cooling strength gain for concrete and steel reinforcement is not considered in the values given in Figures (1.1 and 1.2), and the issue of strength gain after cooling is discussed in the following section.

1.4 Behavior after Cooling

When compared to the behavior under elevated temperatures, RC members behave differently after cooling (Mohamedbhai, 1953; Harada et al., 1972; Papayianni and Valiasis, 1991; Poon et al., 2001; Chen et al., 2009; Gernay, 2012). Post-cooling behavior can be separated into two stages. At the first stage after cooling to ambient temperatures, it is observed that the strength of concrete may be further reduced from its strength under high temperatures until a period of time because of continuing disintegration of the microstructure in concrete. This is shown as one reason that a more conservative strength reduction factor to assess the residual strength of the concrete is given in Concrete Society (2008) report (hereafter CS-68). The first stage of post-fire cooling period is reported as about 1 month from the beginning of cooling by Harada et al. (1972) and Papayianni and Valiasis (1991). These researches reported that the reduction in compressive strength of concrete continues during 30 days after fire exposure. Because of the reaction between the concrete and moisture in the air (needed for re-hydration of cement), after 30 days, recovery in compressive strength begins referring to the second stage of cooling period.

It should be noted that there is a great variation in the residual strength of concrete after cooling depending on the maximum temperature attained, duration of heating

exposure, mix proportions, aggregates, conditions of loading during heating and stress level (Concrete Society, 2008). Although EC-2 curves consider the loss of strength at the first stage of cooling, it neglects the second stage of the cooling in which a strength gain is expected. Furthermore, since the effects of creep are not explicitly considered in EC-2 curves as well as other investigated codes, previous researches (Franssen, 2004; Gernay and Franssen, 2010) report that the EC-2 curves are not valid for structural assessment for the cooling phase since the irreversibility of transient creep is not considered. The EC-2 model with recommended value of the peak stress strain leads to overestimated elongations (i.e. approximately 50% larger values with respect to the test results), because of a highly underestimated transient creep strain (Gernay and Franssen, 2010). CS-68 recommends a curve for residual compressive strength reduction which is valid for the cooling phase considering the poor behavior after being exposed to temperatures above 300 ˚C unlike 500 °C isotherm approach given in EC-2 in which the design methodology discounts the strength of concrete exposed to temperatures higher than 500°C. Therefore, it can be concluded that CS-68 approach is more conservative than the one according to EC-2 (Figure 1.3). It should be noted that due to the variety of residual compressive strength depending on the aggregate type and loading conditions, only the values for the siliceous concrete are shown in Figure 1.3 for comparison. Similarly, CS-68 recommends a curve for yield strength of steel reinforcement in terms of post-fire strength reduction (Figure 1.4). According to fib bulletin No.46 (2008), the concrete incorporating siliceous aggregate resulted with a marginally-lower residual strength, compared to the calcareous aggregate after cooling. Siliceous aggregates (like basalt and quartzite), make the concrete more temperature-sensitive than calcareous aggregates (like carbonate and sandstone, the latter being partly siliceous). Fib bulletin No.46 also reports that a compressive load applied during heating and cooling, may increase the residual compressive strength by 20-40%. Keeping this in mind, ACI 216.1 (1997) gives the relationship between reduction in compressive strength and temperature for varying aggregate (siliceous or carbonate) and loading cases. According to ACI 216.1 (1997), compressive behavior of concrete under high temperature is better than the cooled one since the loss of humidity still continues for a period after cooling as defined in previous section (first stage of cooling). Bazant and Kaplan (1996) reports results of an experimental work under the temperatures 200, 400, 600 and 800 °C and demonstrates that residual compressive strength (after cooling) for these temperatures are resulted with strength

reductions as 70, 60, 40 and 25% of their initial values (Figure 1.3). It should be noted that, concrete that is exposed to an elevated temperature up to 500 ˚C, recovers 90% of its original strength in one year (second stage of cooling) (Lie, 1992). Cooling will often restore the material to its original state for temperatures up to 450 °C for cold work steel reinforcement and 600 °C for hot rolled steel reinforcement (Lie, 1992; Concrete Society, 2008). Above these temperatures, a simple approach is suggested by CIB (Schneider and Nagela, 1990) in which for every 100 °C increase in temperature, 7.5% of the yield strength is reduced (Figure 1.4). On the other hand, Fletcher et al. (2007) recommended to reduce the load bearing capacity of steel reinforcement about 20% of its design value when exposed to temperatures of the order of 700 °C as similarly reported by CS-68. Felicetti and Meda (2005) presented an experimental work that has also been considered by FIB bulletin No. 46 (2008) and showed that the deformed bars exhibited a sizeable decay above 550°C with a loss of 45% in terms of yield strength after being heated to 850°C (Figure 1.4). This study shows that CIB approach (Schneider and Nagela, 1990) on reducing yield strength is unsafe when compared to experimental findings.

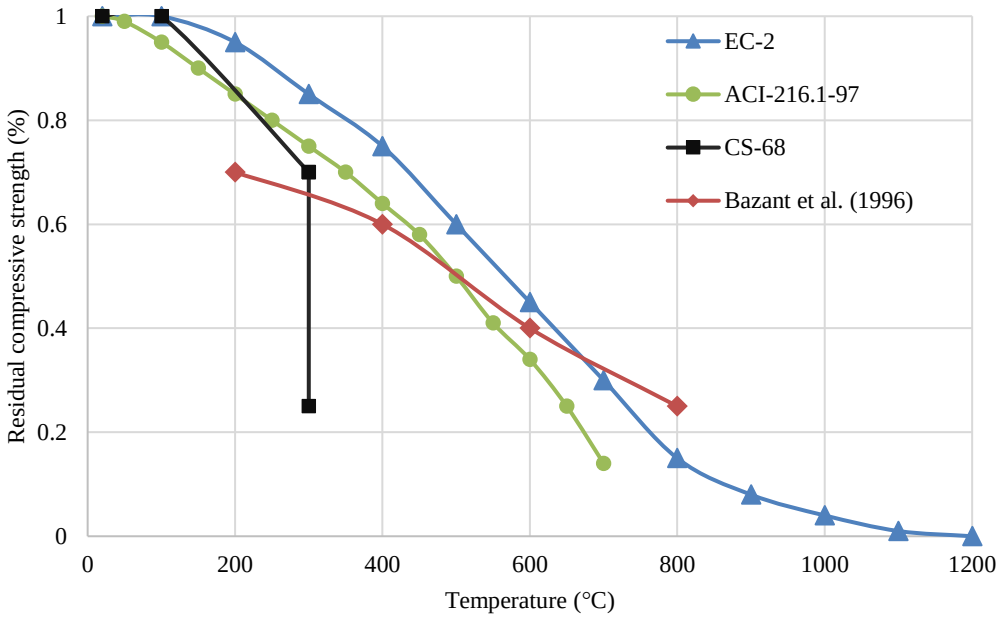

Figure 1.3 : Residual compressive strength of concrete after cooling.

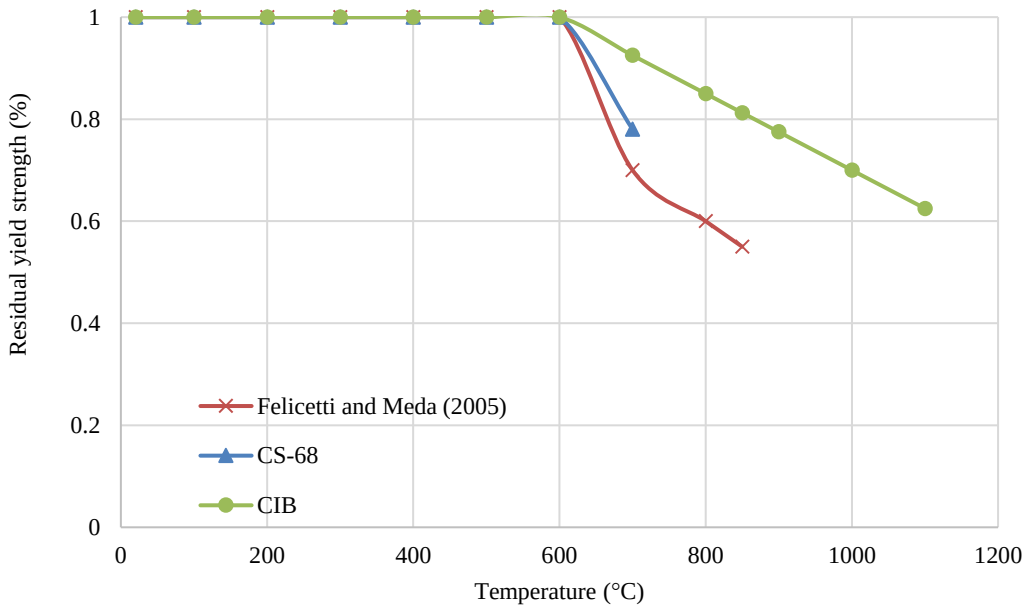

Figure 1.4 : Residual yield strength of reinforcement steel after cooling.

2. EFFECT OF FIRE DAMAGE ON SEISMIC BEHAVIOR OF CAST-IN-PLACE REINFORCED CONCRETE COLUMNS

2.1 Abstract

This paper presents the results of an experimental study that was conducted to investigate the post-fire seismic behavior of reinforced concrete columns. Five full-scale, flexure-critical code-complying (e.g. ACI 318-19) cast-in-place reinforced concrete columns were tested to failure under constant axial load and reversed cyclic lateral displacements after being exposed to an ISO-834 standard fire for 30, 60 or 90 minutes. Other than the effects of the duration of the fire exposure, the effects of thickness of concrete cover (25 and 40 mm) on structural performance was also investigated for the short fire exposure duration (30 minutes). The responses of the columns were analyzed in terms of lateral load-displacement relationships, ductility, stiffness, energy dissipation capacities, and residual displacements. The test results indicated that fire exposure reduced the lateral load capacity of the columns whereas the deformability capabilities were found to be satisfactory in terms of structural response. It was also observed that the thickness of the concrete cover had only a slight influence on the post-fire seismic behavior of the columns. Furthermore, a numerical study was conducted to predict the load-displacement response of the fire exposed columns. The comparison of the experimentally and numerically obtained load-displacement relationships indicated that the principles of structural mechanics usually applied to conventional columns are also valid for the columns exposed to fire.

2.2 Introduction

According to world fire statistics, about 1 million deaths were caused by fires between 1993 and 2014, and approximately 40% of all fires around the world originated from structures (Brushlinsky et al., 2016).

This chapter is adopted from the journal paper: Demir, U., Goksu, C., Unal, G., Green, M.F. and Ilki, A. (2020). Effect of fire damage on seismic behavior of cast-in-place reinforced concrete columns. ASCE Journal of Structural Engineering. DOI: 10.1061/(ASCE)ST.1943- 541X.0002794.

For the majority of the fires in reinforced concrete structures, structural damage was observed due to the deterioration of the materials, such as concrete and steel reinforcement. However, traditional design guidelines cannot provide any reliable estimate for the performance of the structures after a fire event, and therefore, the level of safety against the risk of limit states (i.e. collapse) is simply unknown (Usmani, 2008). Furthermore, probable future earthquakes may cause unanticipated strength and stiffness degradation to these types of fire-damaged structures, which may be critical in terms of lateral dynamic instability in earthquake prone areas. This instability may be manifested in reinforced concrete structures as side-sway collapse caused by loss of lateral-force-resisting capacity or substantial increases in peak displacement demands (FEMA, 2009). In other respects, reinforced concrete columns form the main load bearing component of a reinforced concrete structure, and therefore, provision of appropriate fire safety measures is one of the major safety requirements in design. Furthermore, protecting columns from losing the load-carrying capacity is the most crucial part in the ductility design of reinforced concrete frame structures to withstand seismic actions.

It should be highlighted that the post-fire behavior of the reinforced concrete columns is of vital importance for protecting fire damaged structures against future earthquakes and the sequential seismic damage. However, most existing studies considered the behavior after cooling under only service loads combined with uniaxial/biaxial bending (Lie et al., 1986; Jau and Huang, 2008; Chen et al., 2009), whereas the research on the seismic performance of fire damaged reinforced concrete columns has not been extensive even though it is the major concern in terms of structural seismic performance assessment. Studies conducted by Yaqub and Bailey (2012) and Bailey and Yaqub (2012) included seismic retrofitting of shear-critical reinforced concrete columns non-complying with current design codes. Benichou et al. (2013) investigated the impact of fire on seismic resistance of fiber reinforced polymer strengthened reinforced concrete columns, and Mostafaei (2013) implemented hybrid fire testing principles to consider one high strength concrete column under monotonic lateral loading after exposure to fire. Li et al. (2019a and 2019b) investigated the seismic performance of concrete-filled double-skin steel tubes after exposure to fire. None of these studies considered the assessment of post-fire seismic behavior of flexure-critical, conventional reinforced concrete columns.

Hence, the experimental study presented herein specifically aims to systematically investigate the effect of fire damage on the seismic behavior of reinforced concrete columns for the first time. Test parameters include the effects of fire intensity and the thickness of concrete cover on seismic behavior of reinforced concrete columns. In the scope of the current study, five full-scale reinforced concrete columns were designed and constructed in compliance with major design codes. The columns, except the reference one, were exposed to the ISO-834 standard fire (ISO, 1999) for 30, 60 or 90 minutes, and then cooled in air. All columns were then subjected to constant axial loads representing vertical loads in mid-rise reinforced concrete structures combined with cyclically reversing lateral displacements simulating seismic loading. The responses of the columns were analyzed in terms of lateral load-displacement relationships, ductility, stiffness, energy dissipation capacities, and residual displacements. In addition, two columns were tested to examine the effect of concrete cover on residual seismic behavior. Finally, the experimentally obtained lateral load-displacement relationships were compared with a prediction model based on the basic principles of structural mechanics to investigate the model's applicability in fire damaged columns.

2.3 Materials and Methods

2.3.1 Material properties

The concrete mix-proportions of the columns are presented in Table 2.1. The aggregate is mainly calcareous (78%). The slump was approximately 200 mm. The mean unheated concrete compressive strength, obtained based on the tests of cylinder specimens (150 mm × 300 mm) at the age of column testing day (at around the age of 16 months corresponding to the age of 60 days after the fire tests) was 36 MPa. The stress-strain relationships of the specimens not exposed to fire (reference – REF), and the specimens exposed to fire for 30, 60, and 90 minutes (30M, 60M, 90M) are presented in Figure 2.1. It should be noted that two cylinder specimens were tested for each case. As observed in this figure, the average concrete compressive strength of the cylinder specimens (4 MPa) exposed to 90 minutes of fire (the most severe fire) was obtained to be approximately 10% of that of the reference specimen (36 MPa). The peak compressive strain corresponding to the peak compressive strength increased

with an increase in temperature while the compressive strength decreased. In other words, concrete softened with increasing temperatures due to loss of elastic modulus.

Table 2.1 : Concrete mix-proportions.

Material	Weight (kg/m^3)
Cement (CEM 42.5 R)	300
Sand (0-4 mm)	920
No I Aggregate (5-12 mm)	507
No II Aggregate (12-22 mm)	490
Superplasticizer (Sikament-300)	3.6
Water	124

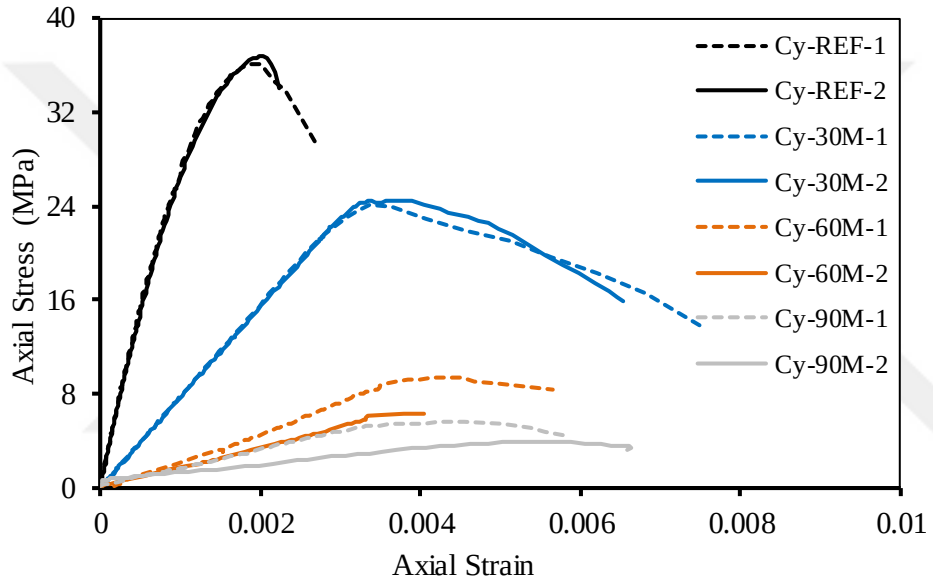

Figure 2.1 : Stress-strain relationships of cylinder specimens.

The mechanical properties of the longitudinal (diameter of the bar, d_b=20 mm) and transverse (d_b=10 mm) reinforcing bars under ambient temperatures, and after post-fire cooling are presented in Table 2.2. For obtaining the mechanical properties of these reinforcing bars, first, 300×300×500 mm reinforced concrete specimens, which had the same cross-section and reinforcing scheme with the full-scale reinforced concrete columns, were cast using the same concrete batch. These specimens were then subjected to the same fire exposure as the full-scale columns. Thereafter, the reinforcing bars were removed after cooling, and then subjected to a uniaxial tension test. As shown in Table 2.2, there is only a minor difference between the mechanical properties of the unheated reinforcing bars and the reinforcing bars exposed to 90 minutes of fire (the most severe fire) since the measured maximum temperatures along the reinforcing bars did not exceed 560 °C in the fire tests. Thus, no residual fire

damage to the reinforcing bars was expected for all fire exposure durations (30, 60 and 90 minutes) as reported by Neves et al. (1996) in these temperature ranges (up to 600 °C).

Table 2.2 : Mechanical properties of reinforcing bars.

Diameter of reinforcing bar (mm)	Fire exposure (minutes)	f_y (MPa)	ε_y	f_{max} (MPa)	ε_{max}	f_u (MPa)	ε_u
20	N.A.	472	0.0023	569	0.0965	525	0.15
10	N.A.	483	0.0025	557	0.0998	525	0.10
20	90	442	0.0024	549	0.0992	516	0.16
10	90	457	0.0024	552	0.0992	522	0.11

N.A.: not available

2.3.2 Test specimens

Five full-scale reinforced concrete columns were constructed with the same geometrical properties and reinforcement detailing as depicted in Figure 2.2. The specimens were cantilevers with cross-sectional dimensions and heights of 300×300 mm and 1500 mm, respectively. The height of the columns represents point of contraflexure (zero moment) of a column with 3000 mm height. Each column incorporated a reinforced concrete foundation block with dimensions of 700×700×500 mm that was connected firmly to the strong floor. Columns were reinforced with four 20 mm diameter longitudinal steel deformed bars placed at the corners. The bars had an average measured yield strength of 461 MPa. Lateral reinforcement (deformed bars) with an average measured yield strength of 472 MPa was provided in the form of 10 mm diameter ties spaced at a 100 mm spacing center-to-center. After casting, columns were cured under ambient temperature and humidity for 14 months before they were transported to the fire facility. For four columns, the clear concrete cover to the longitudinal bars was 40 mm, while one specimen had clear cover of 25 mm. The concrete cover of 40 mm was designed to conform with major building fire codes (ACI 216.1, 1997; EN 1992-1-2, 2004; Turkish Fire Regulation, 2007) while the case of the 25 mm concrete cover was to represent a case of inadequate cover, which may commonly be constructed in practice, particularly, in developing countries (i.e. in Turkey). It should be noted that all the columns complied with the requirements of recent seismic design codes (e.g. ACI-318-19, Eurocode 2) in terms of lateral reinforcement.

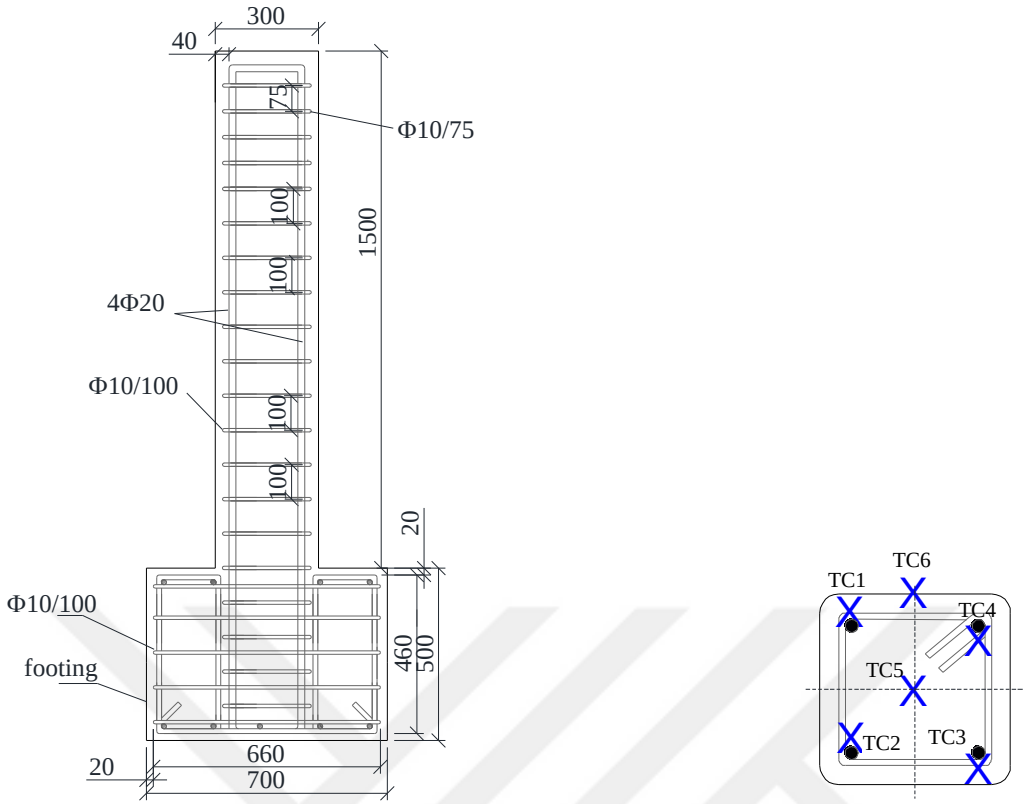

Figure 2.2 : a) elevation, b) plan views of reinforcement and location of thermocouples. Note: Dimensions in mm.

The designation of the columns are as follows: REF (the reference column), 30m-25c, 30m-40c, 60m-40c, 90m-40c. The first term represents the fire exposure duration in minutes (30, 60 or 90), and the second term indicates the thickness of clear concrete cover (25 or 40 mm). The columns were designed to fail in flexure while the foundations were overdesigned to eliminate the possible effect of foundation on the behavior. The shear span to depth ratio (a/h) was 4, which can be assessed as flexure-controlled based on the study by Kuang (2017).

2.3.3 Test furnace

The columns, except the reference one, were exposed to the ISO-834 standard fire for 30, 60 or 90 minutes, on all sides, and along their whole heights. The footings were insulated to protect them from the fire exposure. The fire exposed columns were then cooled in air. The fire tests for each fire exposure duration were executed every other week about 14 months after casting. The tests were conducted at a large-scale multipurpose furnace, which was 3.2 m in depth, 4 m in width and 3 m in height

(Figure 2.3). Heat was provided by eight natural gas burners located within the furnace, positioned on opposite sides containing four burners each. Eight thermocouples were distributed throughout the test chamber to monitor the furnace temperature during the fire tests. Each burner was controlled independently to produce an environment of uniform temperature following the temperature-time curves specified by ISO-834. Six type-K NiCr-Ni thermocouples of 0.91 mm thick were installed at the mid-height cross section in each column for measuring concrete and reinforcing bar temperatures. The locations of the thermocouples in the cross section are shown in Figure 2.2b. The fire tests were executed without any axial loading.

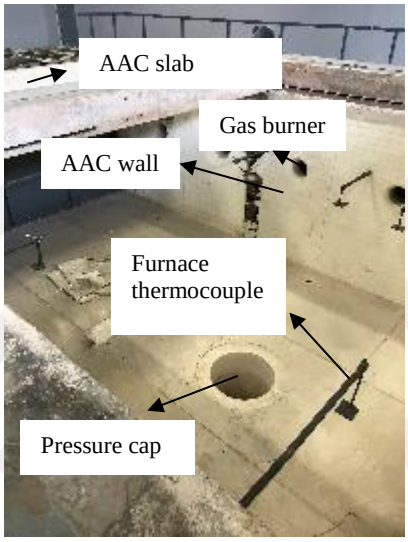

Figure 2.3 : Fire test furnace.

The impact of axial loading in the fire tests is a critical parameter that should be further discussed. Compressive strength tests on concrete after exposing to elevated temperatures demonstrated that the axial loading in fire tests results in an improved concrete residual behavior compared to the unstressed residual tests (Malhotra, 1956; Abrams, 1971; Harada et al., 1972; Papayianni and Valiasis, 1991; ACI 216.1, 1997; fib bulletin-46, 2008). Moreover, presence of a compressive axial load in fire tests increases the fire resistance of RC columns (Salse and Lin, 1976) and neglecting the axial load in the design of RC beams under fire conditions leads to a conservative estimate of the fire resistance (fib bulletin-46, 2008). Therefore, the absence of axial loading in fire tests generally results in a worst-case scenario compared to the presence of axial load which may be beneficial for design concerns and practical applications (Bisby et al., 2011, Yaqub and Bailey, 2012). As a result, the presented test results obtained for columns, which were exposed to fire without axial load can be considered

to represent a worst-case scenario. Nevertheless, it is worth to mention that in unlikely cases where the axial load during the fire test is too high, excessive damage or compression failure may occur in RC structural elements.

2.3.4 Instrumentation, test setup, and loading procedure

The test setup is shown in Figure 2.4. The upper end of the columns was loaded by a hydraulic jack and controlled to provide an axial force of 630 kN corresponding to $0.2f'_cA_g$ (axial load ratio of 0.2) where f'_c is the compressive strength of unheated concrete at the day of seismic test, and A_g is the gross cross-sectional area of the columns. Applied axial load ratio represents common column axial loads in mid-rise reinforced concrete structures. The lateral load was applied at the tip of the columns, 1200 mm above the column-footing interface using an MTS actuator with a capacity of ±250 kN, ±300 mm.

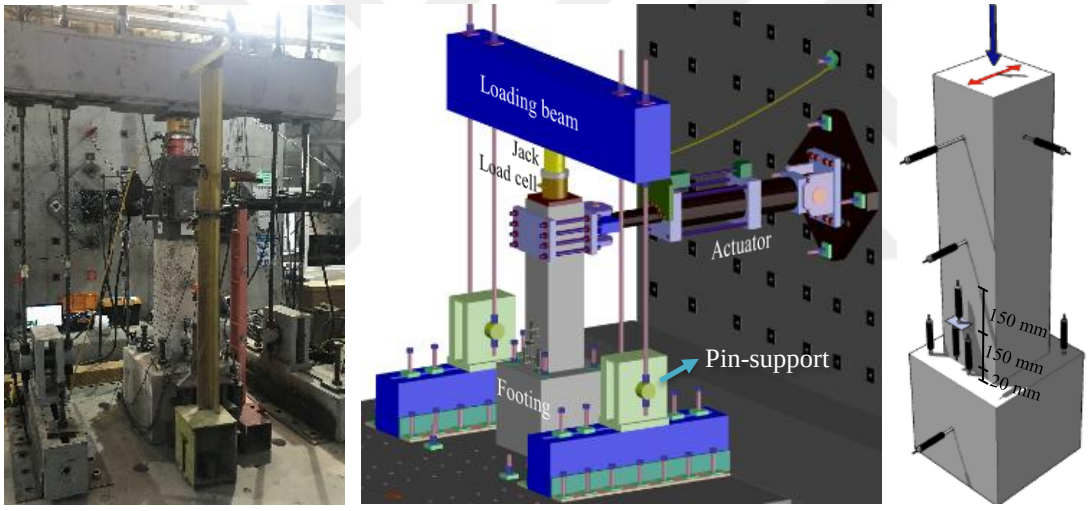

a) b) c)

Figure 2.4 : a), b) test setup, c) locations of LVDTs.

As shown in Figures 2.2c and 2.4c, the instrumentation in the columns included thermocouples and displacement transducers (LVDTs). The instrumentation of the columns consisted of four horizontal and eight vertical LVDTs. Three of horizontal LVDTs were distributed along the height of the column and the footing to measure the in-plane lateral displacements, and one horizontal LVDT was attached at the top of the column to measure the out of plane lateral displacement, which was seen to be negligible. Six of the vertical LVDTs were attached along the potential plastic hinge regions of the columns three for each side in loading direction in different gage lengths (at 0-20 mm, 20-150 mm and 150-300 mm from the column-footing interface) to

measure the variation of vertical displacements, and two LVDTs were fixed to the top of the footing to measure its rotation, which was also seen to be negligible.

A displacement-based lateral loading protocol, shown in Figure 2.5, was applied during the tests based on ACI 374.2R (2013). Reversing lateral displacements were applied to the columns in pushing and pulling cycles to simulate seismic loading. The drift ratio was calculated as the ratio of the lateral displacement to the column height (Δ/l). After a drift ratio of 0.5%, for each target displacement, two cycles of loading were applied.

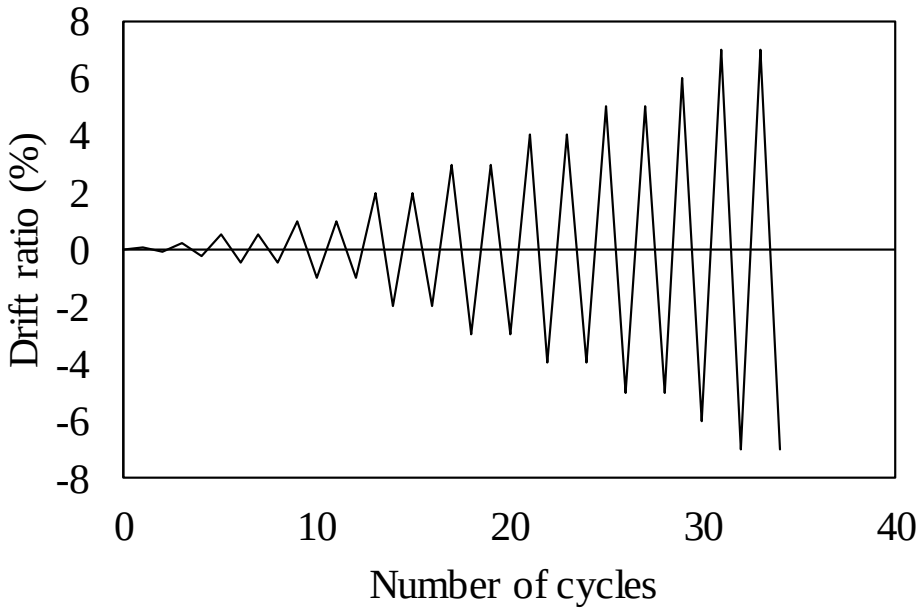

Figure 2.5 : Loading protocol.

2.4 Temperature Distribution of the Columns

Figure 2.6 shows the temperature-time curves in the furnace. Maximum temperatures of 841, 945 and 1005°C were measured for the furnace while average temperatures of 330, 493 and 552°C were measured for reinforcing bars after 30, 60 and 90 minutes of fire exposure, respectively.

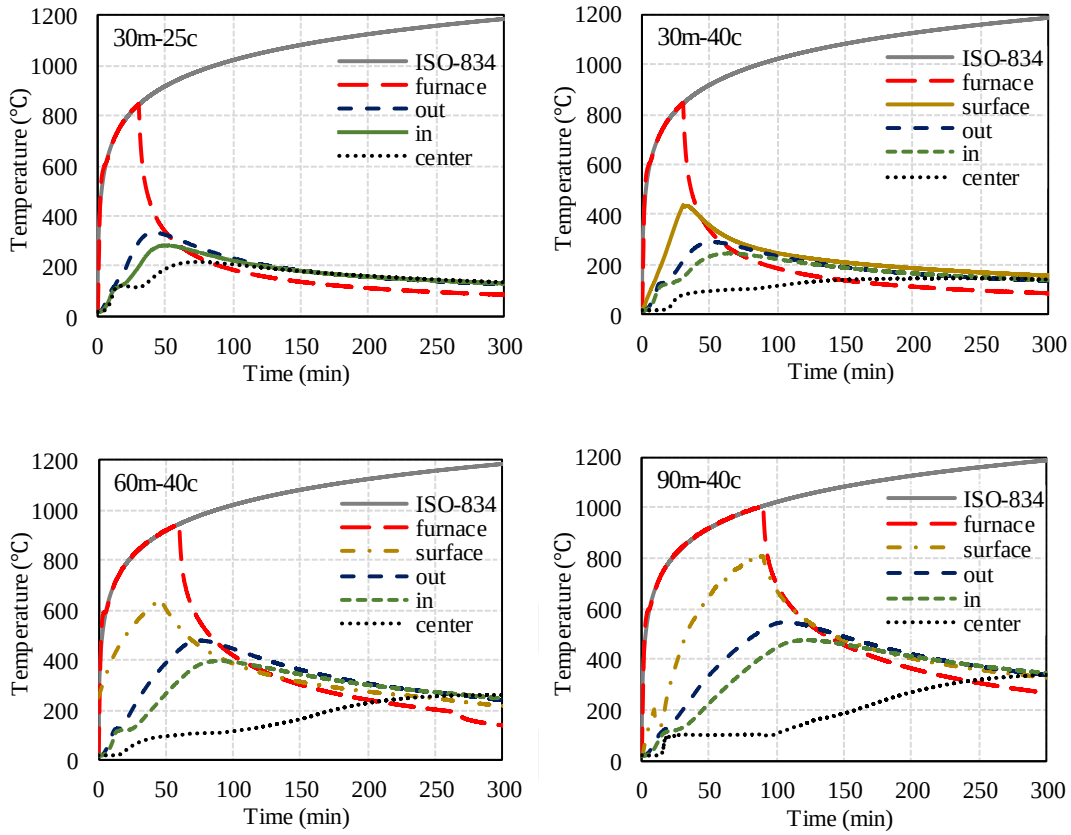

Figure 2.6 : Temperature-time curves of the columns. Note: "surface" temperature is obtained from TC6, "out" temperature is obtained from TC1 and TC3, temperature "in" is obtained from TC2 and TC4, "center" temperature is obtained from TC5. Note 2: Surface temperature of the column 30m-25c could not be measured.

The extent of damage and spalling of the cover concrete of the columns during the fire tests was monitored by making observations through the window ports of the furnace and after the columns were removed from the furnace. Hairline cracking occurred in column 30m-40c. Flaking of concrete was observed on the surface of column 60m-40c while minor spalling occurred in column 90m-40c in the form of small chunks of concrete falling from the surface of the column. As also stated by Raut and Kodur (2011), when the temperature in concrete reaches about 250-300°C, the tensile stresses due to fire-induced pore pressure exceeds the reduced tensile strength of concrete, and at this stage, chunks of concrete fall off from the surface of the column. When the furnace naturally cooled down to room temperature (with a cooling rate around 1, 0.65 and 0.5 °C/min after 30, 60 and 90 minutes of fire, respectively), the columns were taken out of the furnace and stored in the laboratory for 2 months until the time of the seismic tests.

The damages of the columns after fire exposure can be evaluated according to Concrete Society (2008) guideline as shown in Table 2.3. This guideline defines damage classes and corresponding repair requirements for RC columns accounting for the color change, crazing and spalling of concrete, condition of reinforcement and formation of the cracks. As seen in Table 2.3, the damage classes are 1, 2 and 2 for the columns exposed to fire for 30, 60 and 90 minutes, respectively with reference to the guideline. Superficial repair of slight damage is sufficient for the column exposed to 30 minutes of fire, whereas minor structural repair for restoring the damaged parts of the concrete cover is required for the columns exposed to 60 or 90 minutes of fire.

Table 2.3 : Damage classification and repair requirements after fire (Concrete Society, 2008).

Duration of fire (minutes)	Color	Crazing	Damage class	Repair classification	Repair requirements
30	Normal	Slight	1	Superficial	Superficial repair of slight damage not needing fabric reinforcement
60	Yellow/beige	Moderate	2	General	Non-structural or minor structural repair restoring cover to reinforcement where this has been partly lost
90	Yellow/beige	Moderate	2	General	Non-structural or minor structural repair restoring cover to reinforcement where this has been partly lost

Note: Spalling and cracking are minor for all columns. Reinforcing bars are not directly exposed to fire.

The temperature distribution after the fire tests was also calculated using a finite element software program, SAFIR (Franssen and Gernay, 2017) (Figure 2.7), which is used to predict the monotonic lateral load-displacement curves. During these analyses, heat transfer mechanisms were determined through the assumption that heat was distributed through solid structures primarily by conduction, and at the boundary of the structure, heat was exchanged with the environment by convection and radiation. For conduction in the solids, heat exchange was based on a Fourier equation expressed in Cartesian system of coordinates using Eq. (2.1).

$$\frac{\partial}{\partial x}\left[k\frac{\partial T}{\partial x}\right]+\frac{\partial}{\partial y}\left[k\frac{\partial T}{\partial y}\right]+\frac{\partial}{\partial z}\left[k\frac{\partial T}{\partial z}\right]+Q=c\rho\frac{\partial T}{\partial t} \quad (2.1)$$

In this equation, $\{x, y, z\}$ is the vector of Cartesian coordinates (m), T is the temperature (K), k is the thermal conductivity (W/mK), Q is a term that accounts for internal generation of heat (W/m^3), ρ is the specific mass (kg/m^3), c is the specific heat (J/kgK)

and t is time (s). For convection and radiation acting over the boundaries of the structure, heat exchange is determined using Eqs. (2.2 and 2.3).

$$h_c = h(T_g - T_s) \tag{2.2}$$

$$h_r = \sigma \varepsilon {T_s}^4 \tag{2.3}$$

In these equations, h_c is the convective heat flux between gas and solid (W/m²), h is the coefficient of convection (W/m²K), T_g is the temperature of the gas (K), T_s is the temperature at the surface of the solid (K), h_r is the radiative heat flux emitted by a solid (W/m²), σ is the Stefan-Boltzman constant (5.67 × 10-8 W/mK4), ε is the emissivity of the solid (-).

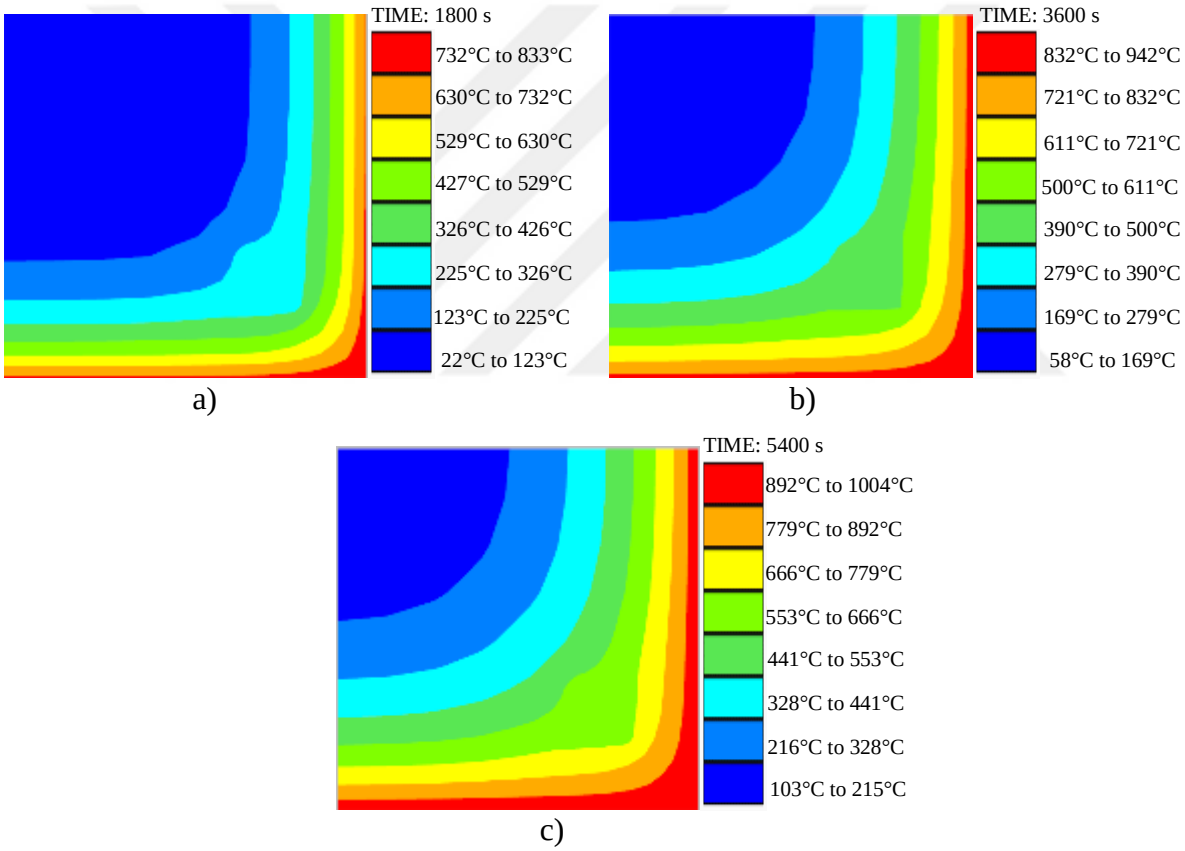

Figure 2.7 : Temperature distributions in SAFIR after a) 30 minutes, b) 60 minutes and c) 90 minutes of fire exposure.

During the thermal analyses, first, the temperatures from two previous time steps, t_{n-1} and t_n, are extrapolated to find a first approximation at a given time $t_n + d_t$ between t_n and t_{n+1}. For the next steps, the next approximations of the temperatures at $t_n + d_t$ are performed until thermal equilibrium is restored. The process continues with extrapolating the temperatures at t_{n+1} from the values at tn and $t_n + d_t$. During the

thermal modelling, the cross-sections of the columns were defined using 144 nodes and 121 solid elements. Calcareous concrete (CALCONC_EN) and steel (STEELEC2_EN) material properties as presented in Eurocodes (EN-1992-1 and 2, 2004) were assigned to the corresponding elements of the cross-section of the columns.

2.5 Experimental Results

2.5.1 Hysteretic load-displacement responses and their envelopes

The hysteretic load-displacement responses of the columns and their envelopes are depicted in Figures (2.8 and 2.9), respectively. These curves, which reflect both the lateral load capacity and ductility variations, can be used to compare the development of the seismic capacity of the columns with increasing drift ratios. When developing the envelope curves, only the first cycle of each lateral load-displacement relationship was considered. Important stages such as the first flexural crack, crushing and spalling of concrete cover, and buckling of the reinforcement are symbolically marked on the plots to aid interpretation. All columns were observed to fail in flexure during the cyclically reversing load tests. The peak lateral loads were achieved at a drift ratio of 2% for all columns. In-cycle strength degradation resulting from repetitive cycles for each displacement level was similar (less than 5%) for all columns irrespective of the duration of fire up to buckling of the reinforcing bars.

Table 2.4 shows the lateral load capacities and displacement ductility factors of the columns. The maximum lateral load values in this table are the average of pushing and pulling directions. As seen in this table, the peak lateral loads for the fire exposed columns 30m-25c, 30m-40c, 60m-40c and 90m-40c are 10, 13, 19 and 19% lower than that of the column REF, respectively. Since the strength recovery of reinforcing bars after cooling is assumed to restore the material strength to its original state (Table 2.2), the rate of decrease in lateral load capacities is driven primarily by the deterioration in concrete properties. Since the residual stress-strain characteristics of the concrete of the columns 60m-40c and 90m-40c were influenced in a similar manner, these columns exhibited similar reductions in lateral load capacity (Figures 2.1, 2.8 and 2.9).

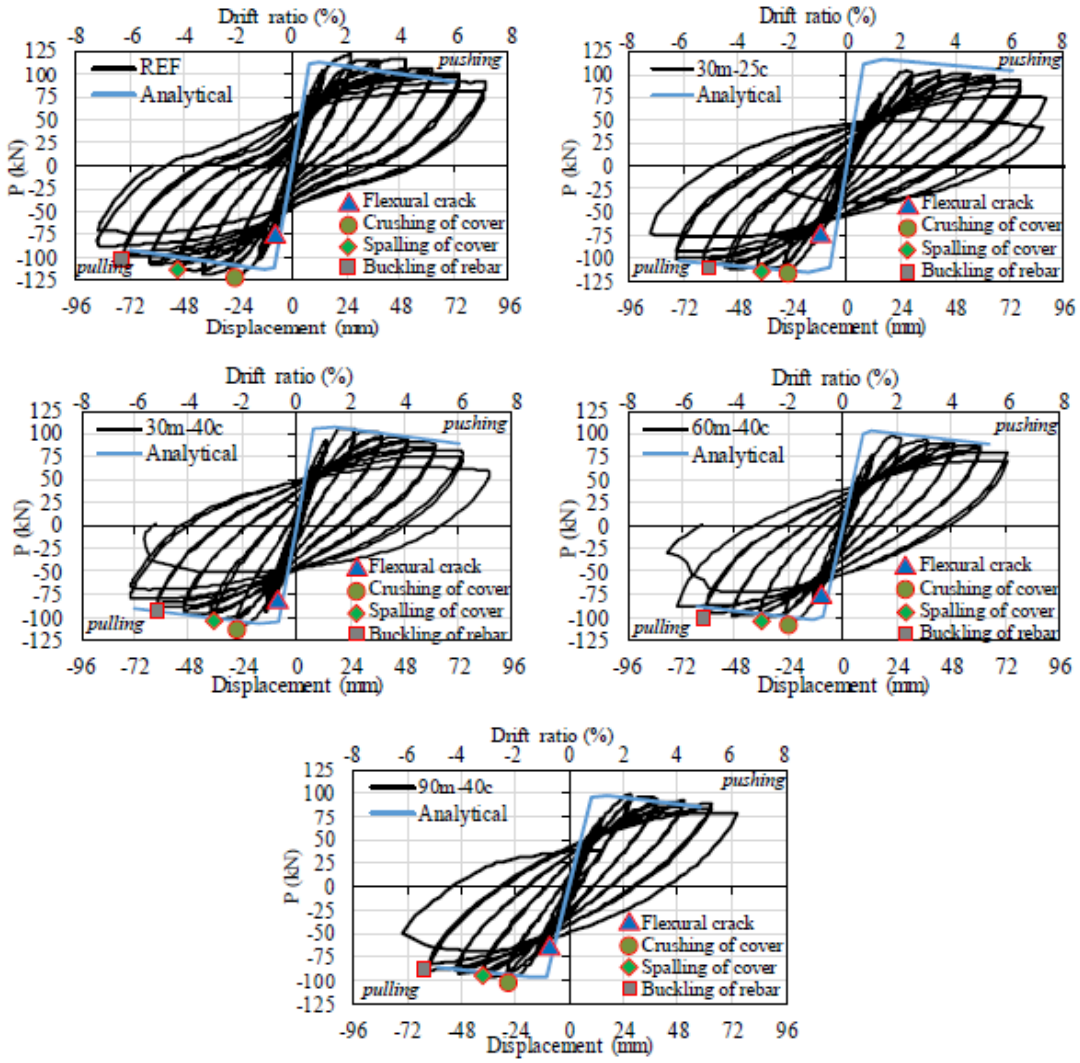

Figure 2.8 : Experimental and numerical lateral load-displacement relationships.

To compare the hysteretic responses of the columns subjected to the same fire exposure duration (the columns 30m-25c and 30m-40c) with different concrete cover thicknesses (25 and 40 mm), the lateral load (P) is normalized with the numerically obtained lateral load capacities (P_0) of their reference counterparts (117.7 kN for the column 30m-25c, 113.4 kN for the column 30m-40c) in order to eliminate the effect of higher bending moment capacity, and thereby, higher lateral load capacity of the column 30m-25c because of its larger effective depth (Figure 2.9). As shown in Figure 2.9, while the concrete cover thickness does not have a significant effect on lateral load capacity (10% and 13% reduction in lateral load capacities of the columns 30m-25c and 30m-40c, respectively, compared to the column REF), the stiffness of the column increases as the thickness of the concrete cover decreases because of the larger effective depth of the column with the smaller concrete cover thickness.

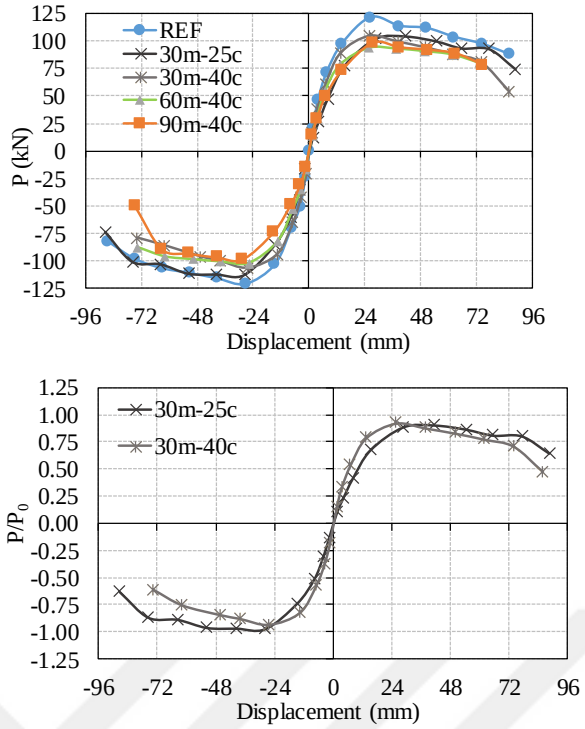

Figure 2.9 : Envelopes of lateral load-displacement relationships for the columns.

Table 2.4 : Lateral load capacities and displacement ductility factors of the columns.

	REF	30m-25c	30m-40c	60m-40c	90m-40c
Experimentally obtained P_{max} (kN)	121.1	108.8	105.6	98.0	98.3
Numerically obtained P_{max} (kN)	113.4	115.9	107.7	103.6	97.1
Δ_y (mm)	16.6	19.9	14.4	15.7	19.7
Δ_u (mm)	74.0	81.3	65.7	73.8	70.5
μ_Δ	4.5	4.1	4.6	4.7	3.6

For better comparison of the column performances in terms of sustaining their ductility, displacement ductility factors (μ_Δ), which were defined as the ratio of the ultimate displacement (Δ_u) to the yield displacement (Δ_y), are calculated. Yielding, ultimate displacements, and corresponding ductility factors of all columns are computed based on the average envelope curve (absolute average of pushing and pulling directions as defined by Memon and Sheikh, 2005) as schematically depicted in Figure 2.10, and listed in Table 2.4. The point on the post peak branch where the lateral strength is 80% of the maximum lateral strength ($P = 0.8P_{max}$) is defined as the failure point, corresponding to Δ_u as recommended by Memon and Sheikh (2005). Additionally, as suggested by Paulay and Priestley (1992), Δ_y is determined by drawing a secant to intersect the lateral load-displacement envelope at 75% of the peak lateral load on ascending portion of the envelope curve. The line is then extended to the

intersection with a horizontal line corresponding to the maximum lateral load, and projected onto the abscissa (Figure 2.10).

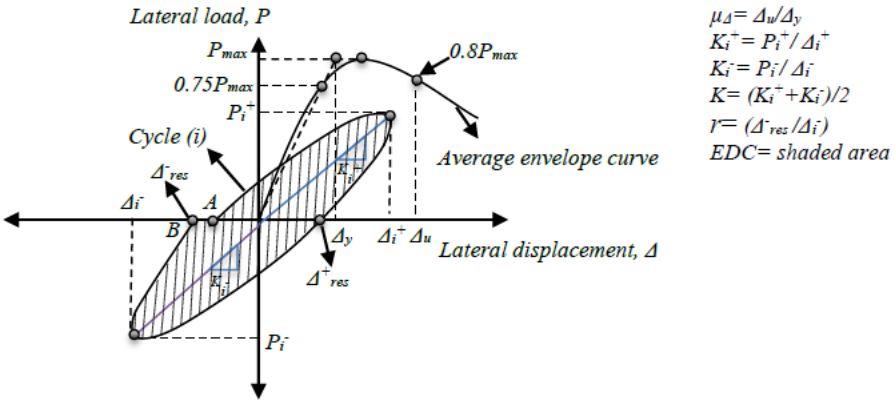

Figure 2.10 : Definition of ductility parameters.

As evident from Table 2.4, for the fire exposed columns complying with the major fire regulations, the ductility of the columns is similar except the column exposed to the severest fire exposure in the test campaign (column 90m-40c). The column 90m-40c exhibited 20% reduction in ductility with respect to the reference column (REF). As observed from this table, the Δ_y of this column is significantly higher than that of the other columns having concrete cover of 40 mm. Stiffness degradation of the column 90m-40c induced from fire exposure, which will be discussed in the following section in detail, can be accounted for higher Δ_y. Furthermore, the increase in Δ_y of the column 30m-25c is also noticeable from Table 2.4 and Figures (2.8 and 2.9). This can be attributed to the axial deformation of the longitudinal reinforcing bars which creates more considerable compressive strains on the concrete cover of the column 30m-25c because of its lower cover thickness. These compressive strains cause a reduction in tensile capacity of concrete in transverse direction, and finally deteriorates the concrete cover (Dhakal and Maekawa, 2002). Nevertheless, the displacement ductility factors higher than 3.5 correspond to a fully ductile response that can reasonably be achieved at carefully identified and detailed inelastic regions (Paulay and Priestley 1992, UBC 1997). When this value (3.5) is compared to the values given in Table 2.4, post-fire ductility factors of all columns appear satisfactory in terms of structural response.

The appearance of the columns at a drift ratio of 4% (prior to buckling of reinforcing bars) are shown in Figure 2.11. The damage progression of the columns throughout the test is tabulated in Table 2.5. First, fine bending cracks were observed at the potential plastic hinge zone at around 0.5% drift ratio for all columns. As the lateral

displacement increased, the flexural cracks extended and widened. Upon yielding of the longitudinal reinforcing bars at around 2% drift ratio, the peak load was achieved, and the cracks developed and extended rapidly. The crushing of cover concrete initiated in the hinging zone at a drift ratio of approximately 2% for all columns. Eventually, the crushed cover concrete was observed to spall off at a drift ratio of 4% for the reference column and at 3% for its fire exposed counterparts. For the columns exposed to fire, outward lateral pressures exerted on the bar from the bulging concrete core accelerated buckling compared to the reference column (Table 2.5). It is noteworthy that the damage was observed to be distributed over a length longer than the potential plastic hinge zone, in other words, the hinging zone was observed to be elongated with an increase in fire duration (Figures 2.11 and 2.12). This behavior can be attributed to a loss of concrete compressive strength, which in turn causes an increase in axial load ratio (applied axial load/axial load capacity).

a) b) c)

d) e)

Figure 2.11 : Appearance of the columns (at drift ratio of 4%) a) REF, b) 30m-25c, c) 30m-40c, d) 60m-40c and e) 90m-40c.

Table 2.5 : Drift ratios (%) for different damage states.

Failure mechanisms	REF	30m-25c	30m-40c	60m-40c	90m-40c
First flexural crack	0.5	0.5	0.5	0.5	0.5
Crushing of concrete cover	2	2	2	2	2
Spalling of concrete cover	4	3	3	3	3
Buckling of reinforcing bar	6	5	5	5	5

In the present study, axial load capacities of the fire exposed columns, which were evaluated based on the actual compressive strengths, decreased about 10% to 50% of their reference value depending on the duration of the fire. In previous research, it has also been reported that the axial load ratio has an important influence on the plastic hinge length of reinforced concrete columns, and particularly, after exceeding 20% of axial load capacity of the column, the plastic hinge length elongates with an increase in the axial load ratio (Bae and Bayrak, 2008). When the tendency towards cracking, and the development of plastic hinging zone for the column exposed to the severest fire exposure (the column 90m-40c) and its reference counterpart (the column REF) are compared, the crack lengths and widths of the column 90m-40c are also observed to be lower than that of the reference column because of the relatively higher axial load ratio in 90m-40c. This in turn caused a significant increase in the compression strains of concrete for the reference column which were greater than that for column 90m-40c. Thereby, the neutral axis depth (z) in column 90m-40c extended more substantially, and the area of the concrete required to be balanced by the area of the reinforcement increased while the strains in reinforcing bars decreased with fire exposure. As a consequence, fixed-end rotation occurred in the reference column resulting in longer crack lengths and larger crack widths than those of column 90m-40c for both pushing and pulling directions. This brought about concentration of the curvatures along a shorter plastic hinging zone for the reference column. On the other hand, curvatures were distributed along a comparatively longer hinging zone for the fire exposed columns because of the shorter crack length at identical drifts as shown in Figure 2.12.

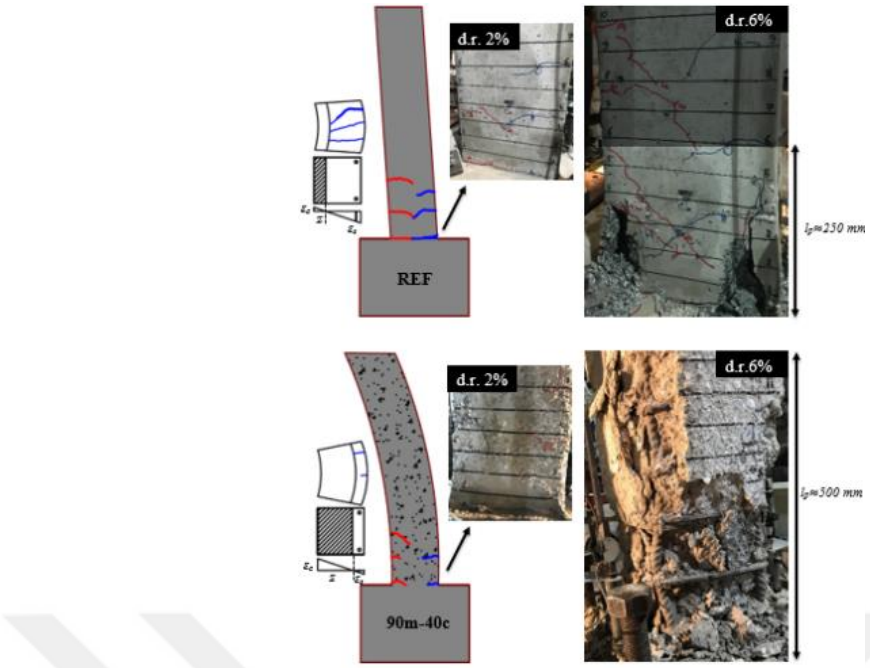

Figure 2.12 : Plastic hinging zone for the columns.

This observation was also examined through the compression strains of the concrete cover (ε_c) and confined concrete (ε_{cc}) extracted from the fiber analysis at the onset of yielding of the reinforcing bars (ε_y=0.0023). The numerically obtained strains are presented in Table 2.6. As shown in this table, the compression strains of the concrete cover and confined concrete increase as the fire duration increases. It is noteworthy that, while yielding of reinforcing bar is followed by crushing of concrete cover for the column not exposed to fire, for the 30-minute fire exposed columns (30m-25c and 30m-40c) yielding of the reinforcing bars and crushing of the concrete cover occurred simultaneously. For the columns exposed to more severe fire exposure (60m-40c and 90m-40c), crushing of concrete cover initiated before yielding of the reinforcing bars.

Table 2.6 : Numerically obtained compressive strains of confined concrete and concrete cover.

	REF	30m-25c	30m-40c	60m-40c	90m-40c
ε_c	0.0018	0.0020	0.0020	0.0026	0.0031
ε_{cc}	0.0010	0.0012	0.0011	0.0016	0.0020

One of the most basic tools to define limit state curvatures is the M-ϕ analysis of reinforced concrete sections. The experimentally obtained M-ϕ relationships for the columns at a drift ratio of 4% (at 48 mm displacement) (before buckling of reinforcing bars) are presented in Figure 2.13. The base moment was calculated by multiplying

the lateral load with the shear span of 1200 mm extending between the acting point of the lateral load and the interface of the column-footing, which was then summed to obtain the contribution of the axial load. The curvature distributions of the columns were obtained using LVDTs deployed at different gage lengths over 0-20 mm, 20-150 mm and 150-300 mm above the interface of the column-footing (Figure 2.4c). As depicted in Figure 2.13, the curvature was concentrated mainly over a height of approximately 0-20 mm for the reference columns and 30-minute fire exposed columns. For these columns, maximum curvatures over a 0-20 mm gage length were measured in the order of 0.6 1/m. On the grounds that the curvature values of the columns measured in 300 mm gage lengths above the footing are even smaller, these results are not presented in the figure. However, for columns 60m-40c and 90m-40c, maximum curvature values were in the order of 0.1 1/m, for each gage length. This occurred because the hinging zone was observed to enlarge with an increase in fire duration as previously discussed. Therefore, for columns 60m-40c and 90m-40c, the deformations were distributed over a longer plastic hinging zone (larger than 300 mm), which is outside the measurement zone (Figures 2.4c, 2.11, 2.12).

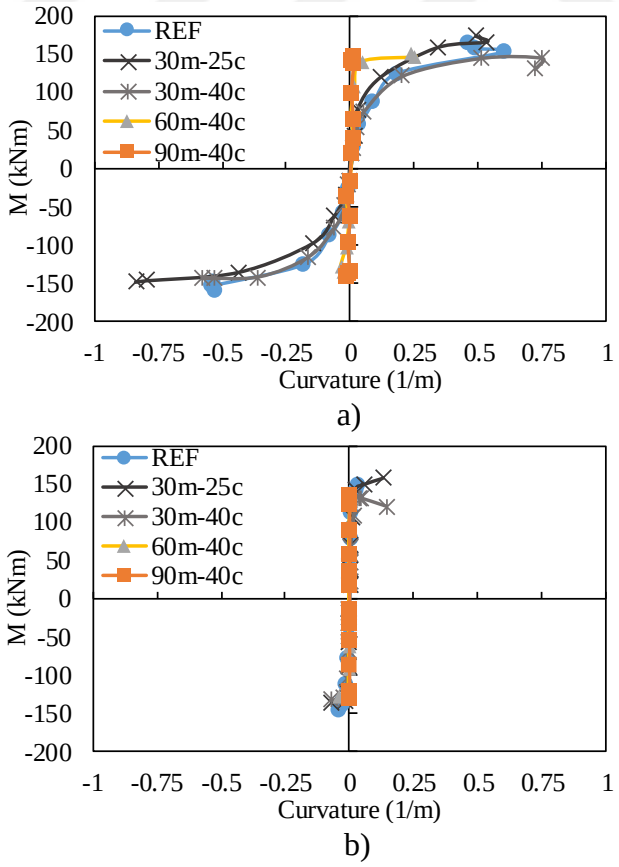

Figure 2.13 : Moment-average curvature relationships over the gage lengths a) 0-20 mm, and b) 20-150 mm.

2.5.2 Stiffness degradation and energy dissipation capacity

Many structural components and systems will exhibit some level of stiffness degradation when subjected to reversed cyclic loading. Particularly, in short-period structures as considered in the presented study, cyclic strength degradation can lead to significant increases in peak displacement demands as well (FEMA P440A, 2009). Fire exposure is a parameter that may potentially exacerbate this trend.

The secant stiffness (*K)* in this study is obtained by dividing the maximum lateral load in the first loop within each cycle by the displacement at the peak of each loading cycle, and pursuing, the average values of the stiffness in pushing (K_i^-) and pulling (K_i^+) directions are considered (Figure 2.10). As shown in Figure 2.14, the cyclic *K* decreases as the fire exposure duration increases as a consequence of the concrete cracking resulted from the loss of tensile strength of concrete and the formation of plastic hinges. It should also be noted that the magnitude of decrease in *K* is greater than the magnitude of the reduction in lateral load capacity. For instance, for the column 90m-40c, the decrease in *K* during the initial stage of loading is around 40% while the reduction in lateral load capacity is 19%. This discrepancy occurs because the behavior under lateral loads is controlled by concrete residual properties up to yielding, whereas after yielding, reinforcement characteristics which have been restored after cooling are more effective for all columns as similarly reported by Ni and Birely (2018). As aforementioned, reinforcement residual properties were not influenced from fire exposure and therefore, despite relatively large degradation in cyclic stiffness in the initial stage of loading, the difference between the stiffness values became comparatively lower after the drift ratio of 2% (around yielding). Column 30m-25c demonstrated relatively lower initial stiffness and stiffness degradation, and this was attributed to the higher yield displacement of this column as discussed previously. These observations can also support the conclusion that beyond the capacity related issues discussed in this paper, peak displacement demands in fire exposed columns are sensitive to Δ_y and will increase because of the reduced stiffness caused by fire.

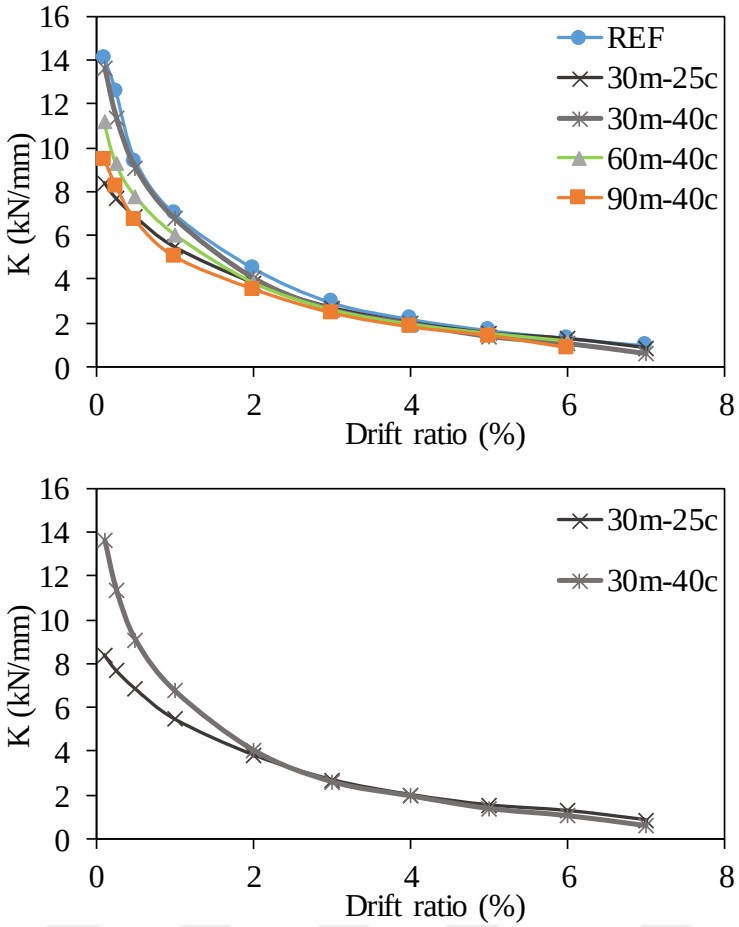

Figure 2.14 : Stiffness degradation of columns.

The energy dissipation capability of a structure has a strong influence on its seismic response. It can be simply defined as the ability to consume seismic energy under lateral loads through plastic deformations. The energy dissipation per each cycle can be evaluated as the area enclosed by the first hysteretic loop of each displacement level and the cumulative energy dissipation capacity (EDC) can be computed through the summation of these areas (shaded area in Figure 2.10). The EDC due to cyclic loading is presented in Figure 2.15 as a function of drift ratio. Total dissipated energy mainly consists of two components as follows: (i) dissipated energy during the formation of new cracks and the friction of existing crack surfaces, and (ii) dissipation of energy through reinforcing bars (Li et al., 2019). As shown in this figure, in the earlier stages of the loading (up to 1% drift ratio), the lateral loads were not high enough to cause considerable damage (e.g. cracks) and therefore, the EDC of the columns was almost negligible. The effect of fire exposure duration on the energy dissipation is quite pronounced particularly after 2% drift ratio (around yielding). After this drift ratio, the EDC of the reference column is higher than that of the columns exposed to fire, and

as the fire exposure duration increases, the EDC of the columns decreases. In particular, for the fire exposed columns, cracks that occurred after the fire tests widened and the number of new cracks were limited up to yielding. After yielding, new cracks occurred, the energy dissipation increased in an accelerated way, and most of the energy was consumed by the inelastic deformation of the columns including the formation of new cracks and the yielding of reinforcing bars. It should be noted that concrete cover did not have a significant effect on the EDC.

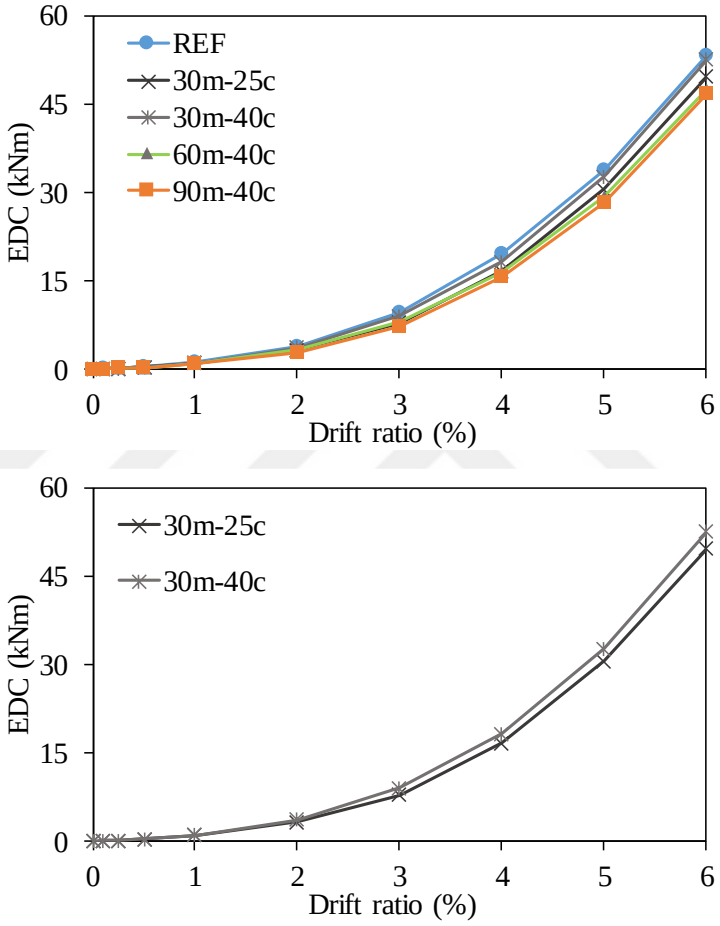

Figure 2.15 : Cumulative energy dissipation capacities of columns.

2.5.3 Residual plastic deformation

The reinforced concrete columns are expected to exhibit ductile behavior and undergo large inelastic deformations under severe earthquakes. However, columns that exhibit high ductility demands tend to retain large residual displacements after earthquakes. These residual displacements are one of the most important measures in terms of post-earthquake functionality and feasibility of repairing fire-damaged structures. It is even arguable that residual displacements are ultimately more important than maximum

displacements, given the difficulty of straightening a bent building after an earthquake (Priestley, 1993). However, the study of the residual displacements of reinforced concrete columns after fire exposure has received no attention in the literature. Therefore, in this paper, attention is paid to report the level of post-earthquake residual displacements for fire exposed reinforced concrete columns. The residual plastic displacement ratios (r) of the columns are obtained by dividing the residual lateral plastic displacements after unloading, when the applied lateral load is zero (Δ_{res}) to the specified peak displacement for each drift ratio (Δ_{un}) in pushing direction which is illustrated in Figure 2.10, and presented in Figure 2.16. As shown from Figures (2.8 and 2.16), the r values of the columns exposed to fire obviously increased as an outcome of the fire damage. The maximum residual displacement ratio of the column 90m-40c (0.63) is about 28% higher than that of the reference column (0.49). It must be emphasized that concrete cover did not have a significant influence on the residual displacements.

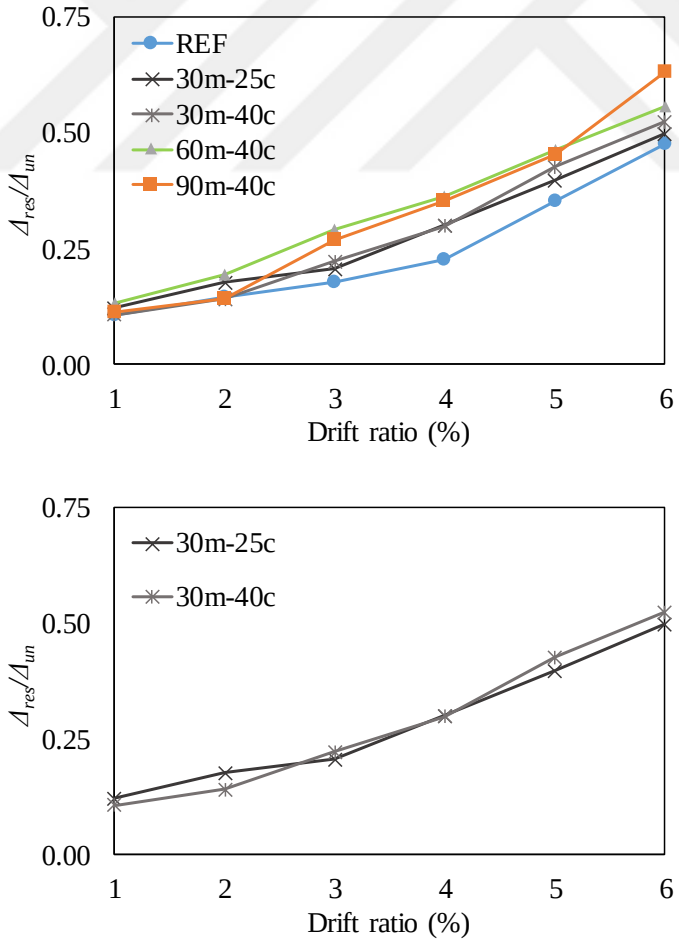

Figure 2.16 : Residual displacements of the columns.

2.6 Prediction of Post-fire Seismic Response

A numerical study is conducted to predict the seismic response of the columns. Figure 2.17 shows the step-by-step calculation process of the predicted post-fire lateral load-displacement response of the columns.

The predicted post-fire seismic response of the fire exposed and reference columns is calculated considering Moment (M)-Curvature (ϕ) relationships of the columns at the critical sections based on a fiber analysis approach combined with a plastic hinge concept. For the fiber analysis, the cross-section is defined in terms of its geometry, reinforcement type and arrangement in transverse and longitudinal directions, and the effect of axial loading is considered in the fiber analysis. For the monotonic stress-strain relationship of the reference column, the model proposed by Mander et al. (1988) is used based on the actual characteristics of unconfined (Figure 2.1, Figure 2.17 Step A) and confined concrete. For fire exposed columns, the cross-sections of the columns are first divided into 36 finite elements each having a dimension of 50×50 mm (Figure 2.17 Step 1, Figure 2.18). For each finite element, the temperatures attained during the whole course of heating and cooling stages are taken from SAFIR and verified by thermocouple readings obtained from fire tests (Figure 2.7, Figure 2.17 Steps 2-3). As shown in Figure 2.18, the mean temperature value interpolated based on the temperatures obtained from SAFIR along both the diagonal section and symmetry axis of the section as similarly conducted by Lie et al. (1986) and Mostafaei et al. (2009). Then, stress-strain relationship for each of the finite elements are determined using the residual stress-strain relationships using Eqs. (2.4-2.5) as recommended by Chang et al. (2006) (Figure 2.17 Step 4). More details about the model can be found in the original paper.

$$\frac{f'_{cT}}{f'_c} = \begin{Bmatrix} 1.01-0.00055T & (20°C<T\leq 200°C \\ 1.15-0.00125T & (200°C<T\leq 800°C \end{Bmatrix} \tag{2.4}$$

$$\frac{\varepsilon_{0T}}{\varepsilon_0} = \begin{Bmatrix} 1 & (20°C<T\leq 200°C \\ \left\{(-0.1f'_c+7.7)\left[\frac{\exp(-5.8+0.01T)}{1+\exp(-5.8+0.01T}\right]-0.0219\right\} & (200°C<T\leq 800°C \end{Bmatrix} \tag{2.5}$$

In these equations, f'_{cT} is the residual compressive strength, ε_{oT} is the compressive strain corresponding to f'_{cT} after exposure to temperature T, f'_c and ε_o are concrete compressive strength and strain of peak stress at ambient temperature, respectively.

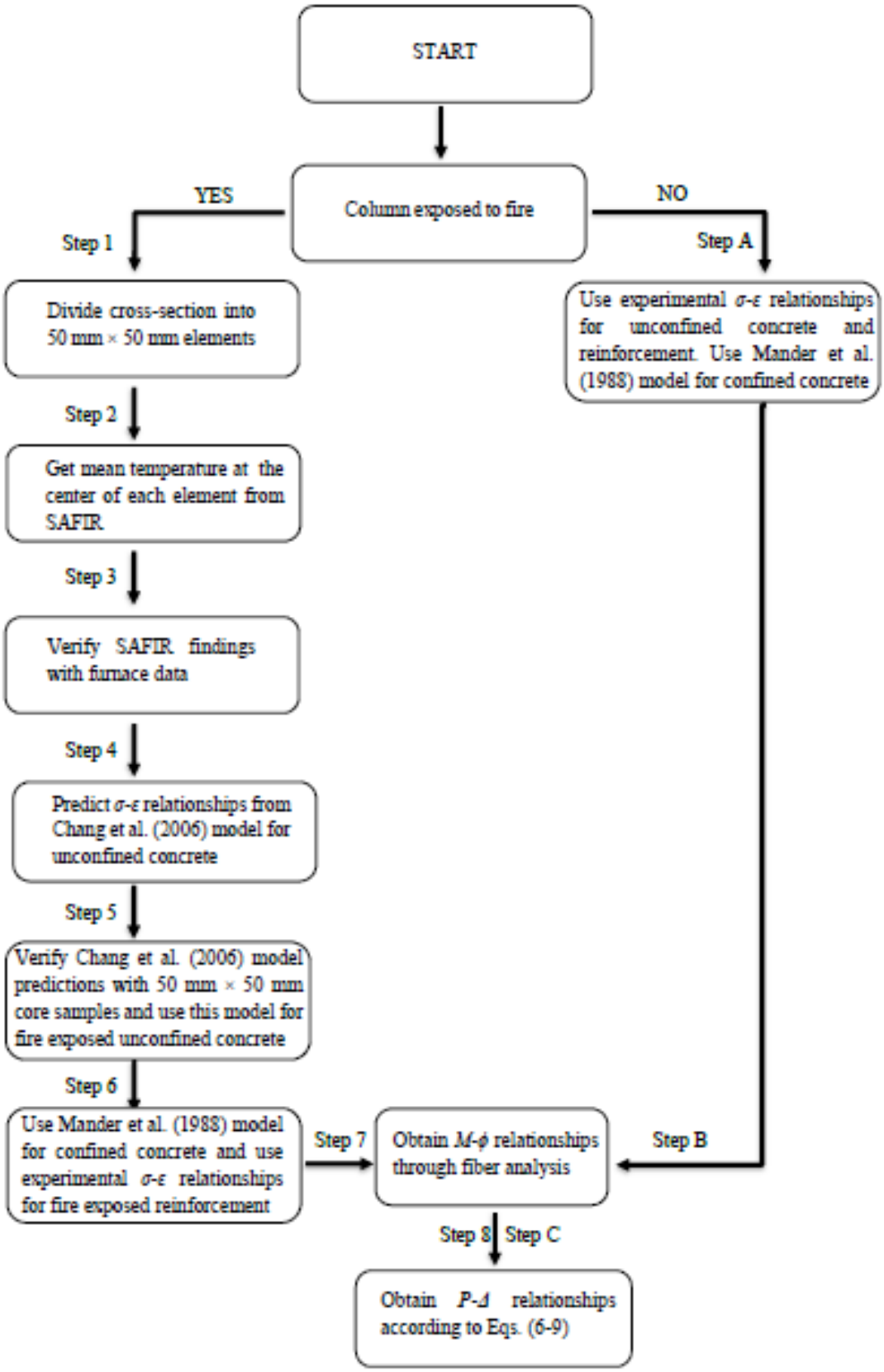

Figure 2.17 : Calculation procedure for the prediction of post-fire seismic response of the columns.

In order to verify the model (Chang et al., 2006), core specimens were drilled from the undamaged parts of the tested columns after the seismic tests on the test days corresponding to about the age of 60 days after the fire tests (approximately 16 months after the production of the column specimens) (Figure 2.17 Step 5). Two single core samples along the whole width and depth of each column with dimensions of 100 (diameter)×300 (height) mm were taken. Each sample was then divided into six elements each having a height of 50 mm to correspond to mesh size in the cross-sectional analysis. These core samples were then tested under uniaxial compression in order to obtain their stress-strain relationships. The average compressive strengths of the core samples, which corresponded to the compressive strength of the elements located over distances of 50, 100 and 150 mm from the edge of the columns (Figure 2.18a), are given in Figure 2.19a. It should be noted that core compressive strengths were converted to standard cylinder strengths with a conversion factor calculated based on the ratio of cylinder to core compressive strengths obtained from unheated specimens (i.e. 36.2/30.8 in Figure 2.19a). The predictions of Eqs. (2.4 and 2.5) were then validated by core strengths (converted to cylinder strengths) and cylinder strains given in Figure 2.19a, and Figure 2.1, respectively with a reasonable agreement. Therefore, model predictions obtained using Eqs. (2.4-2.5) are used in the structural analysis for defining unconfined concrete properties after fire exposure. The unconfined and confined stress-strain relationships of the unheated and 90 minutes heated elements used in the fiber analysis are given in Figures 2.19b and 2.19c, respectively.

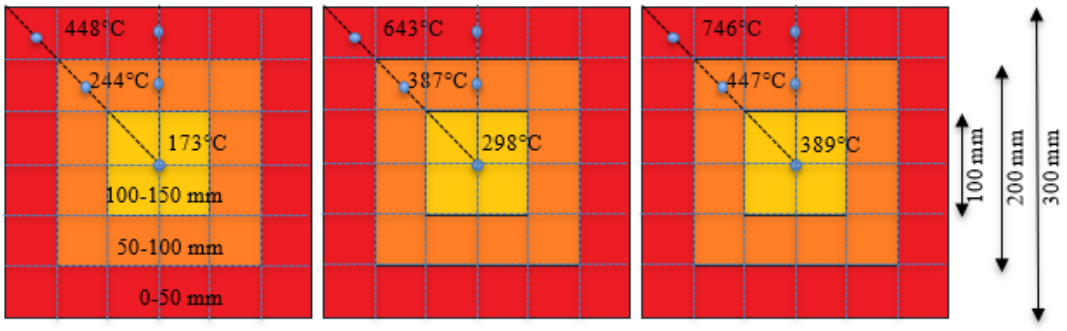

a) b) c)

Figure 2.18 : Temperatures including cooling stages after a) 30 minutes, b) 60 minutes and c) 90 minutes.

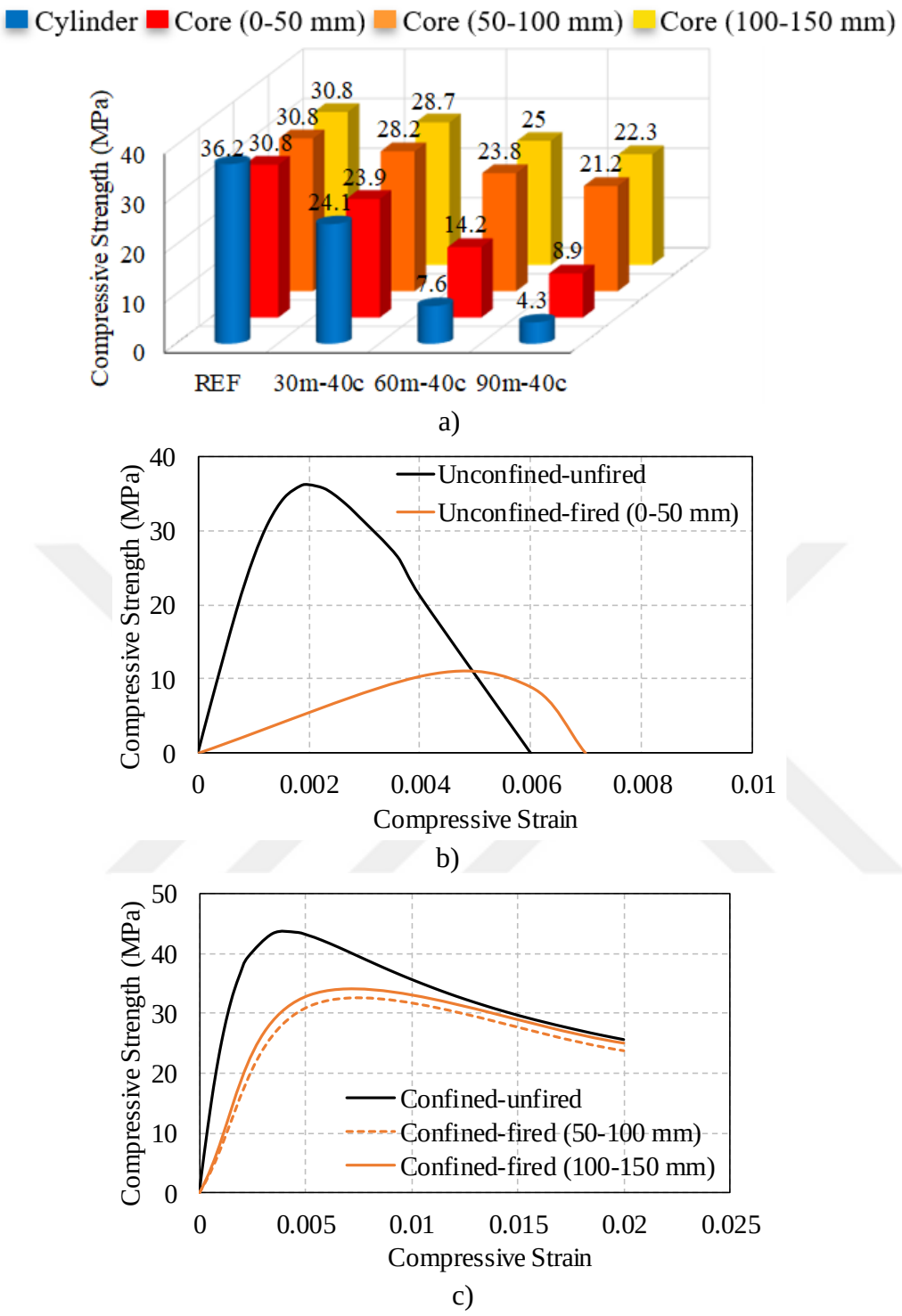

Figure 2.19 : a) compressive strength for cylinder and core samples, b) unconfined concrete model and c) confined concrete model used in fiber analysis.

The monotonic stress-strain relationships for confined concrete in the fire exposed columns are estimated based on the study by Mander et al. (1988). Besides, for fire exposed columns, an elastoplastic steel stress-strain relationship with strain-hardening is assumed in fiber analysis based on the actual uniaxial tension test results obtained for the worst-case scenario (90 minutes of fire exposure) (Table 2.2, Figure 2.17 Step

6). As aforementioned, only a slight variation in mechanical properties of reinforcing bars was observed even after 90 minutes of fire exposure, which forms the idea behind using the same mechanical properties for the specimens exposed to 30, 60 and 90 minutes of fire.

At the next step (Figure 2.17 Steps 7 and B), monotonic M-ϕ relationships of the column sections are obtained as shown in Figure 2.20 for the columns REF and 90m-40c. The M-ϕ analysis is terminated when the confined concrete reaches its ultimate strain capacity. It is well-known that the plastic hinging starts after the maximum moment capacity of the member section is reached (Figure 2.21). As shown in Figure 2.21, a potential plastic hinge is located at the lower part of the column, where the plastic deformations are distributed. On the other hand, the upper part of the column out of the plastic hinge length, which is assumed to remain elastic, is subdivided into 5 elements of equal heights so that the effective flexural stiffness of each piece can be considered properly at each stage of loading. It should be noted that the rotations are lumped at mid-height of each piece for calculation of lateral load-displacement relationship.

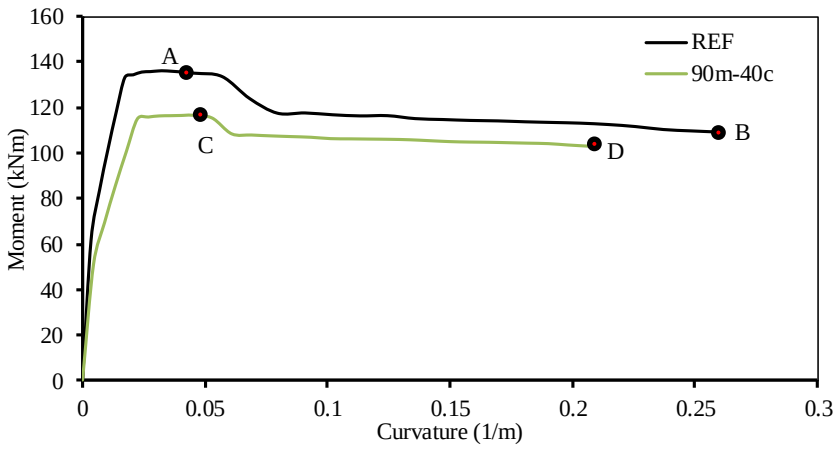

Figure 2.20 : Moment-curvature relationships for the columns REF and 90m-40c.

The numerical P-Δ relationship of the column is obtained based on M-ϕ relationship (Figure 2.17 Steps 8 and C). The tip displacement is the sum of the elastic displacement (Δ_e) and the plastic displacement (Δ_p). The elastic displacement (Δ_e) can be obtained as follows: first, for each lateral load increment (P_i), the bending moment values (M_i) on each piece are obtained using Eq. 2.6. In this equation, h_i is the distance between

the center of the respective piece and the tip of the column, where the lateral load is applied (Figure 2.21).

$$M_i = P_i \cdot h_i \tag{2.6}$$

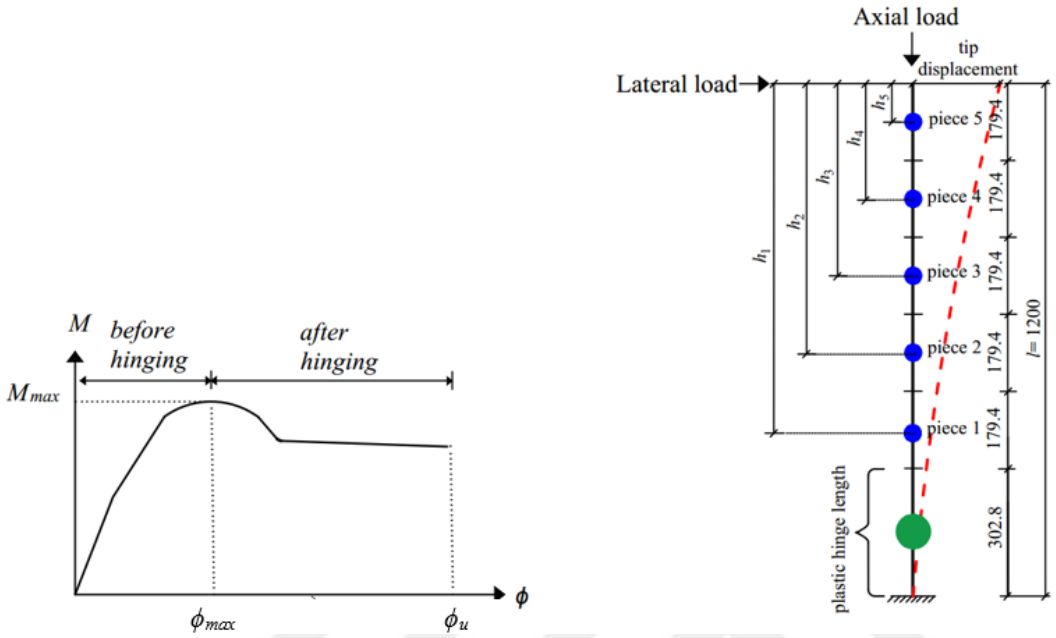

Figure 2.21 : The calculation of tip displacement for the columns.

Subsequently, the curvature value of each piece (ϕ_i) is ascertained on the ascending portion of the M-ϕ curve corresponding to the respective bending moment M_i. Finally, the displacement induced from the elastic part (Δ_e) is calculated using Eq. (2.7). In this equation, l_i is the length of the respective part.

$$\Delta_e = \sum_{i=1}^{5} \phi_i . l_i . h_i \tag{2.7}$$

The plastic displacement (Δ_p) induced from the plastic hinge can be obtained using Eq. (2.8).

$$\Delta_p = (\phi_u - \phi_y) . l_p . (l - \frac{l_p}{2}) \tag{2.8}$$

The plastic hinge length (l_p) is obtained to be 303 mm using Eq. (2.9), which also makes allowance for additional rotation at this zone resulting from strain penetration of the longitudinal reinforcement into the footing (Priestley et al. 1996). In Eq. (2.9), d_b and f_y are the diameter and the yield strength of the longitudinal bar, respectively.

$$l_p = 0.08l + 0.022 d_b . f_y \tag{2.9}$$

The numerically obtained monotonic *P-Δ* curve is assumed to be similar for both pushing and pulling loading directions, and serves as the envelope for the hysteretic response. The comparison of the numerical and experimental lateral load-displacement relationships is presented in Figure 2.8. As seen in this figure, the predicted results are in good agreement with the experimental results in terms of estimating the load bearing capacity and deformability. As it is also evident from the figure, the use of the conventional principles of structural mechanics used for unheated columns results in reasonably overestimation of the stiffness of the columns. This may be due to the facts that only flexural displacements are considered while shear and slip components of the tip displacement are neglected. As aforementioned, the uniaxial monotonic concrete model developed by Chang et al. (2006) is used for numerical analysis in this study. According to the best literature survey of the authors, there is no cyclic concrete model in the literature considering post-fire cooling. In case of fire exposure and particularly after cooling, even the monotonic concrete models in the literature are extremely rare. Although Chang et al. model does not account for any concrete damage due to cyclic loading, usage of the model results in a reasonable prediction of lateral load capacity and ductility of the tested columns. On the other hand, relatively lower accuracy of predictions in terms of flexural stiffness of the columns can partly be stemming from negligence of damage due to cyclic loading. Consideration of cyclic characteristics of fire exposed concrete is a challenging issue and necessitates further studies. Nevertheless, the conventional principles of structural mechanics used for unheated columns can also be used for the columns exposed to fire in case the aforementioned algorithm is followed.

2.7 Conclusions

This paper presents the seismic behavior of five full-scale reinforced concrete columns after fire exposure. The parameters are the duration of fire and the thickness of concrete cover. The following conclusions can be drawn from the observed performances of the tested columns.

- The failure of the columns was dominated by flexural behavior characterized by initial yielding of the longitudinal reinforcing bars followed by crushing of the concrete cover. The lateral load capacities of the fire exposed columns were observed to be lower than the reference column that was not exposed to fire. The average

reductions in ultimate loads with respect to the reference column were found to be 13%, 19% and 19% for fire exposure durations of 30, 60 and 90 minutes, respectively. Since the strength of the hot rolled reinforcing bars were mitigated after cooling, the concrete residual properties were found to be the reason for the reduction in lateral load capacity. Therefore, similar reductions in lateral load capacities were observed for the columns subjected to 60 or 90 minutes of fire exposure, which had similar residual stress-strain characteristics of concrete.

- The ductility of the columns was found to be similar to each other except the column 90m-40c in which higher yield displacement based on stiffness degradation resulted with lower ductility. Nevertheless, ductility factors of all columns were larger than 3.5, which implies satisfactory structural response in terms of ductility.
- The initial stiffness of the columns decreased with an increase in fire duration because of concrete cracking resulting from the loss of tensile strength of concrete and the formation of plastic hinges.
- The energy dissipation capacity of the columns decreased while the tendency of the columns towards plastic deformation increased with an increase in fire duration.
- For the columns subjected to the same fire exposure duration but with different concrete cover thicknesses, it was observed that while the concrete cover thickness does not have significant effect on lateral load capacity, it adversely effects the stiffness of the column. The lower concrete cover thickness of the column 30m-25c was responsible for the larger stiffness degradation than its counterpart, which in turn caused an increase in Δ_y of the column leading to lower ductility. The thickness of concrete cover did not significantly affect the residual displacement and energy dissipation capacity.
- The proposed numerical model predicts the post-fire seismic behavior of reinforced concrete columns in a reasonable manner.

Since limited test data are available, it is clear that further research is necessary for generalizing the outcomes of the study.

3. POST-FIRE SEISMIC PERFORMANCE OF PRECAST RC COLUMNS

3.1 Abstract

Quantifying the seismic resistance of reinforced concrete (RC) buildings after fire is currently difficult because of the lack of information regarding their strength and ductility under earthquake loads. In this study, four nearly full-scale, flexure-controlled precast RC columns were subjected to a quasi-static reversed cyclic lateral loading under constant axial load to examine the seismic response of precast RC columns damaged by 30, 60 and 90 minutes of ISO-834 fire. For the first time, the impact of fire damage on force-displacement behavior, moment-curvature relationship, stiffness, energy dissipation capacity, and residual displacements was investigated through post-fire seismic tests. Test results clearly indicated that the fire exposure did not remarkably influence the lateral load bearing capacity, failure modes, and ductility of the columns with the exception of the specimen subjected to 90 minutes of fire. The analytical study consisting of thermal and fiber based structural analysis demonstrated that, conventional principles of structural mechanics are valid for estimation of the post-fire seismic behavior of precast RC columns in case the deteriorations in materials are realistically taken into account and the given algorithm is followed.

3.2 Introduction

Over the last few decades, precast structural members have been a product of choice anywhere people need to rapidly build many homes and industrial facilities in the US (New York Times, 2018). With this popularity, precast RC structural members widely form structural systems of buildings in seismic zones of both developed and developing countries.

This chapter is adopted from the journal paper: Demir, U., Green, M.F. and Ilki, A. (2020). Post-fire seismic performance of precast RC columns. PCI Journal. DOI: 10.15554/pcij65.6-01.

Generally, socket base connections are the simplest way to connect precast RC columns to foundations, and are mostly used for low-rise buildings, bridge piers and other light facilities (fib, 2004). In such column-to-foundation connections, the bottom of the column is inserted into a RC hollow core body and grouted in place. Precast RC columns are prominent load bearing members in frame buildings in the case of seismic loading, and particularly in industrial facilities, lateral forces are resisted through cantilever action of the precast RC columns. The majority of European industrial facilities consist of precast RC frames and these structures have demonstrated poor seismic behavior when connections were insufficiently detailed (Brunesi et al., 2015); potentially threatening the life safety of occupants after an earthquake. When precast RC structures have not been properly designed and constructed according to the valid codes, serious damage, large lateral displacements, and total collapse have been observed in previous earthquakes (Sezen and Whittaker, 2006; Brunesi et al., 2015).

Most building codes require that the RC structural members remain standing after a fire event as well as after a design earthquake, in order to provide that occupants are able to escape from the building and rescue operations can be conducted safely. However, fire damage complicates the assessment of the seismic behavior of structural members depending on the deterioration of the materials such as concrete and steel reinforcement which is not generally taken into account during the design stage and is of vital importance in terms of post-fire performance assessment. In post-fire performance assessment, it should be decided to repair, strengthen, or demolish and rebuild the entire structure considering service and earthquake loads during the remaining service life of the structure. Furthermore, in addition to post-fire performance assessment need in case of individual fires, structural fires may also occur collectively because of earthquakes, and thus implicitly causing significant number of casualties. The collective fires following the San Francisco 1906 and Tokyo 1923 earthquakes rank as the two largest urban fires in history and after these two major earthquakes, fires caused about 150,000 people killed and over 150,000 buildings destroyed (Scawthorn et al., 2005). It is noteworthy that severe earthquakes are generally followed by aftershocks, and thus structures, which have been exposed to collective fires, may be exposed to seismic actions again. The risk of aftershocks following the main shock addresses the obvious need of a post-fire seismic performance evaluation (Benichou et al., 2013). Therefore, this study is focused on estimation of the post-fire seismic performance of flexure dominated precast RC

columns which has not been investigated to date. Although behavior of cast-in-situ RC columns under elevated temperatures have been extensively investigated under service loads (Lie and Irwin, 1990; Franssen and Dotreppe, 2003; Tan and Yao, 2003; Benichou et al., 2011; Khaliq and Kodur, 2013), and under service loads combined with uniaxial/biaxial bending after cooling (Lie et al., 1986; Jau and Huang, 2008; Chen et al., 2009; Yaqub et al., 2013), experimental studies on the post-fire seismic behavior of cast-in-place RC columns are extremely rare. Yakub and Bailey (2012) and Bailey and Yakub (2012) described the results of an experimental study to investigate the seismic performance of post-heated shear critical repaired RC columns. A uniform temperature exposure was applied and the influence of fire damage on hysteretic response was addressed in case of FRP retrofitting. It should be noted that these studies considered the cast-in-situ RC columns with insufficient shear capacity and focused on the retrofitting issues in order to enhance the lack of shear capacity addressing sub-standard existing buildings. Benichou et al. (2013) presented the results of a study on seismic resistance of FRP strengthened concrete members after fire exposure. Two square and five circular RC columns with FRP confinement and fire insulation were exposed to 4 hours of standard fire. Then, a pushover lateral load was gradually applied. Since a specimen that has been exposed to fire was not available in the study for the columns without FRP confinement, a simplified approximation using ASFI method (Mostafaei and Hum, 2010) was employed to estimate the unfired lateral load capacity of one of the columns. Furthermore, a numerical evaluation was conducted using the structural analysis software SAFIR (Franssen and Gernay, 2017). It was numerically reported that the bare (unconfined and 4h fire exposed) column experienced a 55% reduction in its maximum lateral load capacity due to fire damage and the maximum drift estimated for this column was 0.03 corresponding to about 200% increment in deformation capacity compared to reference specimen that was kept at room temperature.

It should be noted that, according to the best knowledge of the authors, there is no experimental study in the literature considering the post-fire seismic behavior of flexure critical RC columns which are commonly used all over the world. Furthermore, in terms of post-fire seismic behavior of precast RC columns, the current study is also unique. With the above points in mind, the residual structural capacity of fire damaged precast RC structures subjected to earthquakes is not well known, meaning that many fire-damaged structures will need to be demolished after a fire even if it is not

necessary (New York Times, 1997; Almand, 2013). The objective and novelty of the current paper are to determine the post-fire seismic behavior of precast RC columns and to have this knowledge serve as a basis for the development of safer and more cost effective post-fire structural repair and remediation methods through enhanced post-fire performance assessment.

3.3 Materials and Specimen Details

Four precast RC columns with 2800 mm (110.3 in.) height and 300 x 300 mm (11.8 x 11.8 in.) cross-sectional dimensions were manufactured. The precast columns were then inserted into RC footing sockets. The embedded part of the columns within the footings were 600 mm long with a gap of 25 mm on all sides. The outer dimensions of the footings were 700 x 700 x 825 mm (27.6 x 27.6 x 32.5 in.). The 25 mm wide gap between the column and the inner walls of the footing was then grouted in-situ. The surfaces of the embedded parts of the precast columns and inner walls of the footing socket were not subjected to any special treatment (Fig. 3.1). The ready-mixed concrete used in the production of the specimens was provided by a private precast company representing the common practice. The properties of concrete are given in Table 3.1. Concrete contains 78% calcareous aggregates and concrete cylinder tests on the 28^{th} day gave a concrete compressive strength of 32.4 MPa (4.7 ksi). Columns were fitted with 4 of 20 mm longitudinal steel deformed bars placed at the corners with a 50 mm (2 in.) concrete cover from the edge of the specimen to the center of the longitudinal bar. These bars had a yield strength of 461 MPa (66.9 ksi). Lateral reinforcement with a yield strength of 472 MPa (68.5 ksi) was provided in the form of 10 mm ties spaced at 100 mm (3.94 in.) spacing center-to-center. Along the top 600 mm (23.6 in.) length of the columns, ties were placed at a spacing of 75 mm (2.96 in.). The ratio of the longitudinal and the lateral reinforcement of the columns at the core concrete section, which were calculated according to Eqs. (3.1, 3.2), are 2.5% and 0.7%, respectively. In these equations, ρ_{cc} is the ratio of longitudinal steel, A_s is the area of longitudinal steel, A_{cc} is the area of core of section, ρ_s is the ratio of lateral reinforcement, A_o is the area of lateral reinforcement, s is the spacing of the lateral reinforcement and d_c is the concrete core dimension to center line of the perimeter hoop. The seismic design of the specimens was accomplished in accordance with Turkish seismic design code (2007). Socket foundations were overdesigned and

insulated against fire. A commonly used cement based, non-shrink and expanding grout (SikaGrout-214) was used to fill the gap between the column and the socket foundation. At the age of 28 days, cube (70 mm) compressive strength of the grout was 65 MPa whereas the flexural strength was obtained as 9 MPa.

$$\rho_{cc} = \frac{A_s}{A_{cc}} \tag{3.1}$$

$$\rho_s = \frac{A_0}{s} d_c \tag{3.2}$$

Table 3.1 : Mix proportions and properties of concrete.

Material	Weight
Portland cement-42.5R, kg/m^3 (lb/yd^3)	300 (506)
Sand (0-4 mm), kg/m^3 (lb/yd^3)	920 (1551)
No I Aggregate (5-12 mm), kg/m^3 (lb/yd^3)	507 (855)
No I Aggregate (12-22 mm), kg/m^3 (lb/yd^3)	490 (826)
Superplasticizer-Sikament 300, kg (lb)	3.6 (7.9)
Water, kg/m^3 (lb/yd^3)	124 (209)
Slump, mm (in.)	200 (7.9)
28-day compressive strength, MPa (ksi)	32.4 (4.7)
Test day compressive strength, MPa (ksi)	36.2 (5.3)

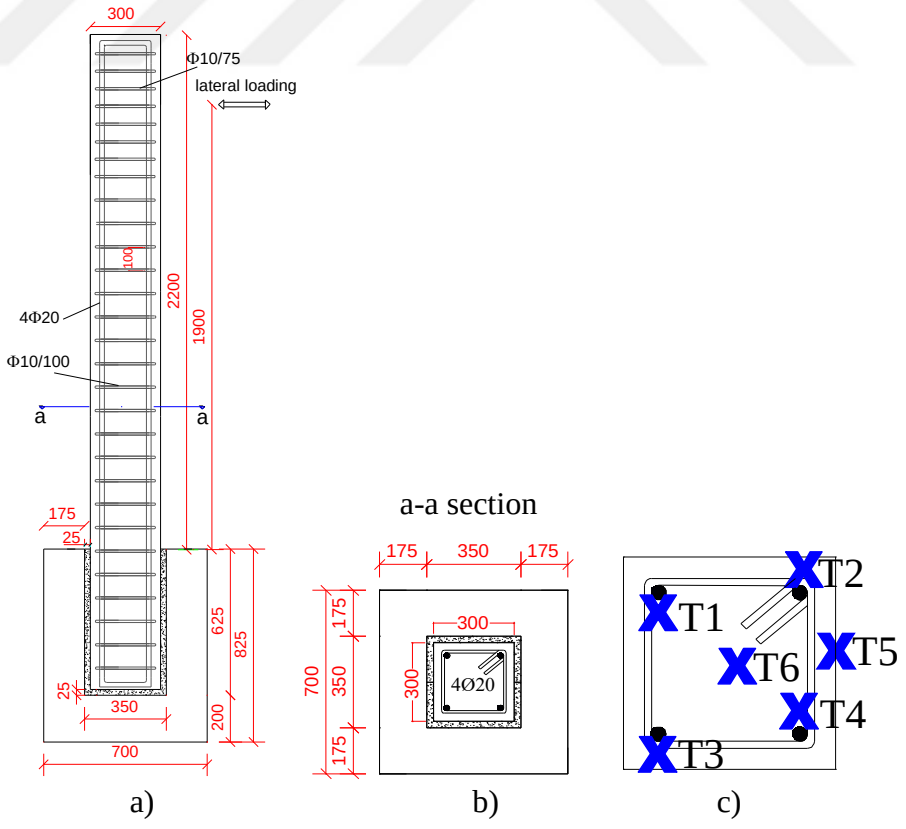

Figure 3.1 : a) longitudinal section of the specimens, b) transverse section of the specimens, c) thermocouple locations. All dimensions are mm, 1 mm=0.0394 in.

3.4 Fire Tests

The columns were cured under ambient temperature and humidity for 14 months before being transported to the fire facility for the fire tests. Then, the fire tests were carried out in Turkish Standard Institution (TSE) fire facility in Istanbul, Turkey. The fire furnace had 3.2 x 4.0 m (10.5 x 13.1 ft.) dimensions in plan and 3 m (9.8 ft.) of height (Figure 3.2). The furnace was consisted of aerated autoclaved concrete (AAC) walls and slab. The heat was provided by a total of 8 gas burners, positioned on opposite sides of the furnace.

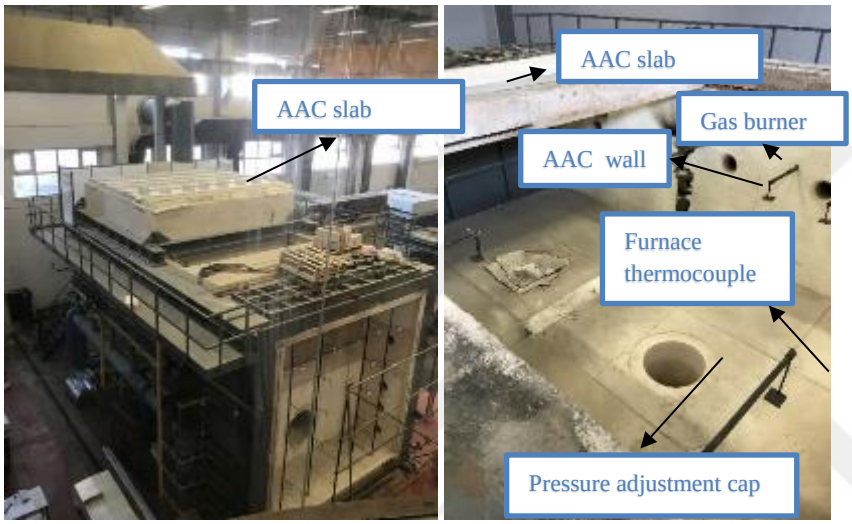

Figure 3.2 : Fire test furnace.

Furnace temperature was set in accordance with ISO (1999) standard fire during the heating stage which is calculated using Eq. (3.3) where T is the furnace temperature in °C (1 °F = 1 °C × 1.8 + 32) and t is the time in minutes. After following the fire curve for 30, 60 and 90 minutes, furnace was switched off and natural air cooling was adopted until the specimens cooled down to room temperature (Figure 3.3). As shown in Figure 3.3, the furnace was able to provide required performance in terms of following the ISO time-temperature curve which is also quite similar to ASTM (2012) fire curve.

$$T = 20 + 345\log(8t + 1) \tag{3.3}$$

The temperatures of concrete and reinforcement were monitored by a total of six K-type NiCr-Ni thermocouples pre-embedded within each specimen during casting (Figure 3.1). Thermocouples located at various locations of the furnace (Figure 3.2) were used to measure the furnace temperature. After 30, 60 and 90 minutes of fire

exposure, maximum furnace temperatures of 841, 945 and 1005 °C (1545, 1733, 1841 °F) were measured, respectively (Figure 3.3). In all fire tests, after about 10 minutes of heating, vapor began to come out of the furnace and continued until the end of the tests. No spalling sound was observed during the test of PC-30M specimen. However, many irregular hairline cracks appeared on the concrete surfaces in this specimen after heating. On the other hand, after 25 minutes of heating, minor spalling of few chunks of concrete was observed in PC-60M specimen. Moreover, a great amount of spalling occurred in PC-90M in the form of spalling of small concrete chunks. Since the fire induced pore pressure increased, spalling was a larger factor for this specimen.

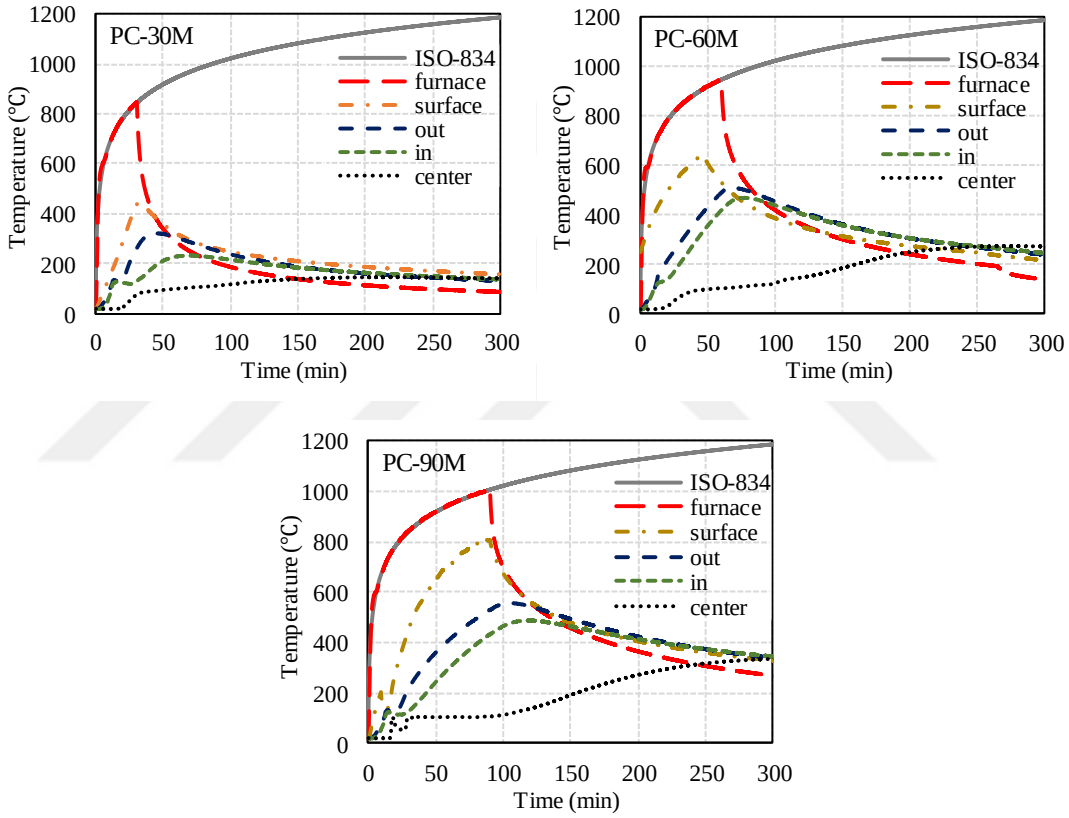

Figure 3.3 : Time – temperature curves in the furnace during the fire tests and after cooling (Note: 1 °F = 1 °C × 1.8 + 32, “surface” is obtained from TC5, “out” is obtained from TC-2 and TC-3, “in” is obtained from TC1 and TC-4, “center” is obtained from TC-6).

The appearance of the heated columns after cooling is shown in Figure 3.4. Because of the dehydration, light grey formations were observed over concrete surfaces for PC-30M and PC-60M specimens whereas the color of the column surfaces was yellowish for PC-90M after heating. During the cooling stage, the temperature continued to rise toward the center of the specimens up to around 5 hours depending on the duration of

the fire exposure before it started to decrease at a slower rate until the heat balance was achieved. After the first 30 minutes of cooling, furnace temperatures were decreased to about half of the maximum temperatures where the cooling rate was reduced to about 2 °C/min (67.6 °F/min) after the first half an hour. It should be noted that the furnace door was kept closed about 24 hours after cooling has started.

a) b) c)

Figure 3.4 : Post-cooling appearance of the columns a) PC-30M, b) PC-60M and c) PC-90M.

3.5 Theoretical Post-fire Seismic Capacities

The impact of post-fire seismic loading on the precast RC columns was estimated through combined thermal and structural modelling. At the thermal analysis stage, SAFIR (Franssen and Gernay, 2017), a finite element analysis software was used to determine cross-sectional thermal numerical evaluation over a quarter of the column cross-section (Figure 3.5). The software assumes that heat is distributed in solid structures essentially by conduction and at the boundary of the structure, heat is exchanged with the environment by convection and radiation. For conduction in concrete, heat exchange is based on Fourier equation expressed in Cartesian system of coordinates as shown in Eq. (3.4) where $\{x, y, z\}$ is the vector of Cartesian coordinates (m), T is the temperature (K), k is the thermal conductivity (W/mK), Q is a term that accounts for internal generation of heat (W/m³), ρ is the specific mass (kg/m³), c is the specific heat (J/kgK) and t is time (s). For convection and radiation acting over the boundaries, heat exchange is evaluated using Eqs. (3.5-3.6) where h_c is the convective

heat flux between gas and solid (W/m²), h is the coefficient of convection (W/m²K), T_g is the temperature of the gas (K), T_s is the temperature at the surface of the solid (K), h_r is the radiative heat flux emitted by a solid (W/m²), σ is the Stefan -Boltzman constant (5.67 × 10-8 W/mK^4) and ε is the emissivity of the solid (-). The software first extrapolates the temperatures from two previous time steps, t_{n-1} and t_n, to a first approximation at a given time t_n + dt comprised between t_n and t_{n+1} and then refines this first approximation of the temperatures at t_n + dt until thermal equilibrium is restored.

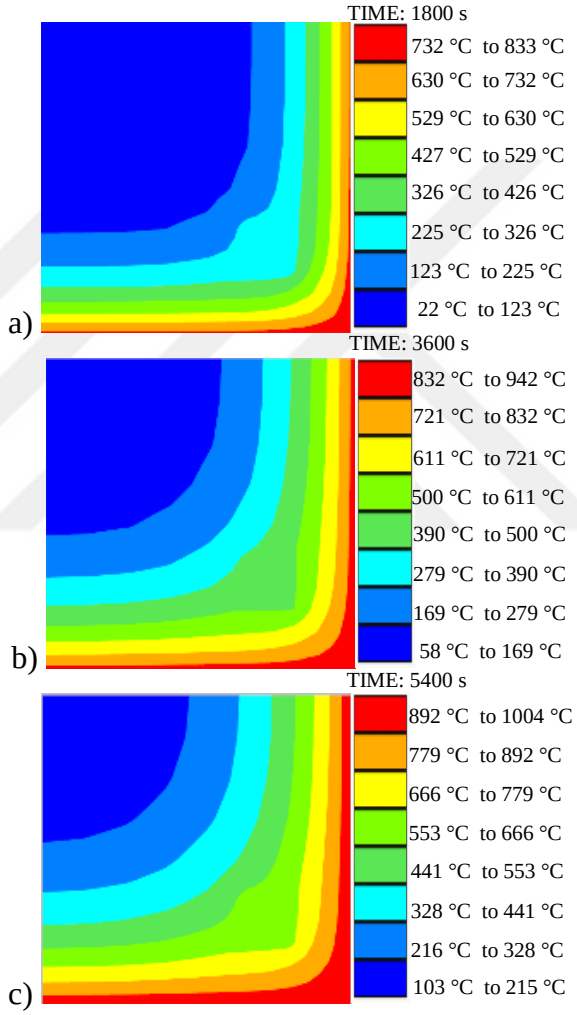

Figure 3.5 : Temperature distributions in fire tests obtained from SAFIR for a) 30 minutes, b) 60 minutes and c) 90 minutes (Note: 1 °F = 1 °C × 1.8 + 32).

In thermal modelling with SAFIR, column cross-sections were defined by 144 nodes and 121 solid elements and then experimentally obtained time-temperature relationships including cooling phase was defined to the fire exposed edges of the section. Calcareous concrete and steel material properties were assigned to the corresponding elements of the cross-section as given by Eurocodes (CEN, 2004). It

should be noted that experimentally measured thermocouple readings (Figure 3.3) were used to verify the findings of SAFIR (Figure 3.5), and findings of the SAFIR were found to be satisfactory.

$$\frac{\partial}{\partial x}\left[k\frac{\partial T}{\partial x}\right]+\frac{\partial}{\partial y}\left[k\frac{\partial T}{\partial y}\right]+\frac{\partial}{\partial z}\left[k\frac{\partial T}{\partial z}\right]+Q=c\rho\frac{\partial T}{\partial t} \quad (3.4)$$

$$h_c = h(T_g - T_s) \quad (3.5)$$

$$h_r = \sigma\varepsilon {T_s}^4 \quad (3.6)$$

Thermal analysis results were then implemented into structural modelling to predicted the post-fire lateral load-displacement response of the columns. The step-by-step procedure of structural analysis is shown in Figure 3.6.

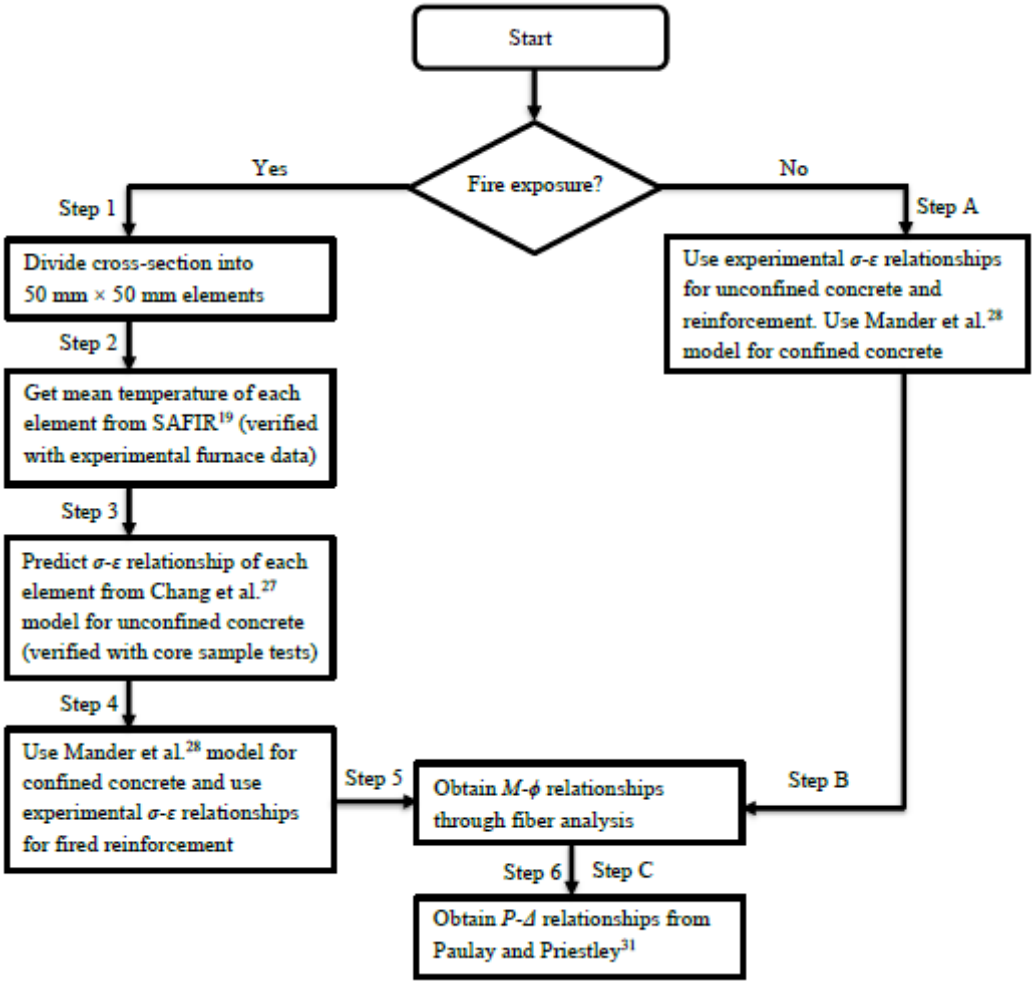

Figure 3.6 : Calculation procedure for the prediction of post-fire P-Δ relationships of the columns.

The theoretical seismic responses of the fired and unfired columns are calculated considering Moment (M)-Curvature (ϕ) relationships of the columns at the critical sections based on fiber analysis approach and plastic hinge concept. The effect of axial

loading is considered in the fiber analysis. In the fiber analysis, RC column cross-sections are divided into 36 finite elements each having dimensions of 50 x 50 mm (2 x 2 in.) as shown in Figure 3.7 (Figure 3.6 Step 1). Average temperatures for each element, attained during the whole course of heating and cooling, are taken from thermal analysis conducted by SAFIR which are verified by thermocouple readings obtained from fire tests (Figures 3.3-3.5, Figure 3.6 Step 2). The average temperatures for the elements are then interpolated based on the temperatures calculated along both the diagonal section and symmetry axis of the section as shown in Figure 3.7 and as similarly carried out by Mostafaei et al. (2009). Using the calculated temperatures, residual stress-strain relationship for each of the finite elements are determined using Eqs. (3.7-3.8) as recommended by Chang et al. (2006) (Figure 3.6 Step 3). In these equations, f'_{cT} and ε_{oT} are the residual compressive strength and peak compressive strain of concrete after exposure to temperature T, f'_c and ε_o are concrete compressive strength and compressive peak strain at ambient temperature, respectively.

$$\frac{f'_{cT}}{f'_c} = \begin{cases} 1.01 - 0.00055T \ (20\,°C < T \leq 200\,°C) \\ 1.15 - 0.00125T \ (200\,°C < T \leq 800\,°C) \end{cases} \tag{3.7}$$

$$\frac{\varepsilon_{0T}}{\varepsilon_0} = \begin{cases} 1 & (20\,°C < T \leq 200\,°C) \\ \left\{\left(-0.1f'_c + 7.7\right)\left[\frac{\exp(-5.8+0.01T)}{1+\exp(-5.8+0.01T)}\right] - 0.0219\right\} & (200\,°C < T \leq 800\,°C) \end{cases} \tag{3.8}$$

In order to verify the actual compressive strength of each finite element, concrete core samples were taken from undamaged regions of the RC columns after the seismic tests were carried out. A total of 2 single core samples along the whole width and depth of each column were taken with dimensions of 100 (diameter) x 300 (height) mm (3.94 x 11.8 in.) and each sample was then divided into six parts each having a diameter of 100 mm (3.94 in.) and height of 50 mm (2 in.). These samples were tested under uniaxial compression loads to verify the compressive strength of each fire exposed concrete element given in Figure 3.7. Since measuring compressive strains over these core samples would not be realistic due to the unconventional dimensions of the samples, 150 x 300 mm (5.9 x 11.8 in.) standard cylinders were also subjected to the same fire tests with the RC columns. Stress–strain behavior of these cylinder specimens is obtained under uniaxial compression loads. The variations of stress-strain relationships obtained from standard cylinder specimens after fire tests, and variations of average compressive strengths of the cores and the cylinder samples are given in Figure 3.8. In Figure 3.8, for instance, REF represents unheated specimen whereas C1-

30M-1 represents the first cylinder specimen of the sample series exposed to 30 minutes (30M) of fire. Experimentally obtained compressive strengths and strains are found to be in reasonable agreement with the analytically estimated model findings estimated using Eqs. (3.7-3.8). It should be noted that core compressive strengths were converted to standard cylinder strengths with a conversion factor calculated based on the ratio of cylinder to core compressive strengths obtained from unheated specimens (i.e. 36.2/30.8 in Figure 3.8). Therefore, model predictions obtained using Eqs. (3.7-3.8) are used in the structural analysis for defining unconfined concrete properties after fire exposure which were validated by core strengths (converted to cylinder strengths) as given in Figure 3.8b and heated cylinder peak compressive strains given in Figure 3.8a. The stress-strain relationships used in the fiber analysis are given in Figures (3.8c and 3.8d) for the unheated (unfired) and 90 minutes heated (fired) elements. Mander et al. (1988) model is used for estimating confined concrete properties after fire exposure and actual uniaxial tensile test results obtained from reinforcements are used in the analysis (Figure 3.6 Step 4). For obtaining the mechanical properties of the reinforcements, first, 300×300×500 mm RC specimens, which have the same reinforcing scheme with the full-scale RC columns, were cast using the same concrete batch. These specimens were then subjected to the same fire exposure with the full-scale columns. Thereafter, the reinforcing bars were taken out after cooling, and then subjected to uniaxial tension tests. The mechanical properties of the longitudinal (ϕ20) and transverse (ϕ10) reinforcing bars under ambient temperatures, and after cooling are presented in Table 3.2. It is also noteworthy that the average of 4 samples is given in the table and it was observed that the differences of the tensile test results were almost negligible (less than 5%).

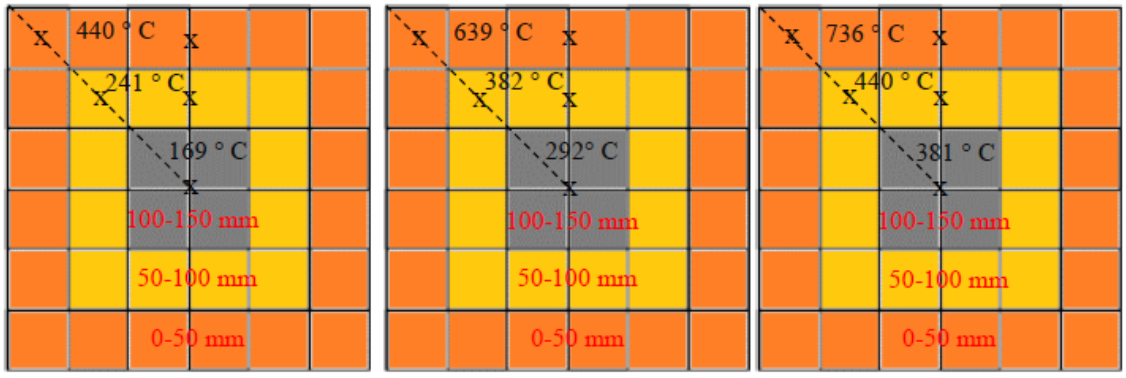

a) b) c)

Figure 3.7 : Maximum temperatures including cooling stages after a) 30 minutes, b) 60 minutes and c) 90 minutes.

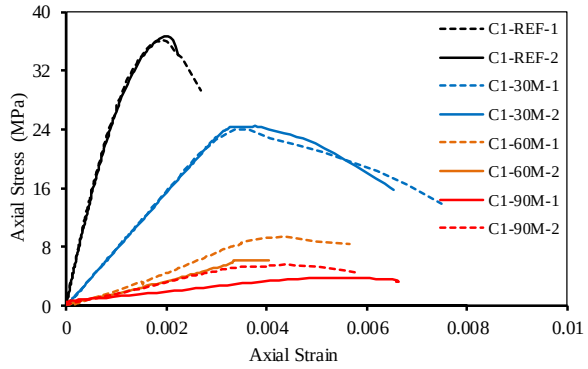

a)

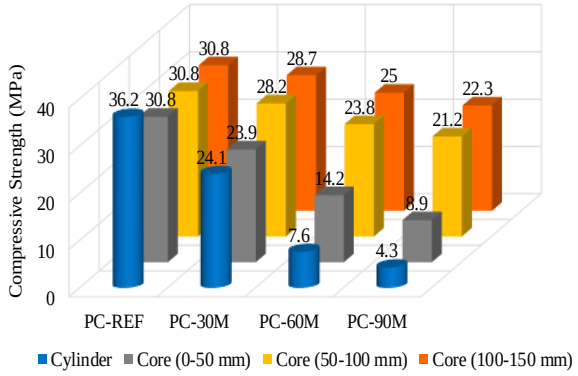

b)

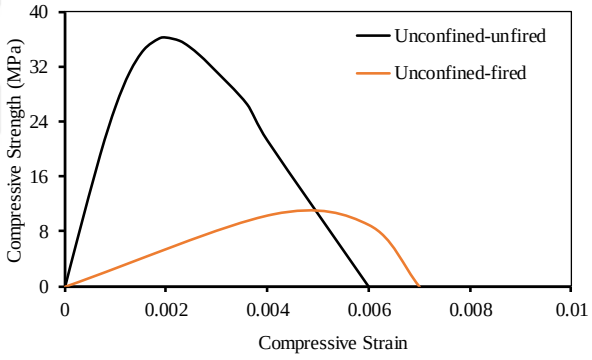

c)

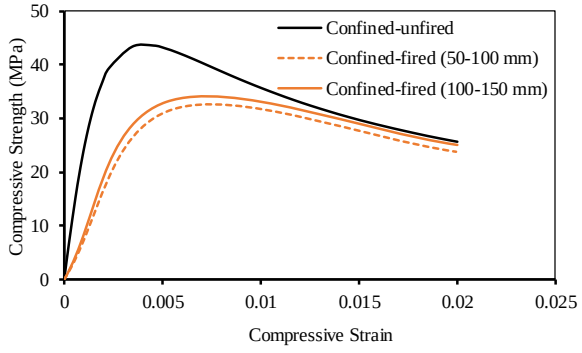

d)

Figure 3.8 : a) Stress-strain relationships for standard cylinder specimens, b) compressive strength for cylinder and core samples, c) unconfined concrete model and d) confined concrete model used in fiber analysis (Note: 1 MPa= 0.145 ksi).

As seen in Table 3.2, there is no remarkable difference between the mechanical properties of the unfired reinforcing bars and the reinforcing bars exposed to 90 minutes of fire (the most severe fire) since the measured maximum temperatures along the reinforcements did not exceed 510°C during the fire tests including cooling phase (Figure 3.3). The residual properties of the reinforcing bars are thus estimated to be almost recovered for all fire exposure durations (30, 60 and 90 minutes) as experimentally shown in this study (Table 3.2), and also reported in the literature in these temperature ranges (Neves et al., 1996). It should be noted that, for the sake of conservatism, the small difference between the residual properties of the fired and unfired reinforcements was also considered in the fiber analysis and the test results of 90 minutes of fire exposed specimens were used in modelling all fire exposed reinforcements (Figure 3.6 Step 4). Steel reinforcing bars were assumed to behave in an elastoplastic manner with strain hardening in fiber the analysis. For the unfired columns, the actual stress-strain relationships obtained from unheated cylinder specimens (Figure 3.8) are used for defining unconfined concrete properties whereas Mander et al. (1988) model is used for confined concrete (Figure 3.6 Step A). For the reinforcement, experimentally obtained mechanical properties were used (Table 3.2).

Table 3.2 : Mechanical characteristics of reinforcing bars.

Reinforcing bars	Fire exposure	f_y MPa (ksi)	ε_y	f_{max} MPa (ksi)	ε_{max}	f_u MPa (ksi)	ε_u
Φ20	n/a	472 (68.5)	0.0023	569 (82.3)	0.0965	525 (76.1)	0.15
Φ10	n/a	483 (70.1)	0.0025	557 (80.8)	0.0998	525 (76.1)	0.10
Φ20	90 min.	442 (64.1)	0.0024	549 (79.6)	0.0992	516 (74.8)	0.16
Φ10	90 min.	457 (66.3)	0.0024	552 (80.1)	0.0992	522 (75.7)	0.11

Once the residual mechanical properties of the concrete and reinforcement were determined, monotonic moment-curvature relationships for the columns are obtained at the critical sections of each RC column through a fiber analysis approach using a commercial software (Chadwell and Imbsen, 2004) for predicting the load–displacement relationships (Figure 3.6 Step 5, Step B). Theoretically obtained moment-curvature relationships for the columns PC-REF and PC-90M are given in Figure 3.9.

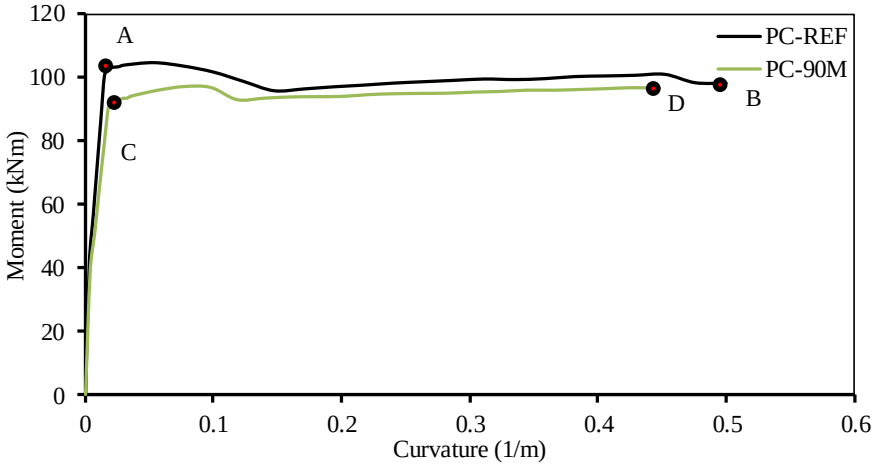

Figure 3.9 : Moment-curvature relationships for the columns PC-REF and PC-90M (obtained through fiber analysis) (1kNm= 0.74 kips.ft, 1 m= 3.28 ft.).

The strains computed for unconfined concrete (extreme concrete compression fiber on cover) (ε_c), confined concrete (extreme concrete compression fiber on core) (ε_{cc}) and longitudinal reinforcing bars in tension (ε_s) corresponding to specific points on moment-curvature relationships are shown in Table 3.3 (ie. for points corresponding to yielding (A and C) and ultimate (B and D) curvatures where the analysis has stopped). After obtaining the moment–curvature relationships, the total top displacements of the columns are estimated considering the elastic and inelastic deformations using the approximation defined by Paulay and Priestley (1992) for prismatic RC cantilever columns (Figure 3.6 Step 6, Step C). The curvature distribution at yield is adopted by linear approximation and can be estimated using Eq. (3.9), where Δ_y is the yield displacement, ϕ_y is the yield curvature and l is the shear span of the RC column. Assuming that the plastic rotations to be concentrated at mid-height of the plastic hinge length (l_p), the plastic displacement at the cantilever tip is calculated using Eqs. (3.10-3.12), where Θ_p is the plastic rotation along the equivalent plastic hinge length and Δ_p is the plastic displacement. For the sake of simplicity, the recommendation of Turkish seismic design code was utilized in the evaluation of the plastic hinge length as half depth of the cross-section. Consequently, theoretically obtained load–displacement relationships are compared to experimental behavior which is discussed below.

Table 3.3 : Theoretically obtained strains.

	PC-REF		PC-90M	
	Point A	Point B	Point C	Point D
ε_c	0.0011	0.006	0.0018	0.007
ε_{cc}	0.0007	0.020[b]	0.0014	0.020[b]
ε_s	0.0024[a]	0.083	0.0024[a]	0.072

a: yielding of reinforcing bar, *b*: crushing of core concrete

$$\Delta_y = \phi_y l^2/3 \tag{3.9}$$

$$l_p = h/2 \tag{3.10}$$

$$\theta_p = \phi_p l_p \tag{3.11}$$

$$\Delta_p = \theta_p(1 - 0.5 l_p) \tag{3.12}$$

3.6 Seismic Tests

Seismic performance at different seismic displacement demands of the precast cantilever columns considered in this study is expected to be larger due to higher flexibility induced from higher inter-story height observed in industrial building columns and relatively lower flexibility of supports compared to cast-in-situ columns. Since this is the first study considering post-fire seismic behavior of precast RC columns, there is an obvious need to better understand hysteretic response in order to predict seismic performance at different seismic displacement demands for a comprehensive post-fire structural performance estimation. By this way, hysteretic models capable of representing all important phenomena related to deterioration observed in experimental studies which are required in collapse assessment can be developed. Therefore, to determine the seismic performance, after exposed to the standard heating, all columns were transported to ITU Structural and Earthquake Engineering Laboratory for seismic testing. Seismic tests were carried out under constant axial loads with an axial force level of 315 kN (70.8 kips) and uni-axial lateral load reversals. In Europe, the common practice in precast industrial buildings is to keep normalized axial load level between 0.05-0.20 (Fischinger et al., 2014). Therefore, in order to reflect the actual axial loads in practice, the axial load in the presented study corresponded to 10% of the axial load bearing capacity which was calculated using Eqs. (3.13-3.14) where N is the applied axial load, N_0 is the axial load bearing capacity of the column considering only the contribution of the concrete, f'_c is

the mean compressive strength of the standard concrete cylinders around the testing days and A_g is the gross cross-sectional area of the column.

$$n = N/N_0 \tag{3.13}$$

$$N_0 = f'_c A_g \tag{3.14}$$

Seismic tests were carried out 75 days after fire tests corresponding to the approximate date where the structural performance assessment procedure including the residual structural analysis is completed. Figure 3.10a shows the seismic test setup. All columns were fixed to a strong floor by 4 strong steel bolts of 32 mm (1.3 in.) diameter. A hydraulic jack was used between the top of the columns and the steel frame to apply axial loads and the load-cell was inserted between the jack and the loading beam to measure the applied axial loads. Axial loads were applied by pinned connection supported steel frame at the base fixed to the adaptor foundation by steel rods prior to application of lateral loads simulating seismic loading. Cyclic lateral loads were applied at the top of each specimen at 1900 mm (74.8 in.) height from the base by a hydraulic actuator with a capacity of ±250 kN (56.2 kips) and ±300 mm (11.8 in.) connected to a strong reaction wall. In order to monitor the lateral and longitudinal displacements as well as rotations, numerous displacement transducers were installed at various locations along the height of the columns as shown in Figure 3.10b. ACI-374 (2013) lateral loading protocol was utilized in seismic tests (Figure 3.11). Target drift ratios calculated as the ratio of the lateral displacement at the top of the specimen to the specimen height, were ±0.1, ±0.25, ±0.5, ±1, ±2, ±3, ±4, ±5, ±6, ±7 and ±8% in pushing and pulling directions corresponding to top displacements of ±1.9 mm (0.075 in.), ±4.75 mm (0.19 in.), ±9.5 mm (0.37 in.), ±19 mm (0.75 in.), ±38 mm (1.50 in.), ±57 mm (2.24 in), ±76 mm (3.0 in.), ±95 mm (3.74 in.), ±114 mm (4.49 in.), ±133 mm (5.24 in.) and ±152 mm (5.98 in.), respectively. All displacement cycles were repeated twice as recommended by ACI-374.

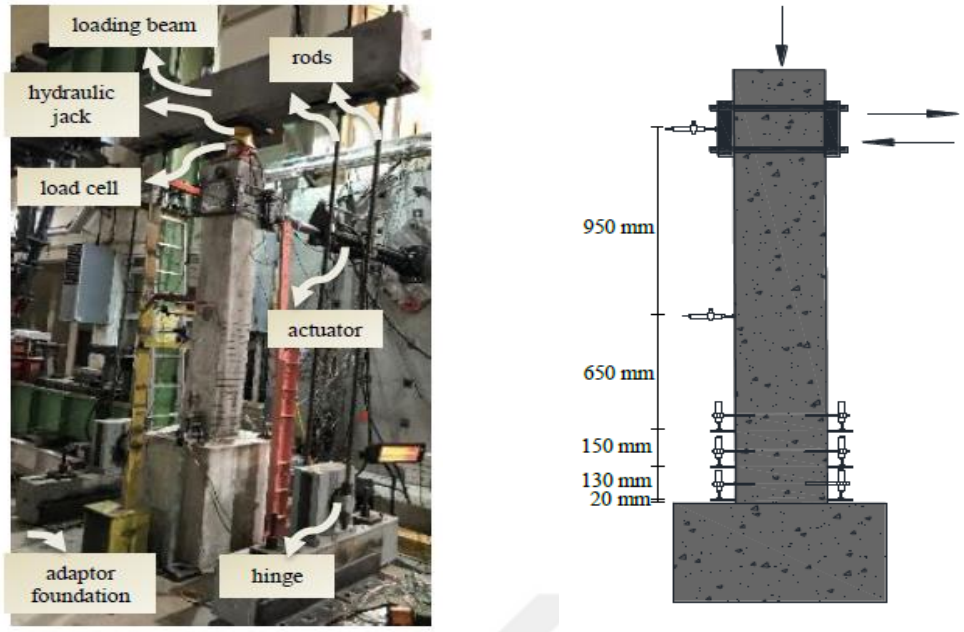

a) b)

Figure 3.10 : Seismic test set-up and arrangement of LVDTs (Note: 1 mm= 0.0394 in.).

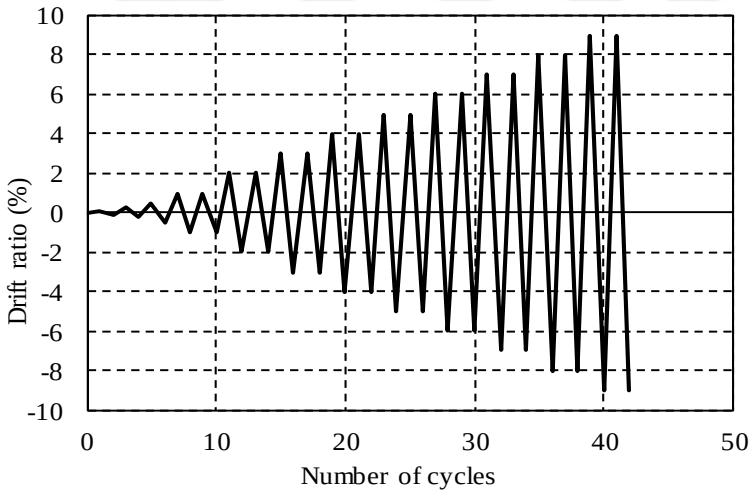

Figure 3.11 : Cyclic lateral loading protocol.

Lateral load-displacement hysteretic curves and their envelopes obtained for the tested columns are shown in Figures (3.12 and 3.13), respectively, where *P* denotes applied lateral load. In the figures, the negative drift ratios correspond to pushing direction whereas the positive ones are the pulling direction values. Analytical modelling results given in Figure 3.12 are good in predicting the lateral load-displacement behavior of precast RC columns. In analytical evaluation, all of the specimens failed with the crushing of the confined concrete since the buckling is not included in the fiber analysis whereas in the experimentally obtained load-displacement curves, failure was caused by the buckling of the longitudinal bars at further drifts (around 6% drift ratio).

It is evident from the analytical findings of this study that, when the residual properties after fire such as stress-strain behavior of concrete and reinforcement are realistically taken into account, basic principles of the structural mechanics are also applicable in the case of post-fire seismic performance assessment. As seen in Figure 3.12, all tested columns reached to their theoretical capacities indicating that inelastic response of the columns was ultimately dominated by flexure resulting with a ductile behavior. Peak lateral loads were observed at around 2% drift ratio for the columns PC-REF and PC-30M, whereas PC-60M and PC-90M columns reached their lateral load capacities at around 3% drift ratio. Damages on the potential plastic hinge region of the columns after reaching to their lateral load capacities at around 2% drift ratio and at the end of the tests are shown in Figures (3.13 and 3.14), respectively. The columns exhibited quite stable deterioration response up to a drift ratio around 6%, where buckling of the longitudinal reinforcing bars led to subsequent failure and the strength of the columns dropped following strength degradation. Mean values of pulling and pushing direction peak loads given in Table 3.4 show that, for PC-30M and PC-60M, lateral load capacities are not remarkably influenced by fire exposure whereas in PC-90M, approximately 10% reduction in ultimate lateral load is observed. This can be explained by more remarkable reduction in compressive strength for this specimen leading to lower bending moment capacity thereby lower lateral load capacity with respect to the other specimens. However, the reductions in lateral load capacities are found to be lower than that of the compressive strengths. This can be explained by the low axial loads (315 kN (70.8 kip)) applied during the seismic tests (usually experienced in such kind of precast RC columns in practice as explained above) which minimize the impact of compressive strength on the behavior as shown on axial load-moment interaction diagrams (Figure 3.14). Theoretically obtained lateral load capacities are in reasonable agreement with experimental peak lateral loads as shown in Table 3.4 (less than 7% error).

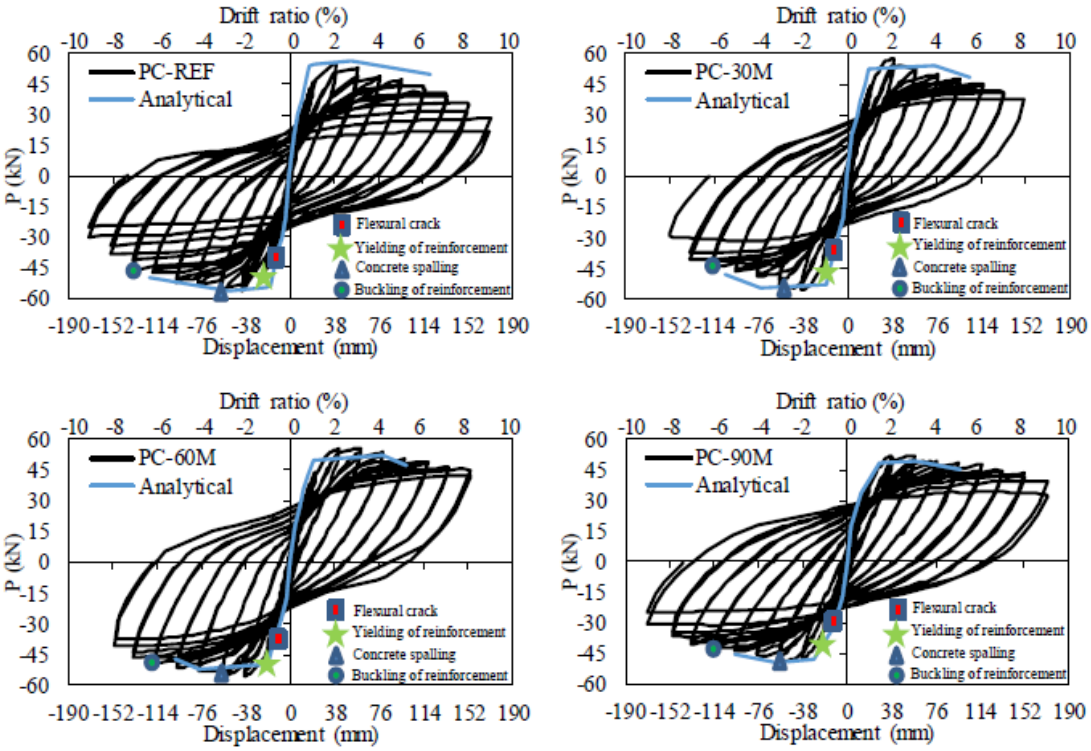

Figure 3.12 : Load-displacement curves of the columns (Note: 1 kN = 0.225 kip., 1 mm=0.0394 in.).

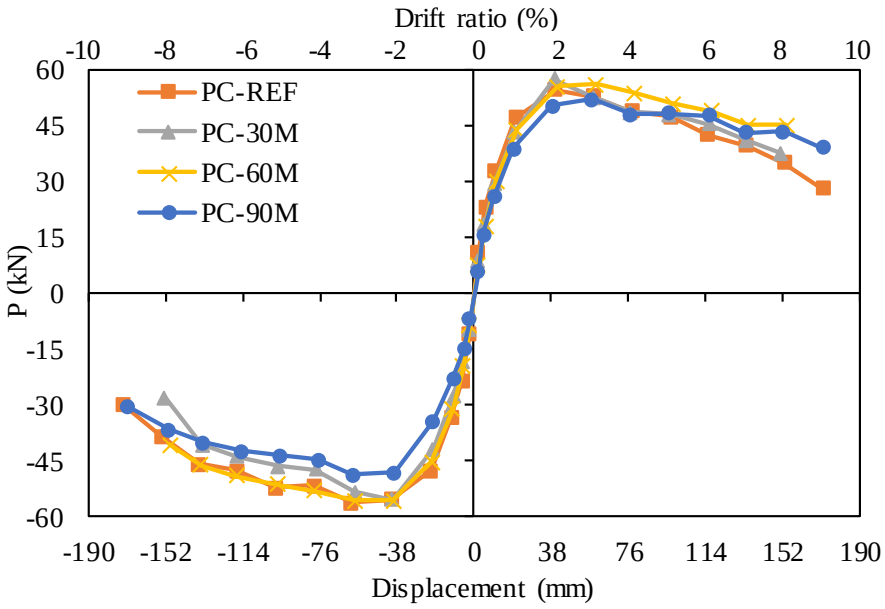

Figure 3.13 : Envelope curves of the columns (Note: 1 kN = 0.225 kip., 1 mm=0.0394 in.).

a) b) c) d)

Figure 3.14 : Damage in the plastic hinge region after 2% drift a) PC-REF, b) PC-30M, c) PC-60M, d) PC-90M.

a) b) c) d)

Figure 3.15 : Damage in the plastic hinge region at the end of the test a) PC-REF, b) PC-30M, c) PC-60M, d) PC-90M.

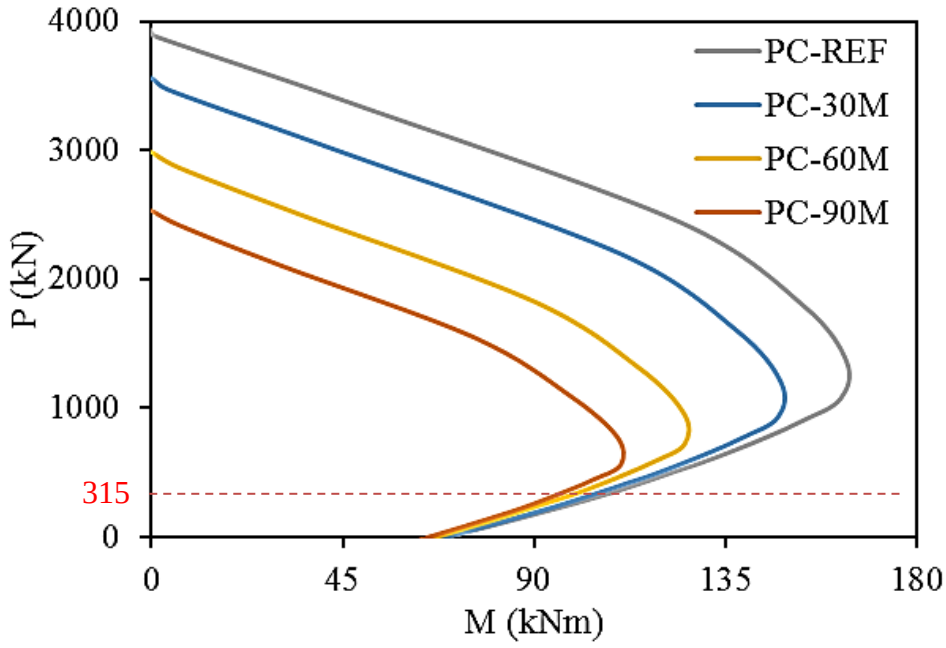

Figure 3.16 : Axial load-moment interaction diagram for the columns (1 kN = 0.225 kip., 1kNm= 0.74 kips.ft.).

Table 3.4 : Lateral load capacities and ductility parameters for the columns.

	PC-REF	PC-30M	PC-60M	PC-90M
Experimentally obtained P_{max} (kN)	55.0	56.5	55.9	50.5
Theoretically obtained P_{max} (kN)	55.2	53.7	51.9	51.0
Δ_y (mm)	22.2	26.4	25.3	29.8
Δ_u (mm)	124.9	112.3	142.4	147.1
μ_Δ	5.6	4.3	5.6	4.9

(Note: 1 kN = 0.225 kip., 1 mm = 0.0394 in.)

For comparison of the column performances in terms of sustaining their ductility, displacement ductility factor (μ_Δ), which is the ratio of the ultimate displacement (Δ_u) to the yield displacement (Δ_y) is calculated for each column as schematically shown in Figure 3.17. Ultimate displacement is defined as the point on the post peak branch of the average envelope curve (absolute average of pushing and pulling directions) where the lateral strength is 80% of the maximum lateral strength ($P = 0.8P_{max}$) as recommended by previous researchers (Sheikh and Khoury, 1993; Sheikh and Yau, 2002; Iacobucci et al., 2003; Memon and Sheikh, 2005). Yield displacement is also obtained from the average envelope curve as the displacement corresponding to the maximum lateral load (P_{max}) on straight line joining origin and the point at 75% of the peak load on ascending portion of the envelope curve ($P=0.75P_{max}$) as recommended by previous researchers (Paulay and Priestley, 1992). The ductility of the columns is not found to be influenced from fire exposure up to 60 minutes, whereas the column PC-90M exhibited around 13% ductility reduction with respect to the reference column (Table 3.4).

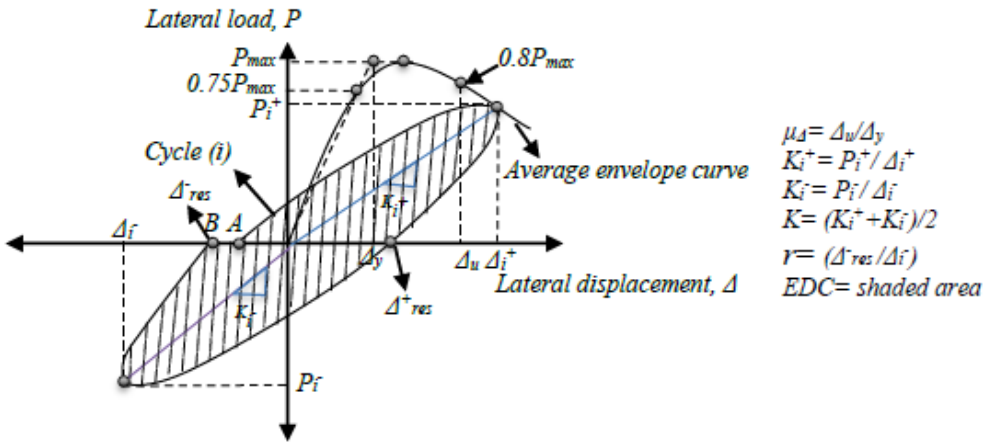

Figure 3.17 : Definition of ductility parameters.

It should be noted that in PC-30M specimen, local defects close to the plastic hinge region in concrete cover were observed after the fire tests. As shown in Figure 3.4,

these fire induced vertical cracks (denoted as vertical black lines) advanced remarkably at around 0.5% drift ratio (9.5 mm (0.37 in.) top displacement). This defect caused premature spalling of concrete cover for this specimen which resulted with relatively higher yield displacement (lower stiffness), lower ultimate displacement and ductility factor. Even though fire exposure enhanced both of the yield and the ultimate displacements of the fire exposed specimens, main deficiency related to the fire damage occurred on ductility ratio of the column PC-90M since the enhancement in yield displacement was more remarkable than that of the ultimate displacement. Stiffness degradation of the column PC-90M induced from fire exposure, can be accounted for higher yield and ultimate displacements. Nevertheless, previous researches reported that the displacement ductility factors higher than 3.5 correspond to a fully ductile response that can reasonably be achieved at carefully identified and detailed inelastic regions (Paulay and Priestley, 1992). When this value (3.5) is compared to the values given in Table 3.4, post-fire ductility of all columns appear satisfactory in terms of structural response.

Concrete is known to be more porous and less stiff when exposed to elevated temperatures. Therefore, loss of stiffness induced from fire exposure is a key parameter to be considered in post-fire performance assessment of RC members. In order to clarify the variation of secant stiffness after a fire, stiffness values of the columns are evaluated from the maximum lateral load divided by the displacement at the peak of each load cycle considering the mean value of pushing and pulling directions (denoted as *K* in Figure 3.17). The variation of secant stiffness versus the horizontal displacement is shown in Figure 3.18a. As seen in Figure 3.18a, the initial stiffness values for the fire exposed columns were substantially lower than the PC-REF. The reductions in initial stiffness were around 7%, 20% and 33% for the columns PC-30M, PC-60M and PC-90M, respectively, compared to the column PC-REF. However, the drop in stiffness degradation can be more pronounced in PC-REF compared to the heated columns. New cracks initiated after imposing the cyclic loading for unheated specimen (PC-REF), while fire induced existing cracks advanced for the fire exposed columns. Therefore, slower rate of stiffness degradation was observed in fire exposed specimens with respect to the reference one which is beneficial for precast RC columns in order to compensate seismic actions since brittle failure regarding to sudden loss of stiffness is eliminated. Fire exposure influenced the residual stiffness more remarkably at smaller drift ratios whereas the stiffness of the columns was similar after around 2%

drift ratio (around yielding). This can be explained with the fact that the structural response is governed by concrete residual properties up to yielding, whereas after yielding, reinforcement characteristics which have been restored after cooling are more dominant.

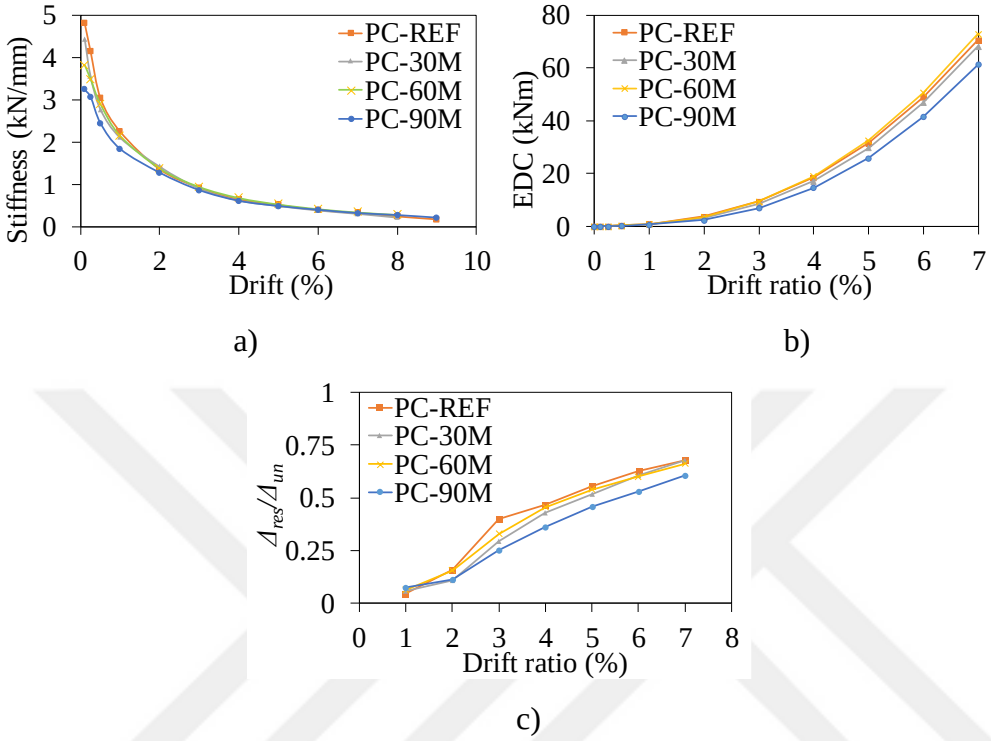

Figure 3.18 : a) Stiffness degradation, b) cumulative energy dissipation capacities and c) residual displacement levels for the columns (1kNmm = 8.85 lbf.in., 1kNm= 0.74 kips.ft.).

The area enclosed by the first hysteretic loop of each target displacement is defined as the energy dissipated by the columns which represents the ability to consume seismic energy through the plastic deformations. Cumulative hysteretic energy dissipation capacities of the columns (EDC), which is the summation of these areas (Figure 3.17), are plotted versus increasing drift ratios (Figure 3.18b). The figure clearly indicates that the lowest energy was dissipated by PC-90M due to the relatively lower lateral load capacity while it was similar among the rest of the specimens. EDC of the columns were similar up to 2% drift ratio (around yielding), whereas the increase rate in EDC was found to be more accelerated for the columns other than PC-90M after yielding. This can be attributed to the fact that after yielding, most of the energy was consumed by the inelastic deformation of the columns including the formation of new cracks and the yielding of reinforcing bars. EDC was reduced about 15% in PC-90M at 7% drift with respect to PC-REF where the difference between the other specimens

was less than 5%. No appreciable pinching was observed in the load-displacement curves of the columns highlighting acceptable performance in terms of energy dissipation.

Residual displacements are one of the most important parameters in terms of measuring post-earthquake functionality and feasibility of repairing fire-damaged structures. The residual plastic displacement ratios (*r*) of the columns are obtained by dividing the residual lateral plastic displacements after unloading, when the applied lateral load is zero (Δ_{res}) to the specified peak displacement for each drift ratio (Δ_{un}) in pushing direction which is illustrated in Figure 3.17. The *r* values are given in Figure 3.18c with increasing drifts. As seen in this figure, after flexural yielding, the *r* values are the lowest for the PC-90M, whereas it is similar for the rest of the columns demonstrating more excessive permanent flexural damage associated with yielding of the reinforcing bars in PC-90M (Goksu et al., 2014). The reason of lower residual displacements for PC-90M can be attributed to potential deterioration in bond between concrete and the reinforcing bars. The limited deterioration in bond can be validated considering the good agreement in the theoretical and experimental test results as shown in Figure 3.12 as well as the minor difference at residual displacements for all specimens as seen in Figure 3.18c. At 7% drift, the ratio was around 0.65 for the columns PC-REF, PC-30M and PC-60M specimens and around 0.6 for PC-90M corresponding to around 10% reduction in plastic deformations for PC-90M with respect to the other specimens. It should be noted that relatively lower residual deformations observed in PC-90M can be deemed as a positive property under seismic loads.

Base moment-average curvature relationships for the columns are presented in Figure 3.19. In the figure, negative values show the values of pushing direction, where the positive ones correspond to pulling direction. The base moment was calculated by multiplying the measured lateral load with the shear span of 1900 mm (74.8 in.) extending between the acting point of the lateral load and the column-foundation interface where the contribution of the axial load was also taken into account. The curvature distributions of the columns are measured using displacement transducers attached at the potential plastic hinge region over 0-20 mm (0-0.79 in.), 20-150 mm (0.79-5.9 in.) and 150-300 mm (5.9-11.8 in.) heights above the column-foundation interface (Figure 3.10b). Due to the low axial forces and closely spaced stirrups providing effective confinement, large plastic rotations in plastic hinge regions are

observed for all specimens. As depicted in Figure 3.19, the curvature was concentrated mainly over a height of approximately 0-150 mm (0-5.9 in.) for PC-REF and PC-30M which is the half depth (h/2) of the column cross section. This height was between 0-300 mm (0-11.8 in.) for PC-60M and PC-90M corresponding to full depth (h) of the column dimensions in loading direction, respectively. This behavior indicates that flexural damage is distributed over a larger plastic hinge length for PC-60M and PC-90M with respect to PC-REF and PC-30M specimens. This is attributed to the considerable loss of concrete compressive strength with an increase in fire duration which results with loss of axial load capacity and thereby an increase in axial load ratio (applied axial load/axial load capacity). Besides, observation of formation of the cracks during the cyclic loading demonstrated that, cracks were distributed over a larger hinging zone with an increase in duration of fire. The widths and lengths of the cracks were also smaller in fire exposed specimens pointing out the larger hinging zone triggered by fire exposure (Figures 3.14 and 3.15). It should be noted that, realistic determination of potential plastic hinge lengths of precast RC columns is of vital importance within the context of post-fire seismic performance assessment of existing buildings. The ratio of the plastic hinge length to the height of the column decreases with an increasing shear span ratio of the precast RC columns (Fischinger et al., 2008). However, there is no study demonstrating the influence of fire on plastic hinge length of the precast RC columns. Hence, there is a strong need to more experimental studies in order to clarify the plastic hinge length after fire damage. It should be noted that no damage, or rotation of any socket foundations of the tested columns were observed during the seismic tests, indicating that the socket foundations provided substantial fixity at the base of the precast columns. Also, no cracks were observed through the grout and thus seismic forces were resisted through the cantilever action of the precast concrete columns resulted by rigid column-to-foundation connection detail. Similar seismic behavior for precast concrete columns with socket foundation was also reported by previous studies in terms of no grout damage even if thicker grout thicknesses are used (Karadogan et al., 1997; fib-27, 2004; Skalko, 2013; Magliulo et al., 2014).

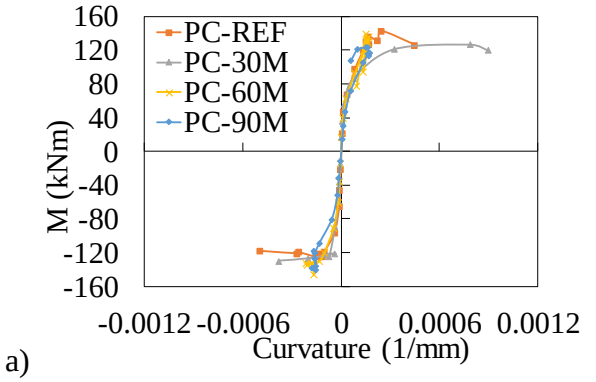

a)

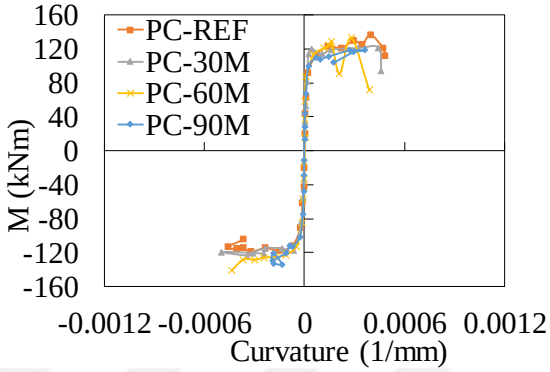

b)

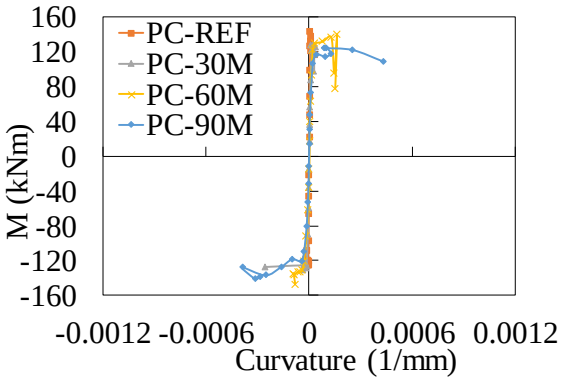

c)

Figure 3.19 : Moment-average curvature relationships over a) 0-20 mm, b) 20-150 mm and c) 150-300 mm (Note: 1kNm= 0.74 kips.ft, 1 mm = 0.0394 in.).

Since precast/prestressed concrete began to emerge in the building marketplace over the last decades, complying with fire resistance became a challenge for engineers in terms of fitting into the prescriptive assembly descriptions of the current design codes, so testing these assemblies became the common method for approval in practical applications (Magliulo et al, 2014). Therefore, the presented experimental research also serves as a basis for development of post-fire seismic resistance assessment procedures for concrete assemblies that could possibly be included in existing performance assessment guidelines. It should be noted that present study focuses on columns of typical low-rise precast RC structures with low axial load (i.e. 10% of the

axial load capacity) in which the effect of axial load on the behavior is quite limited. Therefore, fire tests in this study were conducted without axial load. It should also be noted that fire tests were executed without axial load by other researchers as well (Yaqub and Bailey, 2012; Bailey and Yaqub, 2012).

3.7 Conclusions

Based on the experimental and analytical findings of the study that investigated the post-fire seismic behavior of 4 full-scale precast RC columns, the following conclusions are drawn.

- All specimens reached their theoretical flexural yield capacity and none of the specimens experienced shear failure or noticeable shear damage. The analytical model was in reasonable agreement with the experimental results in terms of predicting the lateral load-displacement envelope and the failure mode. This indicates that basic principles of structural mechanics are applicable in the case of post-fire seismic performance assessment when the effect of fire on material characteristics is carefully considered.

- Post-fire lateral load capacities were not considerably affected with an increase in fire duration up to 60 minutes. For 90 minutes of fire exposure, about 10% reduction in lateral load capacity of the column was observed. Concrete residual properties were seemed to be the reason for the reduction in lateral load capacity of this column. It is worth to note that typical low axial loads in precast RC columns were observed to limit the influence of concrete compressive strength loss on post-fire seismic behavior of the columns. The reduction in lateral load for the column exposed to 90 minutes of fire also caused a slight reduction on the energy dissipation capacity.

- Ductility factors and lateral drift capacities of the columns were not remarkably influenced from fire exposure up to 60 minutes and for the specimen subjected to 90 minutes of fire exposure, ductility reduction was around 13% with respect to the unfired column. This reduction is attributed to the non-proportional increases of the yield and ultimate displacements during post-fire seismic tests

which induced from reduced stiffness after fire. This slight reduction in ductility can be expected for the tested precast RC columns with typical low compressive axial force (as in practice), symmetric reinforcement and considerable lateral confinement.

- Unlike the accumulation of plastic deformations within a height equal to half depth of the column cross section from the column-footing interface in the case of the reference specimen and 30 minutes of fire exposure, plastic deformations were observed to be distributed within a height equal to around full depth of the column cross section during post-fire seismic tests of 60 and 90 minutes heated columns.

- The initial stiffness of the fire damaged specimens was reduced up to around 33% due to the existing cracks induced from fire exposure. Initial stiffness reductions were almost proportional to the duration of the fire exposure. The reductions in stiffness values were observed to be higher than the reductions in the lateral load capacities. Fire exposure influenced the residual stiffness more remarkably up to yielding since the structural response is governed by concrete residual properties up to yielding, whereas after yielding, reinforcement characteristics which have been restored after cooling are more dominant.

It should be noted that these conclusions are based on the results from the specific tests that are presented in this paper. There is an obvious need for more experiments in order to understand the behavior more generally.

4. IMPACT OF TIME AFTER FIRE ON POST-FIRE SEISMIC BEHAVIOR OF RC COLUMNS

4.1 Abstract

Autogenous recovery after fire exposure is known to be effective on the behavior of reinforced concrete structural members. This is substantially attributed to the variations on the residual mechanical properties of concrete as a function of time after fire. For the first time, in this study, an experimental study was carried out to examine the impact of time after fire on (i) post-fire behavior of small-scale specimens (cubes and cylinders), (ii) seismic behavior of full-scale flexure-controlled reinforced concrete columns. Outcomes of the post-fire seismic test results were investigated on a total of four columns one of which was an unheated reference specimen, whereas the other three were heated for 90 minutes following the ISO-834 fire curve. Seismic tests were carried out on fire exposed columns 30, 60 or 360 days after fire exposure. The test results indicated that 90 minutes of fire exposure caused a reduction in lateral load capacity, ductility and stiffness of the columns with respect to the unheated column. On the other hand, impact of time after fire exposure on residual lateral load capacity and ductility of the columns was found to be limited while the column subjected to seismic test 30 days after fire exposure exhibited less stiff behavior with respect to the columns tested later. Furthermore, an analytical study is conducted for the prediction of seismic behavior of reinforced concrete columns after fire exposure considering the variations in residual properties of concrete by time, and the proposed model is found to be in good agreement with the test results.

This chapter is adopted from the journal paper: Demir, U., Goksu, C., Binbir, E. and Ilki, A. (2020). Impact of time after fire on post-fire seismic behavior of RC columns. Structures Journal 26, 537-548.

4.2 Introduction

Reinforced concrete (RC) columns are known to lose a fair amount of compressive strength and stiffness after being exposed to fire (Yaqub et al., 2013). However, the loss of residual mechanical properties of concrete due to fire exposure is largely recoverable in the long-term (Poon et al, 2001). Therefore, autogenous recovery of concrete as a function of time after cooling is of paramount interest. Post-cooling behavior of concrete can be separated into two stages (Ilki and Demir, 2019). At the first stage, after cooling to ambient temperatures, it is observed that the compressive strength and elastic modulus of concrete may be further reduced from its original strength under high temperatures until a period of time because of continuing disintegration of the microstructure in concrete. This first stage of post-fire cooling period is reported to be approximately 30 days from the beginning of the cooling (Harada et al., 1972, Papayianni and Valiasis, 1991). Because of the reaction between the concrete and moisture in the air (needed for re-hydration of cement), after around 30 days, recovery in compressive strength begins referring to the second stage of cooling period and concrete can recover up to 90% of its original strength in one year after being subjected to temperatures of 500 ºC (Lie, 1992). This is attributed to the fact that capillaries initially filled by C-S-H gels are opened during fire exposure and refilled by rehydration products due to the moisture in air owing to the carbonation process (Poon et al, 2001). Hence, this rehydration process reduces the porosity of concrete and results in strength recovery. However, there is not a consensus between the reduction ratios in compressive strength depending on the time after fire due to the fact that residual compressive strength after fire may be affected by various parameters such as concrete composition, heating and cooling scenario, specimen size, axial restraint. For instance, Harada et al. (1972) indicated that residual compressive strength decreases up to 50% of the initial value 30 days after fire, and this reduction ratio does not further vary until 60 days after fire exposure. On the other hand, Papayianni and Valiasis (1991) mentioned that the compressive strength would reduce to about 41% of the original value 30 days after being subjected to fire and then around 15% enhancement on compressive strength is expected for the next 30 days (at the age of 60 days after fire, residual compressive strength ratio is about 48% of the original value). Residual mechanical properties of reinforcement are also effective on the behavior after fire. Cooling would often restore the material to its original state for

temperatures up to 450 °C for cold work and 600 °C for hot rolled steel reinforcement (Lie, 1992; Poon et al., 2001; Concrete Society, 2008) irrespective of time after fire. As can be drawn from the findings of the literature review, the load-bearing capacity of a structure tends to decrease after the maximum temperature is achieved, then reaches to a minimum value, and finally recovers partially or completely after cooling (Gernay and Franssen, 2015). These variations in load-bearing capacity due to the thermal inertia and additional loss of material mechanical properties during cooling stage, may result in structural failure during the cooling phase of a fire rather than under elevated temperatures (Gernay and Dimia, 2011; Behnam, 2018; Lakhani and Osbolt, 2019). This phenomenon is one of the major reasons that formed a motivation for the present study.

In other respects, performance of any building subjected to fire should be inspected considering probable future earthquakes in earthquake prone areas. Weaknesses in RC structures arising from insufficient lateral load capacity and stiffness due to low concrete compressive strength and substandard detailing of reinforcing bars, result with vulnerable buildings during earthquakes (Ilki and Celep, 2012). Fire damage may also cause inadequate concrete compressive strength even for well-engineered structures, and can lead to vulnerable building classes as commonly exist in developing countries. Keeping this issue in mind, post-fire seismic behavior of RC structural elements designed according to current guidelines is simply unknown up to date. Majority of the existing studies considered the behavior after cooling under only service loads combined with uniaxial/biaxial bending (Lie et al., 1986; Jau and Huang, 2008; Chen et al., 2009), and the studies investigating fire-damaged RC columns under seismic loading have not been extensive. Studies conducted by Yaqub and Bailey (2012) and Bailey and Yaqub (2012) included seismic retrofitting of shear-critical RC columns after fire exposure while Mostafaei (2013) pointed out hybrid fire testing principles on a single high strength concrete column under monotonic lateral loading. None of these studies considered the post-fire seismic behavior of conventional flexure-controlled RC columns. Furthermore, impact of autogenous recovery in concrete after fire on the post-fire seismic behavior of RC columns has not been investigated yet neither for shear nor flexure-controlled columns. As mentioned above, structural performance assessment of a fire-damaged structure may lead to misleading results due to the reduction in compressive strength of concrete particularly in the initial days after fire exposure. Therefore, this study presents the experimental findings

on the effect of fire damage on seismic behavior of RC columns for the first time with a particular focus on the impact of autogenous recovery of concrete with time after cooling. In the scope of this study, uniaxial compression tests were carried out on cylinder and cube specimens in order to determine the variation of compressive strength depending on the time after fire. Also, four full-scale RC columns were designed and constructed complying with the major design codes (e.g. ACI-318, 2014). The columns except the reference one, were exposed to ISO-834 (ISO, 1999) standard fire for 90 minutes, and then kept in ambient conditions for 30, 60 or 360 days until the test day. The columns were then subjected to constant axial loads combined with reversed cyclic lateral displacements simulating seismic loading. The responses of the columns were analyzed in terms of lateral load-displacement relationships, ductility and stiffness. However, the column tested 360 days after fire experienced premature buckling of longitudinal bars due to concrete settling problems during casting process and therefore, only the hysteretic response of this column was given in the study, and it was excluded from further discussion. A combined thermal and structural analysis was also conducted to predict the post-fire seismic response of the columns considering the variations in mechanical properties of concrete by time after fire. The results of the analytical work demonstrate that the generated algorithm within the current study is in good agreement with the test results. Demonstrated applicability of the given algorithm within the manuscript in terms of prediction of post-fire seismic response considering the compressive strength variation with time, may serve to the prediction of the response of the column tested 360 days after fire as well.

4.3 Materials and Methods

4.3.1 Materials

The calcareous aggregate concrete mix-proportions of the specimens are presented in Table 4.1. Three cylinder specimens of 150×300 mm size were also reserved for each column to monitor the compressive strength of the columns at the time of seismic tests. The mean unfired concrete compressive strength, obtained based on these cylinder tests at around the age of 16 months corresponding to around 60 days after the fire tests was around 36 MPa. The stress-strain relationships of the unfired specimens and the specimens exposed to fire for 90 minutes are presented in Figure 4.1a, where for

instance 90m-30d stands for the specimen exposed to 90 minutes of fire and tested 30 days after fire. As seen in this figure, the average concrete compressive strength of the cylinder specimens (around 6 MPa) exposed to 90 minutes of fire was obtained to be approximately 15% of that of the unfired specimen (36 MPa). Besides, compressive strain corresponding to the peak compressive strength increased with fire exposure while compressive strength decreased. In order to determine the variation of compressive strength depending on the time after fire, 150×150×150 mm cube specimens (three cubes for each series) were also tested under uniaxial compression. These test results indicated that compressive strength of concrete used in the present study is reduced up to 15 days after fire exposure and then, it reinstates original strength after one year (Figure 4.1b). It should be noted that the increase in dilatancy of the concrete due to heating increases the variability of axial strain measurements, which indicates that non-homogeneities in the concrete are exacerbated by fire exposure. Therefore, Figure 4.1a intentionally shows the trend in axial stress-strain response after fire by selecting the traces best matching with the cube strength results. This is because of improving clarity of the presentation in the paper. There is not a consensus between the findings in the literature on post-fire compressive strength variations in concrete with time after fire as aforementioned and the small-scale compression tests in the present paper are intended only to bring this fact fore. For this respect, rather than considering the experimental compression test results obtained in the current study, the compression test results of Papayianni and Valiasis (1991) is considered for the numerical work, where the compressive strength of concrete is reduced.

Table 4.1 : Concrete mix-proportions.

Material	Weight (kg/m^3)
Cement (CEM 42.5 R)	300
Sand (0-4 mm)	920
No I Aggregate (5-12 mm)	507
No II Aggregate (12-22 mm)	490
Superplasticizer (Sikament-300)	3.6
Water	124

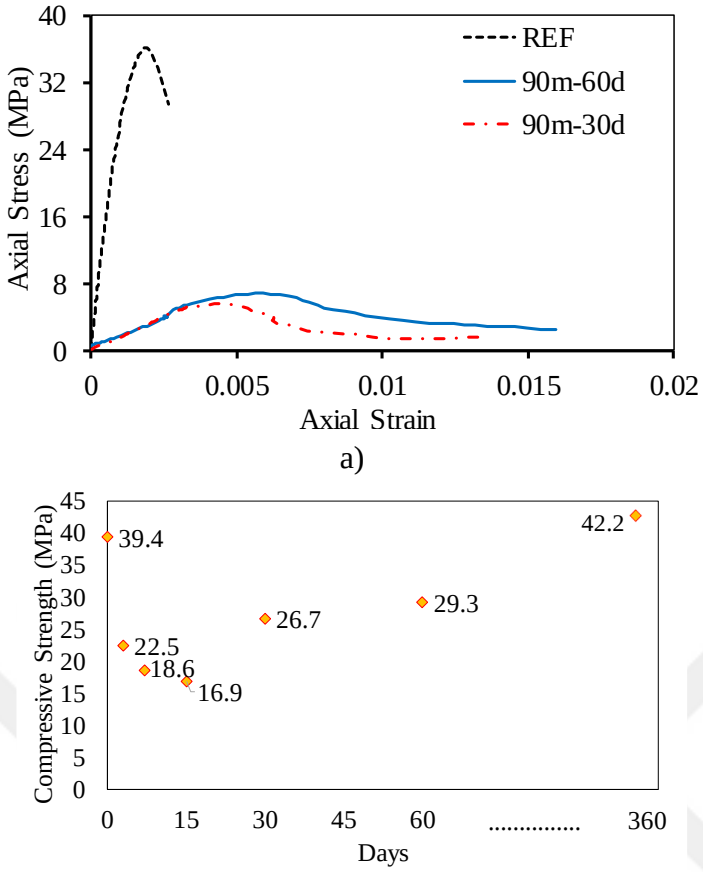

Figure 4.1 : a) Stress-strain relationships of cylinder specimens, b) strength recovery with time in cube specimens. Note: Day 0 refers to the day of fire and after fire exposure.

Four identical cantilever RC columns were cast with cross-sectional dimensions and heights of 300×300 mm and 1500 mm, respectively (Figure 4.2). Each column was manufactured with an RC foundation block with dimensions of 700×700×500 mm that was connected firmly to the strong floor during the seismic tests. Columns were reinforced longitudinally with four 20 mm diameter deformed bars, which had a yield strength of 461 MPa. Lateral reinforcement with a yield strength of 472 MPa was provided in the form of 10 mm deformed bars spaced at 100 mm spacing center-to-center. The concrete cover of 40 mm was designed to conform with the major building fire codes (ACI 216, 1997; CEN, 2004; Turkish fire regulation, 2007). In order to obtain the mechanical properties of the reinforcing bars, 300×300×500 mm RC specimens were cast with the same concrete batch and reinforcing configuration with the tested full-scale RC columns in this study. These specimens were also subjected to the same fire exposure where the maximum temperatures along the reinforcing bars did not exceed 580 °C. Then, reinforcing bars were taken out around the test day, and

subjected to uniaxial tension test. The mechanical properties of the longitudinal (diameter of 20 mm) and transverse (diameter of 10 mm) reinforcing bars under ambient temperatures, and after cooling are presented in Table 4.2 where f_y and ε_y are the yield strength and strain, f_{max} and ε_{max} are the maximum strength and strain, f_u and ε_u are the ultimate strength and strain, respectively. As seen in Table 4.2, the residual properties of the reinforcing bars are recovered as reported by Neves et al. (1996) in this temperature range (up to 600 °C). The columns are designated as REF (the reference column), 90m-30d (exposed to fire for 90 minutes and tested after 30 days) and 90m-60d (exposed to fire for 90 minutes and tested after 60 days). The columns were designed with a shear span-to-depth ratio of 4 resulting with a dominate flexure-controlled failure mode while the foundations were overdesigned for eliminating the possible effects of foundation on the behavior. It should be noted that the columns were conditioned under ambient temperature (around 20 °C) and humidity (around 58%) in the laboratory environment for 14 months after casting until fire tests had been executed. Thus, possible variations in mechanical properties of concrete due to aging was eliminated and the required minimal conditioning duration between casting and the fire test (at least 3 months) to prevent the concrete cover spalling was ensured as recommended by the relevant codes (e.g. EN 1363-1, 2012).

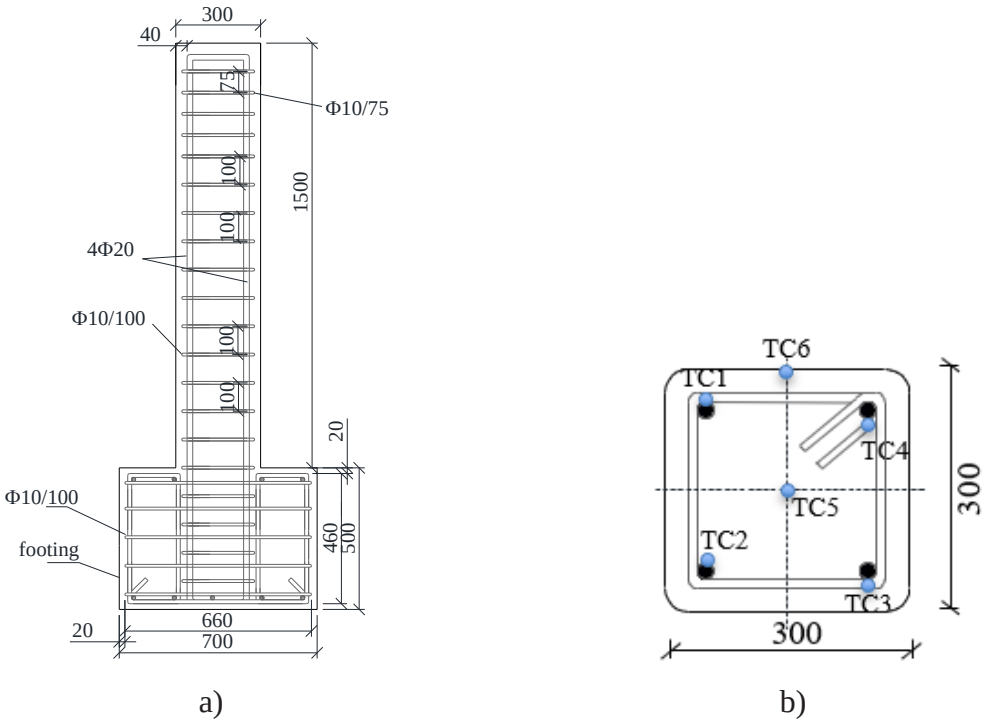

Figure 4.2 : a) Elevation view, b) Plan view and location of thermocouples. Note: Dimensions are in mm.

Table 4.2 : Mechanical properties of reinforcing bars.

Diameter of reinforcing bar (mm)	Fire exposure (minutes)	f_y (MPa)	ε_y	f_{max} (MPa)	ε_{max}	f_u (MPa)	ε_u
20	-	472	0.0023	569	0.0965	525	0.15
10	-	483	0.0025	557	0.0998	525	0.10
20	90	442	0.0024	549	0.0992	516	0.16
10	90	457	0.0024	552	0.0992	522	0.11

4.3.2 Fire tests and thermal modelling

Three columns were exposed to ISO-834 standard fire for 90 minutes except the insulated footings. The fire tests were carried out at a large-scale multipurpose test chamber with 3.2 m in depth×4 m in width×3 m in height (Figure 4.3). The fire furnace is surrounded by aerated autoclaved concrete (AAC) walls and slabs. Heat was provided by eight natural gas burners aligned within the furnace. Eight thermocouples were utilized to measure the furnace temperature. In addition, for measuring the concrete and reinforcing bar temperatures, a total of six thermocouples (type-K NiCr-Ni) of 0.91 mm thick were installed at the mid-height of the cross section for each column as shown in Figure 4.2b. Figure 4.4 shows the time-temperature curves in the fire test. In Figure 4.4, temperature “surface” is obtained from TC6 over the surface of the columns, temperature “out” is obtained from TC1 and TC3 over the outside of the reinforcing bars, temperature “in” is obtained from TC2 and TC4 over the outside of the reinforcing bars, and temperature “center” is obtained from TC5, which is installed at the center of the columns. Maximum temperature of 1005°C was measured in the furnace, which was observed to be well-matching with ISO-834 fire curve. Minor spalling was occurred in the heated columns in the form of falling off small chunks of concrete from the surface of the columns (Figure 4.5). When the furnace naturally cooled down to room temperature with a cooling rate of around 0.5 °C/min (calculated between the end of heating and being cooled down to the room temperature), the columns were taken out of the furnace (around 24h after the end of the heating), and stored in the laboratory for 30, 60 or 360 days until the time of the seismic tests.

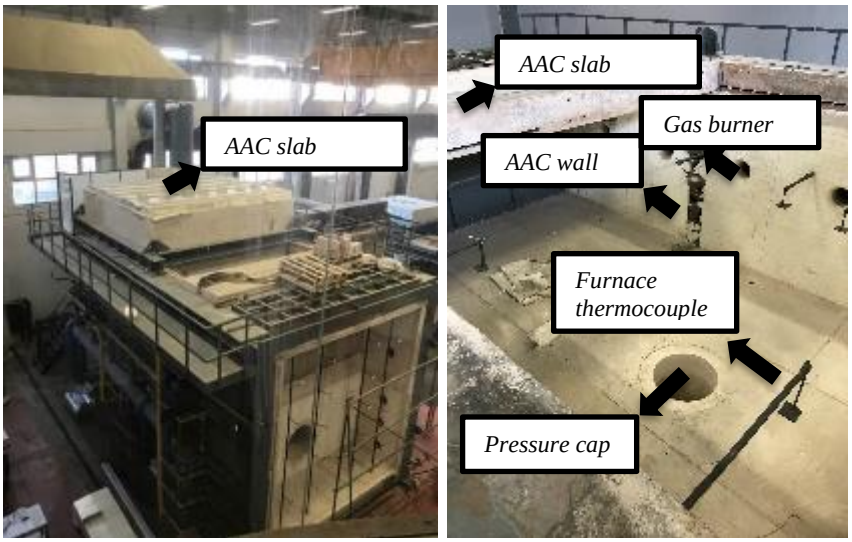

a) b)

Figure 4.3 : a) Outside, b) inside view of the fire test furnace.

Thermal calculations were also executed for estimating the temperature distribution in the quarter column sections throughout the fire test using a finite element software, SAFIR (Franssen and Gernay, 2017) (Figure 4.4d). Calcareous concrete (CALCONC_EN) and steel (STEELEC2_EN) material properties as given in Eurocodes (CEN, 2004) were assigned to the corresponding elements of the cross-sections of the columns. Heat transfer mechanism was determined with the assumption that heat is distributed by conduction at the boundary of the cross section whereas it is exchanged with the environment by convection and radiation. For conduction, heat exchange is evaluated using Fourier heat transfer equation. For convection and radiation, heat exchange is determined using Eqs. (4.1 and 4.2) where h_c is the convective heat flux between gas and solid (W/m²), h is the coefficient of convection (W/m²K), T_g is the temperature of the gas (K), T_s is the temperature at the surface of the solid (K), h_r is the radiative heat flux emitted by a solid (W/m²), σ is the Stefan-Boltzman constant (5.67 × 10-8 W/mK^4), ε is the emissivity of the solid (-).

$$h_c = h(T_g - T_s) \tag{4.1}$$

$$h_r = \sigma \varepsilon {T_s}^4 \tag{4.2}$$

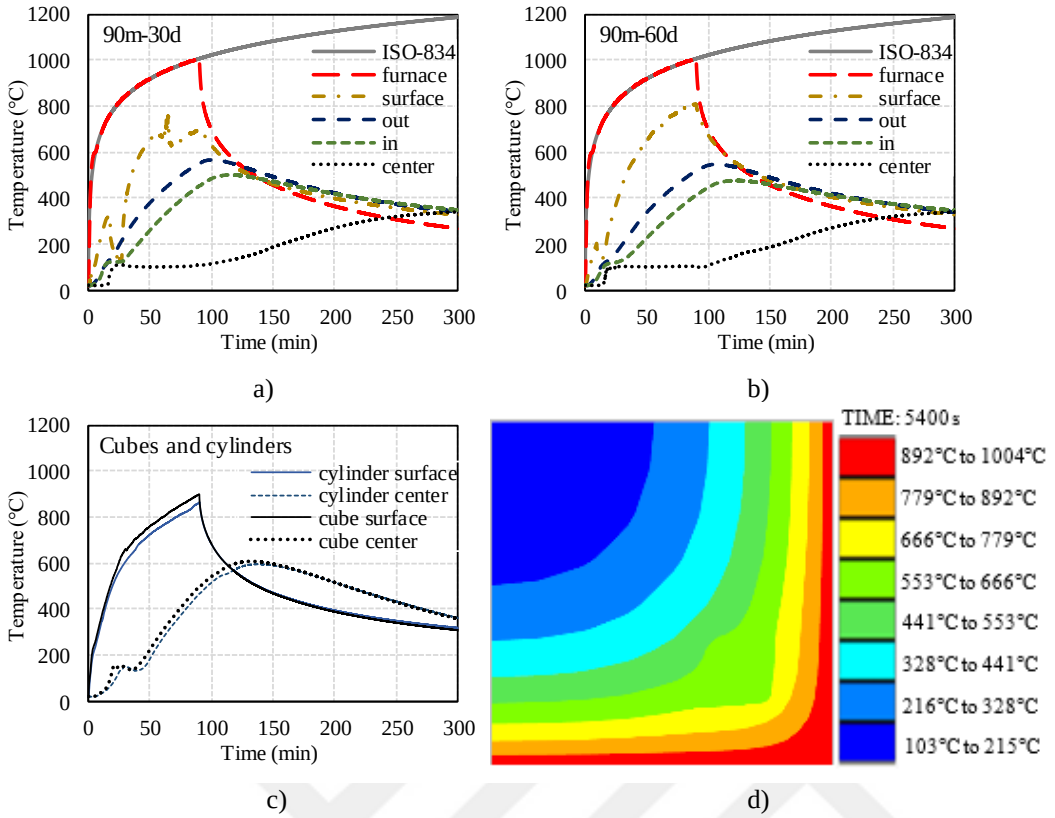

Figure 4.4 : Temperatures in the specimens during the fire tests for the columns a) 90m-30d and b) 90m-60d, c) cubes, d) temperature predictions with thermal calculations.

Figure 4.5 : Comparison of column surfaces for a) unheated, b) heated columns.

4.3.3 Instrumentation, test setup, and loading procedure for seismic tests

Seismic tests were executed 30, 60 or 360 days after the fire tests under constant axial load of 630 kN corresponding to $0.2f'_cA_g$ where f'_c is the compressive strength of unfired concrete at the day of seismic test, and A_g is the gross cross-sectional area of the columns representing common column axial loads in mid-rise RC structures.

Repeated lateral displacement reversals were applied 1200 mm above the column-footing interface using an MTS actuator with a capacity of ±250 kN, ±300 mm which was connected to a strong reaction wall. The seismic test setup is shown in Figure 4.6. All columns were fixed to a strong floor by 4 strong steel bolts of 32 mm diameter. A hydraulic jack was utilized between the top of the columns and a steel loading beam to apply the axial load. The beam was pin supported at the base. A load-cell was used between the jack and the loading beam to measure the applied axial load. As shown in Figure 4.6b, in order to monitor the lateral and longitudinal displacements as well as rotations, numerous displacement transducers were installed at various locations along the height of the columns. It should be noted that out-of-plane tip displacements and rotations in foundation blocks were observed to be negligible. ACI-374 (ACI, 2013) displacement-controlled lateral loading protocol, which is based on yield drift ratios obtained from section analysis, was used in simulating seismic loading as shown in Figure 4.6c.

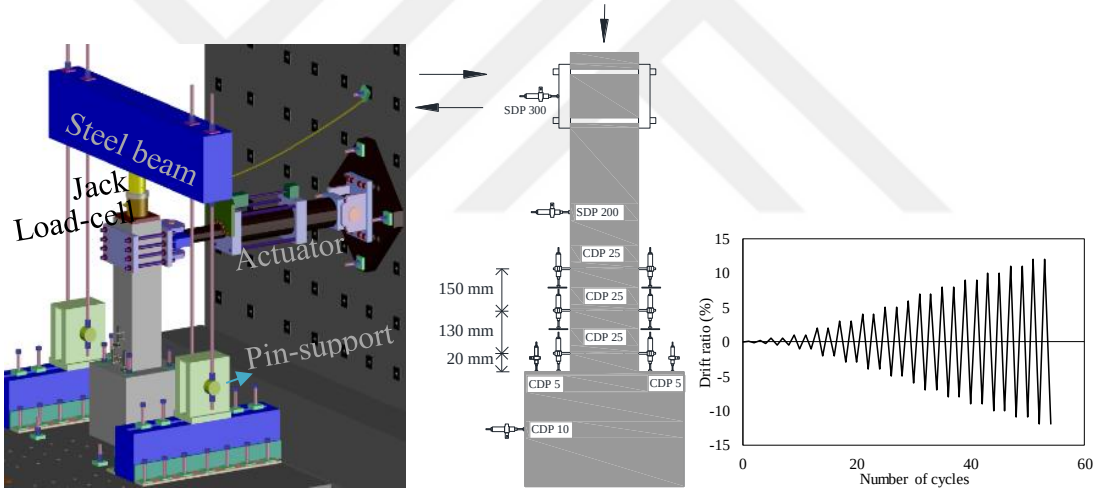

a) b) c)

Figure 4.6 : a) Seismic test set-up, b) arrangement of LVDTs, c) loading protocol.

4.4 Prediction of Post-Fire Seismic Response

Seismic responses of the columns are estimated through a combined thermal and structural modelling. As abovementioned, thermal analysis is conducted using SAFIR software in order to obtain the temperature gradients at various depths in the heated column sections. SAFIR is capable of sequential modelling of the thermal and structural behavior for RC structural members. However, in the presented study, only the thermal behavior (i.e. temperature gradients during the heating and cooling phases) is estimated using SAFIR, while the structural response is determined using

conventional RC theory as defined below. Such way of analysis is preferred in order to investigate the applicability of the conventional theory in case of post-fire seismic actions which may be more practical for the researchers in earthquake engineering area. Furthermore, residual material properties of concrete in SAFIR is considered based on Eurocode approach in which the reductions after fire (i.e. in compressive strength of concrete) are taken into account while the strength gain during cooling phase is neglected. Strength gain with time is also considered in the present study.

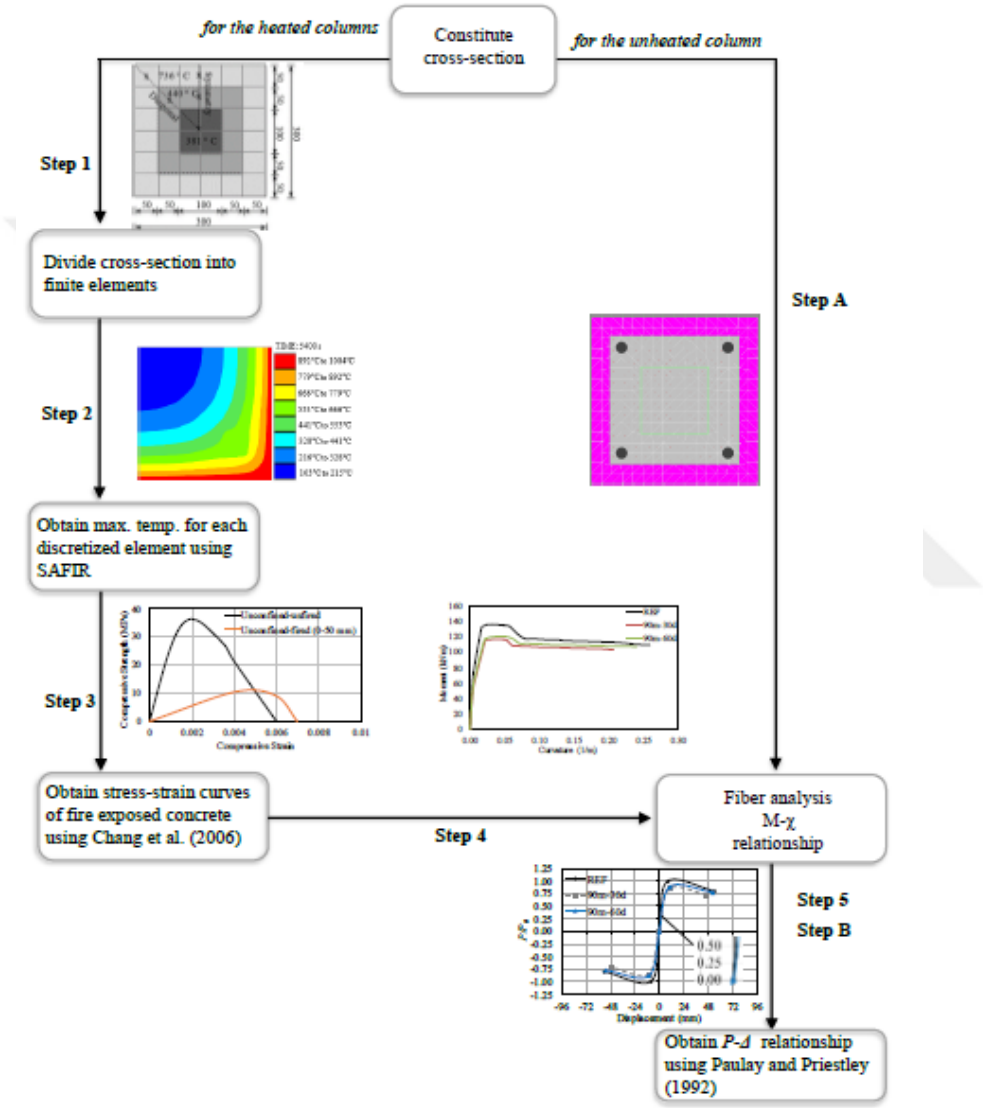

Figure 4.7 : Calculation procedure of the prediction of post-fire seismic response of the columns.

The average temperatures for the elements are evaluated based on the temperatures calculated along both the diagonal and symmetry axis of the section as shown in Figure 4.8 (Step 1). The results estimated from thermal analysis (Figures 4.4a, 4.4b) were first

compared to the experimentally obtained thermocouple readings (Figure 4.4d). The comparison of the temperatures showed reasonable agreement. For example, the average temperature on outer 50 mm zone of the cross-section was estimated to be 736 ºC from thermal analysis (Figure 4.8), while it was obtained to be around 700 ºC from thermocouple readings. Using the estimated maximum temperatures in the cross-section using thermal analysis results (Step 2), residual stress-strain relationship and elastic modulus for each of the elements are determined using Eqs. (4.3-4.5) as recommended by Chang et al. (2006) (Step 3). In these equations, f'_{cT} and ε_{oT} are the residual compressive strength and peak compressive strain of concrete after exposure to temperature T, f'_c and ε_o are concrete compressive strength and compressive peak strain at ambient temperature, respectively, where the E_{cr} and E_c are the residual elastic modulus after fire and under ambient case, respectively. The theoretical seismic responses of the unheated and fire exposed columns are then calculated considering Moment (M)-Curvature (ϕ) relationships of the columns at the critical sections based on plastic hinge concept (Step 4, Step A). The calculated M-ϕ relationships for the columns are shown in Figure 4.9.

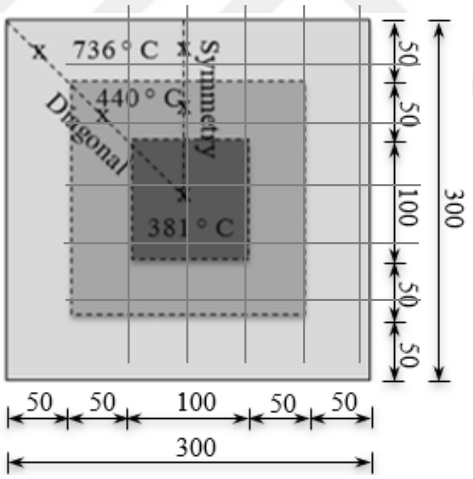

Figure 4.8 : Maximum temperatures including cooling stages after 90 minutes of fire. Note: Dimensions are mm.

$$\frac{f'_{cT}}{f'_c} = \begin{Bmatrix} 1.01 - 0.00055T\ (20\ °C < T \leq 200\ °C) \\ 1.15 - 0.00125T\ (200\ °C < T \leq 800\ °C) \end{Bmatrix} \tag{4.3}$$

$$\frac{\varepsilon_{0T}}{\varepsilon_0} = \begin{Bmatrix} 1 \qquad\qquad\qquad\qquad\qquad\qquad (20\ °C < T \leq 200\ °C) \\ \left\{\left(-0.1f'_c + 7.7\right)\left[\frac{e^{(-5.8+0.01T)}}{1+e^{(-5.8+0.01T)}}\right] - 0.0219\right\} (200\ °C < T \leq 800\ °C) \end{Bmatrix} \tag{4.4}$$

$$\frac{E_{cr}}{E_c} = -0.00165T + 1.033\ (20\ °C < T \leq 600\ °C) \tag{4.5}$$

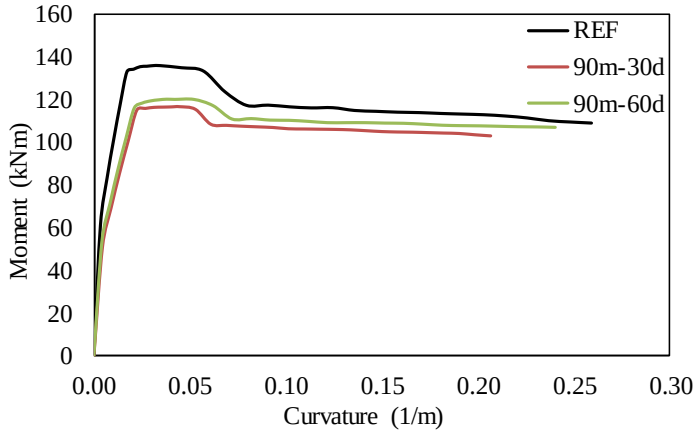

Figure 4.9 : Calculated moment-curvature relationships for the columns.

Chang et al. (2006) mentioned that the model is based on the cylinder tests executed 30 days after heat exposure. Therefore, for the *M-ϕ* analysis of the column 90m-30d, the compressive strength and elastic modulus of concrete are calculated with reference to this model. Besides, Harada et al. (1972) indicated that compressive strength of concrete does not vary between 30 and 60 days after fire exposure whereas Papayianni and Valiasis (1991) mentioned that compressive strength of concrete at the age of 60 days after fire exposure is expected to be around 15% higher than that of after 30 days (Table 4.3). Experimental results shown in Table 4.3 demonstrate that the difference in compressive strengths between 30 and 60 days after fire is around 8%. In the *M-ϕ* analysis, compressive strength of concrete of the column 90m-60d is assumed to be 15% higher than that of the column 90m-30d with reference to the study conducted by Papayianni and Valiasis (1991). It should be noted that as seen in Figure 4.10, Harada et al. (1972) and Papayianni and Valiasis (1991) reported that the trend in strength loss up to first month (between point A and B) and strength gain after this duration (between point B and C) does not vary remarkably with the variations in temperatures. Therefore, the relationship between temperature and time after fire may not be as critical as expected. On the other hand, according to the literature survey of the authors, there is no study revealing the variation in residual elastic modulus of concrete depending on the time after fire exposure in the studied temperature range. However, Mostafaei et al. (2010) indicated that, after fire exposure, there is a linear relationship between the elastic modulus and compressive strength of concrete irrespective of time after fire as shown in Eq. (4.6) where, E_{oT} is the residual elastic modulus after exposure to temperature T, f'_{cT} is the residual compressive strength of concrete after exposure to temperature T, and ε_{oT} is residual peak compressive strain after exposure to

temperature *T*. Therefore, similar to residual compressive strength, elastic modulus of concrete in the present study is assumed to increase by 15% for the column 90m-60d with respect to the column 90m-30d.

$$E_{0T} = \frac{f'_{cT}}{2\varepsilon_{0T}} \tag{4.6}$$

Mander et al. (1988) model is used for estimating confined concrete properties after fire exposure and actual uniaxial tensile test results obtained from reinforcements are used in the analysis (Table 4.2). Steel reinforcing bars were assumed to behave in an elastoplastic manner with strain hardening in *M*-ϕ analysis. For the unheated column, the actual stress-strain relationships obtained from unheated cylinder specimens (Figure 4.1) are used for defining unconfined concrete properties whereas Mander et al. (1988) model is used for confined concrete.

Table 4.3 : Variation in residual compressive strength of concrete with time after fire.

Days	Residual compressive strength (%)		
	Experimental[a]	Harada et al. (1972)[b]	Papayianni and Valiasis (1991)[c]
1	-	0.60	0.50
3	0.57	-	-
7	0.47	-	0.45
15	0.43	-	-
30	0.68	0.50	0.41
60	0.74	0.50	0.48
90	-	-	0.55
360	1.06	0.90	-

[a] 150×150×150 cube, calcareous, w/c: 0.42, ISO-834 standard fire curve is followed for 90 minutes
[b] 50×100 cylinder, siliceous, w/c: 0.60, heating rate 1.5 °C/min, temperature kept constant for 1 hour after 400 °C furnace temperature is reached
[c] 150×300 cylinder, calcareous, w/c: 0.65, heating rate 20 °C/min, temperature kept constant until 3 hours heating after 400 °C furnace temperature is reached

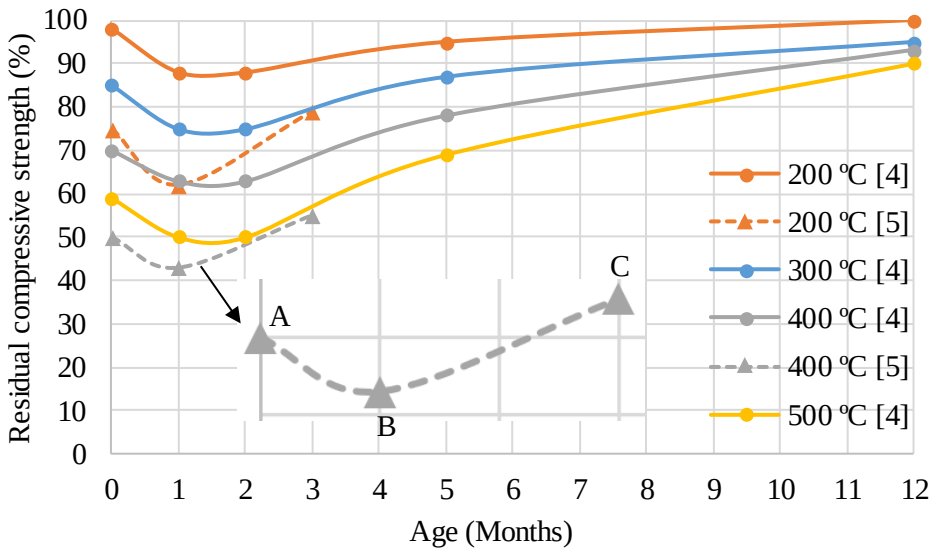

Figure 4.10 : Strength recovery of heated concrete. Note: 4 refers to Harada et al. (1972) and Papayianni and Valiasis (1991), respectively.

After obtaining the *M*-ϕ relationships, the total top displacements of the columns are estimated considering the elastic and inelastic deformations using the definition given by Paulay and Priestley (1992) for RC columns in which the displacement ductility for a cantilever column is defined as the ratio of total lateral tip deflection of the column (Δ) to the yield displacement (Δ_y) (Step 5, Step B). In this definition, yield displacement is assumed to occur simultaneously with the yield curvature at the base of the column. The curvature distribution at yield is adopted by linear approximation and can be estimated using Eq. (4.7), where ϕ_y is the yield curvature and l is the shear span of the RC column. Yield curvature is estimated defining the slope of the elastic portion of the equivalent *M*-ϕ relationships estimated from section analysis, by the secant stiffness at first yield. Assuming that the plastic rotations to be concentrated at mid-height of the plastic hinge length (l_p), the plastic displacement at the cantilever tip is calculated using Eqs. (4.8-4.10), where Θ_p is the plastic rotation along the equivalent plastic hinge length and Δ_p is the plastic displacement. The recommendation of Turkish Building Earthquake Code (TBEC) (2018) was used in the evaluation of the plastic hinge length as half depth of the cross-section. Consequently, theoretically obtained load–displacement relationships are compared with respect to the experimental behavior.

$$\Delta_y = \phi_y l^2/3 \tag{4.7}$$

$$l_p = h/2 \tag{4.8}$$

$$\theta_p = \phi_p l_p \quad (4.9)$$

$$\Delta_p = \theta_p(1 - 0.5 l_p) \quad (4.10)$$

As seen in Figure 4.11, the predicted results match well with the experimental results in terms of load bearing capacity and deformability whereas the stiffness values of the columns are overestimated. This may be attributed to the fact that only flexural displacements are considered while other components of the tip displacements (i.e. strain penetration) are neglected in the theoretical calculations which necessitates more experimental work on this issue. Some variations in assumptions in the present paper would be tolerated in case the given algorithm is followed in most conditions. However, there is also need for further studies under different conditions to generalize the procedure to a wide range of structural members.

4.5 Experimental Results

The seismic responses of the columns are analyzed in terms of their hysteretic behavior. The test data for the hysteretic responses and their envelopes on lateral load versus lateral displacement of the columns are plotted in Figures (4.11 and 4.12a), respectively. Envelopes of the numerical work is shown in Figure 4.12b. Only the first cycle of each lateral load-displacement relationship was considered while developing the envelope curves of the hysteretic response. Important stages such as cracking, crushing of cover and core concrete, and buckling of the reinforcement are symbolically marked on the plots to aid interpretation. During the tests, all columns exhibited a behavior ultimately dominated by flexure and experienced the peak lateral load at around 2% drift ratio (the ratio of the top displacement (Δ) to the shear span (l)) regardless of fire exposure. The maximum lateral load capacities in pushing and pulling directions as well as failure drift ratios corresponding to the failure (80% of the peak lateral strength on the descending branch of the load-displacement response) of the columns are shown in Table 4.4. As seen in this table, the residual lateral load capacities of the fire exposed columns are quite similar, and the peak lateral loads of these columns are approximately 20% lower than that of the column REF. Since the reinforcement reinstated the unheated mechanical properties after cooling, fire induced lateral load capacity reductions can be attributed to the loss of compressive strength in concrete resulting with a lower bending moment capacity and, thereby, lower lateral

load capacity (Figure 4.12c). The similarity of the residual lateral load capacities of the heated columns can be explained by the fact that although the compressive strength of concrete 60 days after fire was improved around 15% with respect to that of after 30 days, the increase in compressive strengths between 30 and 60 days was only around 3 MPa. Therefore, the difference between the lateral load capacities of the columns tested 30 or 60 days after fire exposure remained marginal. On the other hand, contribution of the reinforcement governs the behavior after elastic region (at around peak lateral load) which minimize the impact of autogenous recovery in compressive strength on the post fire seismic behavior as well. For better comparison of the column performances in terms of ductility, displacement ductility factors (μ_Δ), the ratio of the ultimate displacement (Δ_u) to the yield displacement (Δ_y), are calculated. Yielding and ultimate displacements are evaluated on the average envelope curves (absolute average of pushing and pulling directions) as shown in Figure 4.13, and corresponding ductility factors of the columns are listed in Table 4.4.

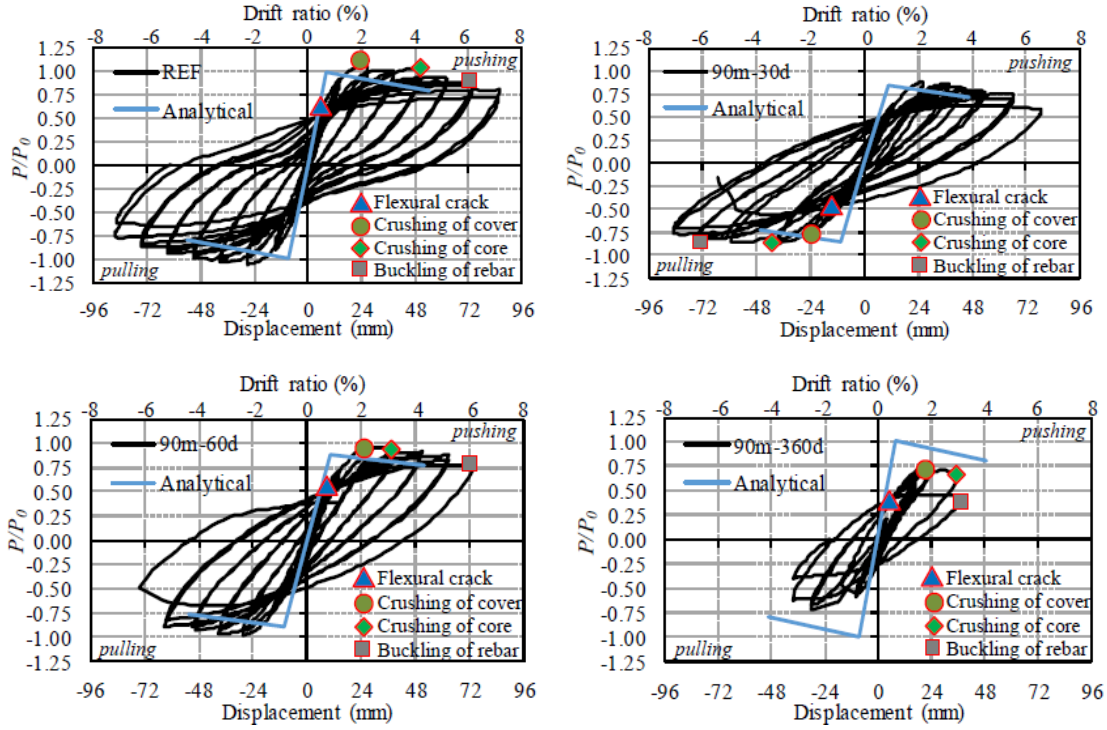

Figure 4.11 : Experimental and theoretical lateral load-displacement relationships. Note: the column 90m-360d experienced premature buckling of longitudinal bars due to concrete settling problems during casting process.

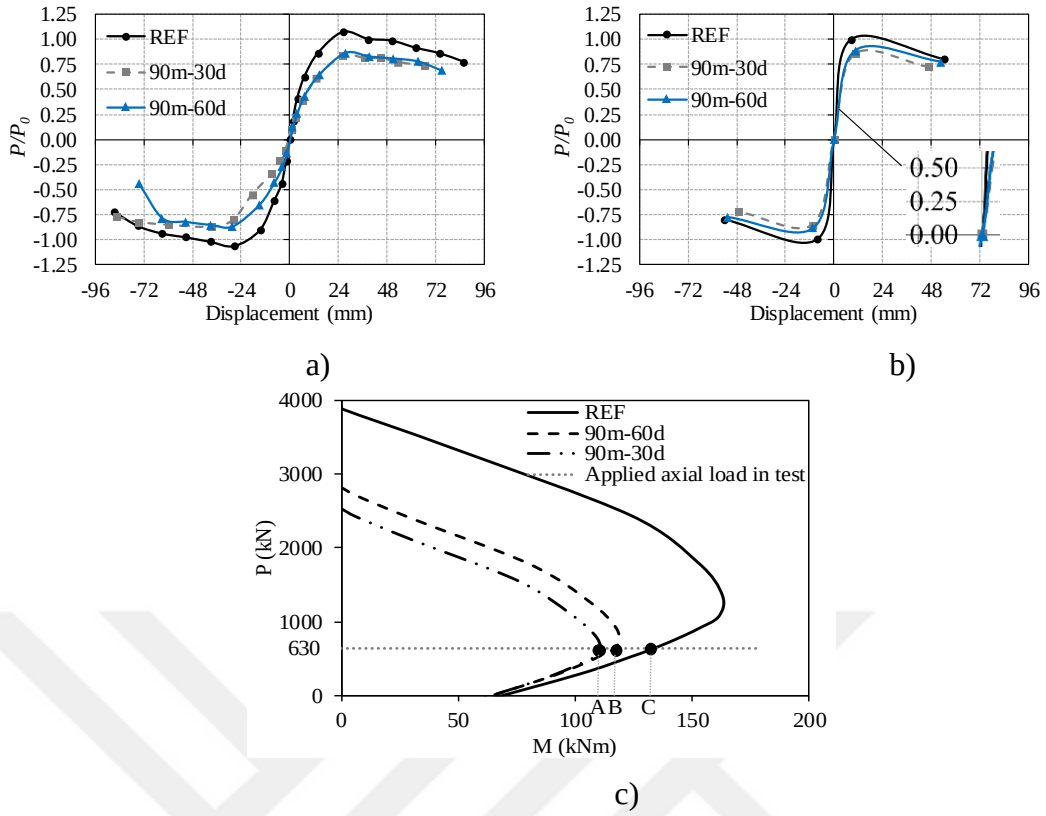

Figure 4.12 : a) Envelopes of hysteretic curves, b) envelopes of numerical work and c) axial load-moment interaction diagrams for the columns. Note: A, B and C correspond to 116.5 kNm, 120.6 kNm and 136.1 kNm, respectively.

As seen in Figure 4.13, Δ_y corresponds to the maximum lateral load on straight line joining origin and the point at 65% of the peak lateral load on ascending portion of the average envelope curve, and Δ_u is the displacement on 80% of the peak load on descending portion of the average envelope curve as defined by Iacobucci et al. (2003). As seen in Table 4.4, yield displacements increased with fire exposure, while the ultimate displacements were not remarkably influenced. The fire induced stiffness degradation is responsible on the increment in the yield displacements. Besides, the mechanical properties of the reinforcing bars reinstated after fire (Table 4.2), and the ultimate displacements are controlled by buckling of the rebars (Figure 4.11) resulting in similar ultimate displacements after fire exposure. This phenomenon resulted with approximately 20% reduction in displacement ductility factors for the heated columns irrespective of time after fire. On the other hand, since the increase in compressive strengths of the concrete between 30 and 60 days was limited, there is no remarkable influence of time after fire on ductility of the columns. Despite this fact, post-fire ductility factors of heated columns appear satisfactory in terms of structural response since the displacement ductility factors higher than 3.5 usually correspond to a fully

ductile response as stated by Paulay and Priestley (1992). ASCE 41 (2017) defines acceptance criteria for RC columns corresponding to related performance levels. These criteria are based on plastic rotations depending on the axial load and lateral reinforcement ratio of the columns as well as failure modes (i.e. *condition i* for flexural failure). For example, the drift ratio limits for IO, LS and CP performance levels for the unheated column are around 0.6%, 2.1% and 2.9%, respectively. These limits are lowered for the heated columns due to the fire-induced reduction in compressive strength, which results in an increase in axial load ratio. The increasing axial load ratios lead to lower plastic rotations, and thereby, results in lower drift limits according to ASCE 41 (2017). Nevertheless, the tests in the present study were terminated at around 6% drift ratio. Thus, all the limits defined in the ASCE guideline were covered in the applied loading protocol.

Table 4.4 : Experimental and theoretical lateral load-displacement results.

Specimen	Failure drift* (%)	Experimental lateral load capacity while pushing (kN)	Experimental lateral load capacity while pulling (kN)	Theoretical lateral load capacity (kN)	Δ_y (mm)	Δ_u (mm)	μ_Δ
REF	6.1	120.7	121.7	113.4	14.9	73.0	4.9
90m-30d	5.9	98.8	95.1	97.1	18.2	71.3	3.9
90m-60d	5.9	98.7	98.0	100.5	17.9	70.5	3.9

* drift corresponding to $0.80P_{max}$ in Fig. 10

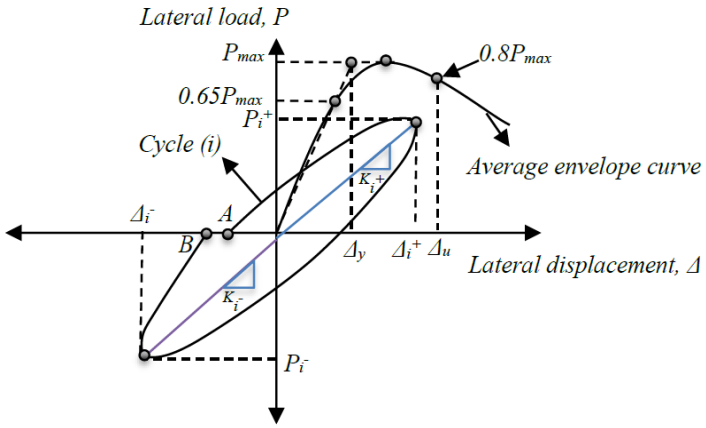

Figure 4.13 : Definition of ductility parameters.

The secant stiffness (K) is computed as the ratio of the maximum lateral load in the first loop within each cycle (P_i) to the displacement at the peak of each loading cycle (Δ_i), and pursuing, the average values of the stiffness in pushing (K_i^-) and pulling (K_i^+) directions are considered (Figure 4.13). Loss of elastic modulus in elastic region and

tensile strength after cracking due to the fire exposure, leads to a decrease in stiffness of the fire exposed columns with respect to the unheated column (Figure 4.14). In addition, as can be seen in Figure 4.14, the main impact of time after fire is observed on post-fire stiffness properties, particularly, at earlier stages of cyclic loading. The column 90m-60d, which was subjected to seismic test 60 days after fire exposure, exhibited around 10% more stiff behavior compared to the column 90m-30d. This can be attributed to the autogenous recovery of compressive strength and modulus of elasticity of concrete in a higher ratio for the column 90m-60d compared to the column 90m-30d. It should also be noted that the ratio of decrease in stiffness is greater than the ratio of the reduction in lateral load capacity with fire exposure. For instance, for the column 90m-60d, the decrease in *K* during initial stage of loading is around 40% while the reduction in lateral load capacity is around 20% with respect to the unheated column. This is attributed to the fact that the modulus of elasticity and tensile strength of concrete is more sensitive to fire exposure than compressive strength of concrete as stated in the study of Ni and Birely (2018). The variation between the stiffness values of the columns became comparatively less after the drift ratio of 2% (24 mm displacement, around yielding) since the reinforcement which is reinstated after cooling is more dominant on the behavior after yielding.

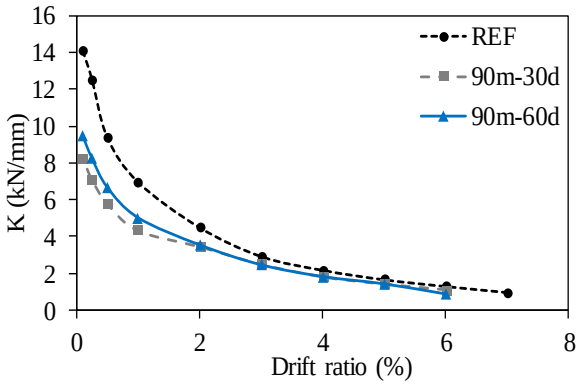

Figure 4.14 : Stiffness degradations.

The appearance of the columns at a drift ratio of 2% (around yielding) and 4% (prior to initiation of buckling of reinforcing bars) are shown in Figures (4.15 and 4.16). The damage progression of the columns throughout the test is tabulated in Table 4.5. The first signs of distress in the tested columns were the initial flexural cracks in the cover concrete which were first observed at a drift ratio around 0.5% (6 mm displacement) within the potential hinging zone. This was followed by yielding of the longitudinal

reinforcing bars and crushing of the cover concrete sequentially at around 2% drift ratio. Then, spalling of the cover concrete, and eventually, buckling of the longitudinal bars were observed. Damage was extended upwards and distributed along a higher portion of the columns with fire exposure while the maximum crack widths reduced with respect to the unheated reference column. In other words, hinging zone is observed to be elongated with fire exposure which is attributed to the increase in axial load ratio (applied axial load/axial load capacity) resulted from the loss of compressive strength of concrete due to fire exposure.

Table 4.5 : Drift ratios (%) for different damage states.

Failure mechanisms	REF	90m-30d	90m-60d
First flexural crack	0.5	0.5	0.5
Crushing of concrete cover	2	2	2
Spalling of concrete cover	4	3	3
Buckling of reinforcing bar	6	5	5

a) b) c)

Figure 4.15 : Seismic damages of the columns a) REF, b) 90m-30d, c) 90m-60d after 2% drift ratio.

a) b) c)

Figure 4.16 : Seismic damages of the columns a) REF, b) 90m-30d, c) 90m-60d after 4% drift ratio.

A critical parameter that should be investigated is the impact of axial loading in the fire test. Compressive strength tests on concrete after exposing to elevated temperatures demonstrated that the axial loading in fire tests results in an improved residual behavior compared to the unstressed residual tests (Malhotra, 1956; Abrams, 1971; Harada et al., 1972; Papayianni and Valiasis, 1991). Moreover, presence of a compressive axial load in fire test increases the fire resistance of RC columns (Salse and Lin, 1976). Therefore, the absence of axial loading in fire tests results in a worst-case scenario compared to the presence of axial restraint which may be beneficial for design concerns and practical applications (Bisby et al., 2011; Yaqub and Bailey, 2012). As a result, the presented tests should be considered as a worst-case scenario.

4.6 Conclusions

This paper investigates the impact of time after fire exposure on seismic behavior of full-scale RC columns. The following conclusions can be drawn from the experimental and analytical campaign.

- Average concrete compressive strength of the heated columns was reduced to around half of the original strength (lower in the surface, higher towards center). This significant loss in concrete compressive strength caused considerable reduction (up to 20%) in lateral load capacities of the fire exposed columns with respect to their unfired counterpart irrespective of time after fire exposure since the mechanical properties of the reinforcing bars recovered after cooling.
- The difference between the lateral load capacities of the columns tested 30 or 60 days after fire was marginal due to the insignificant variation of the concrete compressive strength during this period.
- Stiffness of the columns decreased with fire exposure due to the decrease in elastic modulus and tensile strength of concrete after fire exposure.
- Longer the time after fire, higher is the stiffness of the columns due to the autogenous recovery in compression and tensile strength as well as elastic modulus of concrete with time after fire.
- Ultimate displacements were achieved at around 6% drift ratio, where noticeable buckling of longitudinal reinforcement was observed irrespective of fire exposure. Since the mechanical properties of the reinforcing bars were

recovered after fire, exposure to fire did not affect the ultimate displacements of the columns remarkably.

- Reduction in elastic modulus of concrete due to the fire exposure caused a degradation in flexural rigidity of the columns. As a consequence, yield displacements were increased with fire exposure and thus, ductility factors of the heated columns which were defined as the ratio of the ultimate displacement to the yield displacement, reduced by 20% of that of the initial ductility irrespective of time after fire. Nevertheless, ductility factors of all columns are larger than 3.5, which points out to a satisfactory ductility performance even after fire.
- The suggested numerical procedure, which considers the estimations for thermal gradients, concrete residual properties, and assumes an increase in concrete compressive strength and elastic modulus as a function of time after fire, is in good agreement with the test results in terms of prediction of residual lateral load capacity and ductility.
- The impact of axial loading during the fire tests was not considered herein to represent a worst-case scenario in the present paper. This impact should be further investigated as well as the other parameters which can be influential in the long-term (i.e. concrete mix, compressive strength and cover). Moreover, the impact of time after fire on seismic behavior of RC columns should be investigated in the long term (i.e. after 360 days).

There is a need of more research for further understanding the behavior and generalizing the outcomes of the present work.

5. CONCLUSIONS

In the scope of the thesis, standard fire tests and subsequent seismic tests were conducted for RC cast-in-situ and precast columns.

The first series columns comprised of five full-scale, cast-in-situ RC columns. One of these columns was kept unheated while the other four were exposed to fire following ISO-834 standard fire curve for 30, 60 and 90 minutes. The columns were designed to comply with current seismic and fire design codes in terms of concrete cover (i.e. 40 mm) except for the one which was exposed to 30 minutes of fire with a concrete cover of 25 mm. In the second series specimens, the impact of fire severity (30, 60 or 90 minutes of fire exposure) on post-fire seismic behavior of precast columns is investigated through four full-scale columns. The columns were cast and inserted into socket foundations filling the column-foundation interface with repair mortar to represent the common practice. The third series columns are comprised of four RC columns in order to investigate the impact of time after fire (30, 60 or 360 days) on post-fire seismic behavior of RC columns. Furthermore, a numerical model was developed for tracing the seismic response of RC columns after realistic fire exposure conditions. The model is based on a finite element approach and temperature dependent material properties. The critical factors, namely, different exposure conditions and high temperature material properties that have significant influence on the fire response of RC columns, are accounted for in the analysis. The validated model can reasonably predict the thermal and structural response of an RC column from a fire exposure as well as said columns residual seismic capacity after cooling.

Based on the information presented in this study, the following key conclusions are drawn:

- There is almost no information on the post-fire seismic performance of RC columns, especially under design fire scenarios. Also, to date, there is no

rational approach in determining the residual seismic capacity of RC columns after exposure to fire.

- Fire exposure caused a lateral strength reduction for all columns. The reductions in lateral load capacities for the columns varied between ten percent and twenty percent with respect to the reference column after 30 min, 60 min and 90 min of fire exposure. The level of strength reduction was not proportional to duration of fire exposure or maximum temperature reached during fire exposure. For precast columns, there was no reduction in lateral load capacity for 30 min and 60 min of fire exposure, whereas for 90 min heated column, ten percent reduction was experienced. The difference between cast-in-situ and precast columns is attributed to lower axial load and greater heights of the precast columns making the flexural effects more governing.
- No remarkable reduction was observed in ductility of the columns after post-fire seismic tests up to 60 minutes. On the other hand, the ductility of the columns exposed to 90 minutes of fire exposure experienced higher yield displacement based on stiffness degradation due to fire exposure which is resulted with lower ductility since the deformability of the columns was not considerably affected from fire exposure. Nevertheless, ductility factors of all columns were larger than 3.5, which implies satisfactory structural response in terms of ductility.
- The influence of the concrete cover thickness on the global performance of the tested flexure-critical columns was observed to be limited. This is attributed to the fact that smaller cover thickness results in higher effective depth and thereby higher bending moment capacity and lateral load capacity.
- The initial stiffness of the columns decreased with an increase in fire duration because of concrete cracking resulting from the loss of tensile strength of concrete and the formation of plastic hinges.
- The energy dissipation capacity of the columns decreased while the tendency of the columns towards plastic deformation increased with an increase in fire duration.
- The difference between the lateral load capacities of the columns tested 30 or 60 days after fire was marginal due to the insignificant variation of the concrete

compressive strength during this period. On the other hand, longer the time after fire, higher is the stiffness of the columns due to the autogenous recovery in compression and tensile strength as well as elastic modulus of concrete with time after fire.

- The proposed model can predict the post-fire seismic response of RC columns. The model accounts for critical parameters such as different fire scenarios and high temperature material properties.

The following recommendations are highlighted as a consequence of the presented thesis in terms of future research on this issue:

- Additional post-fire seismic tests are needed to study the influence of other parameters, such as the effect of different cross section sizes, reinforcement ratios and configurations, various levels of confinement of concrete in the column center as well as various restraint conditions. Moreover, the effect that water quenching has on the residual capacity of fire exposed members should be investigated.
- The impact of axial loading during the fire tests was not considered herein to represent a worst-case scenario in the present paper. This impact should be further investigated as well as the other parameters which can be influential in the long-term (i.e. concrete mix, compressive strength and cover). Moreover, the impact of time after fire on seismic behavior of RC columns should be investigated in the long term (i.e. after 360 days).
- Post-fire seismic behavior should also be researched considering more realistic fire scenarios, for example under compartment fires.
- The finite element model can be further advanced by incorporating fire induced spalling of concrete.
- Further research is necessary to realistically address repair/strengthening methodologies for fire damaged structural members considering potential seismic demands in terms of strength and deformation capacity. Although some repair/strengthening techniques for fire damage are defined by several technical documents in the existing literature, none of these recommendations consider post-fire seismic risk.

- One another major concern that should be focused is the realistic estimation of non-destructive testing techniques in order to reveal the first stage of post-fire performance assessment (i.e. diagnosis).

REFERENCES

Abrams, M. S. (1971). Compressive strength of concrete at temperatures to 1600F. *Temperature and Concrete*, *25*, 33-58.

ACI (1997). *Standard method for determining fire resistance of concrete and masonry construction assemblies*. ACI 216.1-97. Farmington Hills, MI.

ACI (2019). *Building code requirements for structural concrete.* ACI 318-19. Farmington Hills, MI.

ACI (2013). *Guide for testing reinforced concrete structural elements under slowly applied simulated seismic loads*. ACI 374. 2R-13. Farmington Hills, MI.

Almand, K.H. (2013). *Structural fire resistance experimental research: priority needs of US industry*. Springer Science and Business Media.

Arioz, O. (2007). Effects of elevated temperatures on properties of concrete. *Fir Safe J*, *42*(8):516-522.

ASCE/SEI, 41 (2017). *Seismic Evaluation and Retrofit of Existing Buildings.* Reston, VA: American Society of Civil Engineers (2017).

ASTM E-119 (2012). *Standard test methods for fire tests of building construction and materials*. ASTM International, West Conshohocken, PA.

Bae, S. and Bayrak, O. (2008). Plastic hinge length of reinforced concrete columns. *ACI Structural Journal*, *105*(3), 290.

Bailey, C. G. and Yaqub, M. (2012). Seismic strengthening of shear critical post-heated circular concrete columns wrapped with FRP composite jackets. *Composite Structures*, *94*(3), 851-864.

Bazant, Z.P. and Kaplan, M. (1996). *Concrete at high temperatures: material properties and mathematical models.* Longman Group, Harlow, UK, 1996.

Behnam, B. (2018). On the interaction between span length and opening ratio of RC frames under natural fires. *Proceedings of the Institution of Civil Engineers–Structures and Buildings*, *171*(6), 472-486.

Benichou, N., Cree, D., Chowdhury, E. U., Green, M. F. and Bisby, L. A. (2011). Fire testing of FRP strengthened reinforced concrete columns. *In International Conference on Durability and Sustainability of FRP Composites for Construction and Rehabilitation*, Québec City, Canada.

Bénichou, N., Mostafaei, H., Green, M. F. and Hollingshead, K. (2013). The impact of fire on seismic resistance of fibre reinforced polymer strengthened concrete structural systems. *Canadian Journal of Civil Engineering*, *40*(11), 1044-1049.

Bisby, L. A., Chen, J. F., Li, S. Q., Stratford, T. J., Cueva, N. and Crossling, K. (2011). Strengthening fire-damaged concrete by confinement with fibre-reinforced polymer wraps. *Engineering Structures*, *33*(12), 3381-3391.

Brunesi, E., Nascimbene, R., Bolognini, D. and Bellotti, D. (2015). Experimental investigation of the cyclic response of reinforced precast concrete framed structures. *PCI Journal*, *60*(2): 57-79.

Brushlinsky, N. N., Ahrens, M., Sokolov, S. V. and Wagner, P. (2016). *World fire statistics*. Center of fire statistics of CTIF. Report No: 20.

CEN (2004). *Design of concrete structures, part 1.1.* Eurocode 2, Brussels, Belgium: CEN.

CEN (2004). *Design of concrete structures, part 1.2.* Eurocode 2, Brussels, Belgium: CEN.

Chadwell, C. B. and Imbsen, R.A. (2004). XTRACT: A tool for axial force-ultimate curvature interactions. *In Structures 2004: Building on the Past, Securing the Future*, Nashville, Tennessee, USA.

Chang, Y. F., Chen, Y. H., Sheu, M. S. and Yao, G. C. (2006). Residual stress–strain relationship for concrete after exposure to high temperatures. *Cement and Concrete Research*, *36*(10), 1999-2005.

Chen, Y. H., Chang, Y. F., Yao, G. C. and Sheu, M. S. (2009). Experimental research on post-fire behaviour of reinforced concrete columns. *Fire Safety Journa*l, *44*(5), 741-748.

Concrete Society (2008). *Assessment, design and repair of rire-damaged concrete structures.* Technical Report 68, The Concrete Society, Camberley, UK.

Demir, U., Goksu, C., Unal, G., Green, M.F. and Ilki, A. (2020a). Effect of fire damage on seismic behavior of cast-in-place reinforced concrete columns. *ASCE Journal of Structural Engineering*, DOI: 10.1061/(ASCE)ST.1943- 541X.0002794.

Demir, U., Green, M.F. and Ilki, A. (2020b). Post-fire seismic performance of precast RC columns. *PCI Journal*, DOI: 10.15554/pcij65.6-01.

Demir, U., Goksu, C., Binbir, E. and Ilki, A. (2020c). Impact of time after fire on post-fire seismic behavior of RC columns. *Structures*, 26, 537-548.

Dhakal, R. P. and Maekawa, K. (2002). Reinforcement stability and fracture of cover concrete in reinforced concrete members. *Journal of Structural Engineering*, *128*(10), 1253-1262.

EN 1363-1 (2012). *Fire resistance tests: General requirements.* European Committee for Standardization, Brussels.

Felicetti, R. and Meda, A. (2005). Residual behaviour of reinforcing steel bars after a fire. *In: Proceedings of FIB Symposium Keep Concrete Attractive.* Budapest, Hungary: 2005. p. 1148-1155.

FEMA (2009). *Effect of strength and stiffness degradation on seismic response.* FEMA P440a. Prepared by ATC, Redwood City, CA.

FIB (2004). *Seismic design of precast concrete building structures (fib Bulletin No. 27).* Lausanne, Switzerland.

FIB (2008). *Fire design of concrete structures- structural behaviour and assessment: state-of-the-art report (fib Bulletin No. 46)*. Lausanne, Switzerland.

Fischinger, M., Kramar, M. and Isaković, T. (2008). Cyclic response of slender RC columns typical of precast industrial buildings. *Bulletin of Earthquake Engineering*, *6*(3): 519-534.

Fischinger, M., Zoubek, B. and Isaković, T. (2014). Seismic response of precast industrial buildings. *In Perspectives on European Earthquake Engineering and Seismology*. Springer, Cham.

Fletcher, I.A, Welch, S., Torero, J.L., Carvel, R.O., Usmani, A. (2007). Behavior of concrete structures in fire. *Therm Sci*, *11*(2):37-52.

Franssen, J.M. (2004). Plastic analysis of concrete structures subjected to fire. *In: proceedings of the Workshop on Fire Design of Concrete Structures: What Now? What Next?*. Milan, Italy.

Franssen, J. M. and Dotreppe, J. C. (2003). Fire Tests and Calculation Methods for Circular Concrete Columns. *Fire Technology*, *39*(1): 89-97.

Franssen, J. M. and Gernay, T. (2017). Modeling structures in fire with SAFIR: theoretical background and capabilities. *Journal of Structural Fire Engineering*, *8*(3), 300-323.

Gernay, T. (2012). Effect of transient creep strain model on the behavior of concrete columns subjected to heating and cooling. *Fir Tech*, *48*(2):313-329.

Gernay, T., Dimia, M.S. (2011). Structural behavior of concrete columns under natural fires including cooling down phase. *In Proceedings of the International Conference on Recent Advances in Nonlinear Models-Structural Concrete Applications*, pp. 637-656.

Gernay, T., Franssen, J.M. (2010). Consideration of transient creep in the Eurocode constitutive model for concrete in the fire situation. *In: Proceedings of the Sixth International Conference Structures in Fire.* Michigan State University, USA. p. 784-791.

Gernay, T., Franssen, J.M. (2015). A performance indicator for structures under natural fire. *Engineering Structures*, *100*, 94-103.

Goksu, C., Yilmaz, H., Chowdhury, S. R., Orakcal, K. and Ilki, A. (2014). The effect of lap splice length on the cyclic lateral load behavior of RC members with low-strength concrete and plain bars. *Advances in Structural Engineering*, *17*(5): 639-658.

Harada, T., Takeda, J., Yamane, S., Furumura, F. (1972). Strength, elasticity and thermal properties of concrete subjected to elevated temperatures. *ACI Special Publication*, *34*:377-406.

Hertz, K.D. (2005). Concrete strength for fire safety design. *Mag Con Res*, *57*(8):445-453.

Ilki, A., Demir, U. (2019). Factors affecting seismic behavior of reinforced concrete structures after fire exposure. *NED University Journal of Research*. doi.org/10.35453/NEDJR-STMECH-2019-0003.

Ilki, A., Celep, Z. (2012). Earthquakes, existing building and seismic design codes in Turkey. *Arab J Sci Eng 37*:365–380.

ISO (1999). *Fire resistance tests: elements of building construction. Part 1: general requirements*. ISO834. Geneva, Switzerland.

Jau, W. C. and Huang, K. L. (2008). A study of reinforced concrete corner columns after fire. *Cement and Concrete Composites, 30*(7), 622-638.

Karadogan, F., Yuksel, E., Ilki, A., Saruhan, H., Darilmaz, K. and Guzel, O. (1997). Seismic behavior of precast RC columns and their socket base connections. *In 4th National Earthquake Engineering Conference (4UDMK)*, Ankara, Turkey.

Khaliq, W. and Kodur, V. (2013). Behavior of high strength fly ash concrete columns under fire conditions. *Materials and Structures, 46*(5): 857-867.

Khoury, G.A. (2000). Effect of fire on concrete and concrete structures. *Prog Struc Eng Mat, 2*(4):429-447.

Kodur, V. K. R. and Raut, N. K. (2008). Fire resistance of reinforced concrete columns-state-of-the-art and research needs. *ACI Special Publication, 255*, 97-124.

Kuang, J.S. (2017). Design considerations for ductile reinforced concrete columns: Hong Kong case studies. *In Annual Concrete Seminar*, Hong Kong.

Lakhani, H., Ožbolt, J. (2019). Structural behaviour of Reinforced Concrete (RC) columns under fire. *In IOP Conference Series: Materials Science and Engineering 615* (1), 12-88.

Li, L.Z., Liu, X., Yu, J.T., Lu, Z.D., Su, M.N., Liao, J.H. and Xia, M. (2019). Experimental study on seismic performance of post-fire reinforced concrete frames. *Engineering Structures, 179*, 161-173.

Li, W., Wang, T. and Han, L.H. (2019a). Seismic performance of concrete-filled double-skin steel tubes after exposure to fire: Experiments. *Journal of Constructional Steel Research*, 154:209-223.

Li, W.., Chen, B. and Wang, T. (2019b). Seismic performance of concrete-filled double-skin steel tubes after exposure to fire: Analysis. *Journal of Constructional Steel Research*, 162, 105753.

Lie, T.T. (1992). *Structural Fire Protection*. American Society of Civil Engineers (ASCE), Committee on Fire Protection. Structural Division, 78.

Lie, T. T. and Irwin, R. J. (1990). *Evaluation of the fire resistance of reinforced concrete columns with rectangular cross-sections*. Technical Paper, Division of Building Research, National Research Council Canada, Report no: 601.

Lie, T. T., Rowe, T. J., and Lin, T. D. (1986). Residual strength of fire exposed RC columns. Evaluation and repair of fire damage to concrete. *ACI Special Publication 92*, 153-174.

Magliulo, G., Ercolino, M., Petrone, C., Coppola, O. and Manfredi, G. (2014). The Emilia earthquake: seismic performance of precast reinforced concrete buildings. *Earthquake Spectra*, *30*(2): 891-912.

Malhotra, H. L. (1956). The effect of temperature on the compressive strength of concrete. *Magazine of Concrete Research*, *8*(23), 85-94.

Mander, J. B., Priestley, M. J. and Park, R. (1988). Theoretical stress-strain model for confined concrete. *Journal of Structural Engineering*, *114*(8), 1804-1826.

Memon, M. S. and Sheikh, S. A. (2005). Seismic resistance of square concrete columns retrofitted with glass fiber-reinforced polymer. *ACI Structural Journal*, *102*(5), 774.

Mohamedbhai, G.T.G. (1953). The residual strength of concrete subjected to elevated temperatures. *Conc*, *17*(12):22-27.

Mostafaei, H. (2013). Residual lateral load capacity of a high strength reinforced concrete column after fire damage. *ACI Special Publication, 293*, 1-12.

Mostafaei, H., Vecchio, F. and Bénichou N. (2009). Seismic resistance of fire-damaged reinforced concrete columns. *In: Proceedings of the ATC and SEI conference on improving the seismic performance of existing buildings and other structures.* San Francisco, California, United States. December 9–11. vol. 1. p.1396–1407.

Mostafaei, H. and Hum, J.K. (2010). *Response simulation of reinforced concrete columns under lateral loads.* NRC Research Report no: 294, p. 55.

Netinger, I., Kesegic, I., Guljas, I. (2011). The effect of high temperatures on the mechanical properties of concrete made with different types of aggregates. *Fir Safe J, 46*(7):425-430.

Neves, I. C., Rodrigues, J. P. C. and Loureiro, A. D. P. (1996). Mechanical properties of reinforcing and pre-stressing steels after heating. *Journal of Materials in Civil Engineering*, *8*(4), 189-194.

New York Times (1997). https://www.nytimes.com.

New York Times (2018). https://www.nytimes.com.

Ni, S. and Birely, A. C. (2018). Post-fire seismic behavior of reinforced concrete structural walls. *Engineering Structures*, *168*, 163-178.

Paulay, T. and Priestley, M. N. (1992). *Seismic design of reinforced concrete and masonry buildings*. John Wiley & Sons, Inc., New York.

Papayianni, J., Valiasis, T. (1991). Residual mechanical properties of heated concrete incorporating different pozzolanic materials. *Mat Struc, 24*(2):115-121.

Poon, C.S., Azhar, S., Anson, M., Wong, Y.L. (2001). Strength and durability recovery of fire-damaged concrete after post-fire-curing. *Cem Conc Res, 31*(9):1307-1318.

Priestley, M. J. N. (1993). Myths and fallacies in earthquake engineering. Conflicts between design and reality. *ACI Special Publication 157*, 231-254.

Priestley, M. N., Seible, F., Calvi, G. M. and Calvi, G. M. (1996). *Seismic design and retrofit of bridges*. John Wiley & Sons, Inc., New York.

Rangan, B.V. and Warner, R.F. (1996). *Large concrete buildings*. Longman Group Limited, England.

Raut, N. and Kodur, V. (2011). Response of reinforced concrete columns under fire-induced biaxial bending. *ACI Structural Journal*, *108*(5).

Salse, E., Lin, T. D. (1976). Structural fire resistance of concrete. *Journal of the Structural Division*, *102*(1), 51-63.

Scawthorn, C., Eidinger, J. M. and Schiff, A. (Eds.) (2005). *Fire following earthquake*. ASCE Publications, 26.

Schneider, U. and Nagele, E. (1990). *Repairability of fire damaged structures* (CIB W14). Conseil International du Batiment (CIB), Delft, The Netherlands.

Sezen, H. and Whittaker, A. S. (2006). Seismic performance of industrial facilities affected by the 1999 Turkey earthquake. *Journal of Performance of Constructed Facilities*, *20*(1): 28-36.

Sheikh, S. A. and Khoury, S. K. (1993). Confined concrete columns with stubs. *ACI Structural Journal*, *90*(4).

Sheikh, S. A. and Yau, G. (2002). Seismic behavior of concrete columns confined with steel and fiber-reinforced polymers. *ACI Structural Journal*, *99*(1), 72-80.

Skalko, S.V. (2013). Building codes evolve through experience, research. *PCI Journal*, *58*(3): 34-40.

Tan, K.H. and Yao, Y. (2003). Fire Resistance of Four-Face Heated Reinforced Concrete Columns. *Journal of Structural Engineering*, *129*(9): 1220-1229.

Turkish Fire Regulation. (2007). *Guideline for protection of buildings in fire* (in Turkish). Official Gazette, Ankara.

Turkish Building Earthquake Code (2018). *Regulations for Buildings to be constructed in Earthquake Prone Areas*, Ankara, Turkey.

UBC (1997). *Uniform Building Code*. International Conference of Building Officials, U.S.A.

Usmani, A. S. (2008). Research priorities for maintaining structural fire resistance after seismic damage. *In Proceedings of the 14th world conference on earthquake engineering*, Beijing, China (pp. 12-17).

Yaqub, M. and Bailey, C. G. (2012). Seismic performance of shear critical post-heated reinforced concrete square columns wrapped with FRP composites. *Construction and Building Materials*, *34*, 457-469.

Yaqub, M., Bailey, C. G., Nedwell, P., Khan, Q. U. Z., Javed, I. (2013). Strength and stiffness of post-heated columns repaired with ferrocement and fibre reinforced polymer jackets. *Composites Part B: Engineering*. *44*(1), 200-211 (2013).

CURRICULUM VITAE

Name Surname **:** Uğur DEMİR

Place and Date of Birth **:** Kars/01.07.1982

E-Mail **:** udemir@itu.edu.tr

EDUCATION **:**

- **B.Sc.** **:** 2007, Kocaeli University, Civil Engineering
- **M.Sc.** **:** 2013, Istanbul Technical University, Structural Engineering Program

PROFESSIONAL EXPERIENCE AND REWARDS:

- 2007-2009 Karstas Construction-Owner
- 2009-2010 Hakkari University, Civil Engineering Department-Research Assistant
- 2010-2020 Istanbul Technical University, Civil Engineering Faculty-Research Assistant

PUBLICATIONS, PRESENTATIONS AND PATENTS ON THE THESIS:

- **Demir, U.,** Goksu, C., Unal, G., Green, M.F. and Ilki, A. 2020. Effect of Fire Damage on Seismic Behavior of Cast-in-place Reinforced Concrete Columns. *ASCE Journal of Structural Engineering*, DOI: 10.1061/(ASCE)ST.1943-541X.0002794.
- **Demir, U.,** Green, M.F. and Ilki, A. 2020. Post-fire Seismic Performance of Precast RC Columns. *PCI Journal*, DOI: 10.15554/pcij65.6-01.
- **Demir, U.,** Goksu, C., Binbir, E. and Ilki, A. 2020. Impact of Time after Fire on Post-Fire Seismic Behavior of RC Columns. *Structures*, 26, 537-548.
- Ilki, A. and **Demir, U.** 2019. Factors Affecting the Seismic Behavior of Reinforced Concrete Structures after Fire Exposure. *NED University Journal of Research*, 1, 31-41.

- Ilki, A. and **Demir, U.** 2019. Factors Affecting the Seismic Behavior of Reinforced Concrete Structures after Fire Exposure. In the First South Asia Conference on Earthquake Engineering (SACEE2019), Karachi, Pakistan. 21-22 Feb 2019. (Invited Keynote Lecture).
- **Demir, U.,** Unal, G., Goksu, C. and Ilki, A. 2019. Impact of Fire Exposure on Seismic Behavior of Full-Scale RC Columns. In the 7th Structural Engineers World Congress (SEWC2019), Istanbul, Turkey. 24-26 Apr 2019.
- **Demir, U.,** Unal, G. and Ilki, A. 2019. Axial Behavior of Square RC Columns Repaired with FRP Sheets after Fire. In the fib Symposium- Innovations in Materials, Design and Structures, Krakow, Poland. 27-29 May 2019.
- **Demir, U.,** Unal, G., Binbir, E. and Ilki, A. 2019. Cyclic Behavior of RC Columns Externally Jacketed by CFRP Sheets after Fire Exposure. In the 7th International Conference on Computational Methods in Structural Dynamics and Earthquake Engineering (COMPDYN2019), in Crete, Greece, 24 – 26 June 2019.
- **Demir, U.,** Unal, G., Sert, AF., Calis, RO. and Ilki, A**.** 2019. Influence of FRP Repair on the Axial Behavior of Fire Damaged Concrete. In the 5th International Conference on Smart Monitoring, Assessment and Rehabilitation of Civil Structures (SMAR2019), in Potsdam, Germany, 27 – 29 August 2019.
- Ilki, A. and **Demir, U.** 2019. Prediction of Seismic Response of Fire-Damaged RC Columns. In the 5th International Conference on Earthquake Engineering and Seismology (5ICEES)-Haluk Sucuoğlu Workshop, in Ankara, Turkey, 08 – 11 October 2019. Published as a book chapter in: Global Advances in Earthquake Engineering (pp. 232-241).

OTHER PUBLICATIONS, PRESENTATIONS AND PATENTS:

- **Demir, U.,** Sahinkaya, Y., Ispir, M. and Ilki, A**.** 2019. Axial Behavior of Noncircular High-Performance Fiber-Reinforced Cementitious Composite Members Externally Jacketed by CFRP Sheets. *ASCE Journal of Composites for Constructon*, 23(4), DOI: 10.1061/(ASCE)CC.1943-5614.0000940.
- Ilki, A., Yazgan, U., Demir, C., Ates, AO., **Demir, U.,** Kupcu, E., Unal, G., Altinok, MA., Karakaya, B., Narlitepe, F. 2019. Development of a Framework for Rapid Earthquake Risk Assessment for Substandard Buildings in Turkey. In the proceedings of fib 2nd International Workshop on Advanced Materials and Innovative Systems in Structural Engineering: Novel Researches (IWAMISSE2019), in Istanbul, Turkey, 20 September 2019.
- Yazgan, U., Ilki, A., Demir, C., **Demir, U.,** Ates, AO., Kupcu, E., Unal, G., Altinok, MA., Karakaya, B., Narlitepe, F. (2019). Challenges in Developing Seismic Vulnerability Models for Substandard Building Stocks in Turkey. In the proceedings of fib 2nd International Workshop on Advanced Materials and Innovative Systems in Structural Engineering: Novel Researches (IWAMISSE2019), in Istanbul, Turkey, 20 September 2019.
- **Demir, U.,** Sahinkaya, Y., Ispir, M. and Ilki, A. 2018. Assessment of Axial Behavior of Circular HPFRCC Members Externally Confined with FRP Sheets. *Polymers*, 10(2), 138.

- Goksu C., Inci P., **Demir, U.,** Yazgan, U. and Ilki, A. 2017. Field Testing of Substandard RC Buildings Through Forced Vibration Tests. *Bulletin of Earthquake Engineering*, 15(8), 3245-3263.
- **Demir, U.,** Sahinkaya, Y., Ispir, M. and Ilki, A. 2017. HPFRCC Members Externally Confined with FRP Sheets. 4th International Conference on Smart Monitoring, Assessment and Rehabilitation of Civil Structures, SMAR2017, Zürich, Switzerland.
- Inci, P., Goksu, C., **Demir, U.** and Ilki, A. 2017. Ambient Vibration Testing of a Three-Storey Substandard RC Building at Different Levels of Structural Seismic Damage. International Conference on Earthquake Engineering and Structural Dynamics (ICESD2017), Reykjavík/Iceland. Published on Springer, Cham. (pp. 219-231).